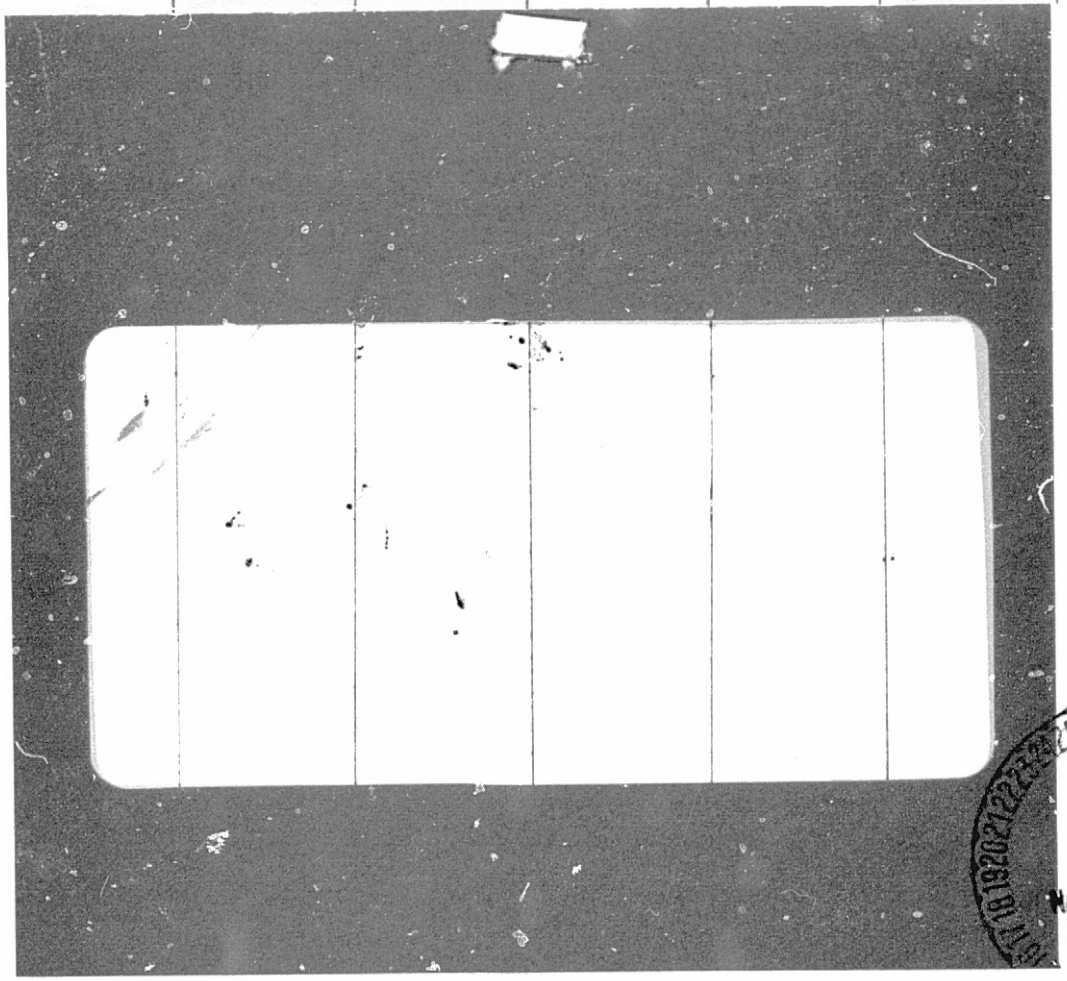

(NASA-CR-144647) SPACE SHUTTLE POST-ENTRY AND LANDING ANALYSIS. VOLUME 1: CANDIDATE SYSTEM EVALUATIONS (Analytic Sciences Corp.) 202 p HC $7.75 CSCL 22C

N76-15242

Unclas
G3/18 08540

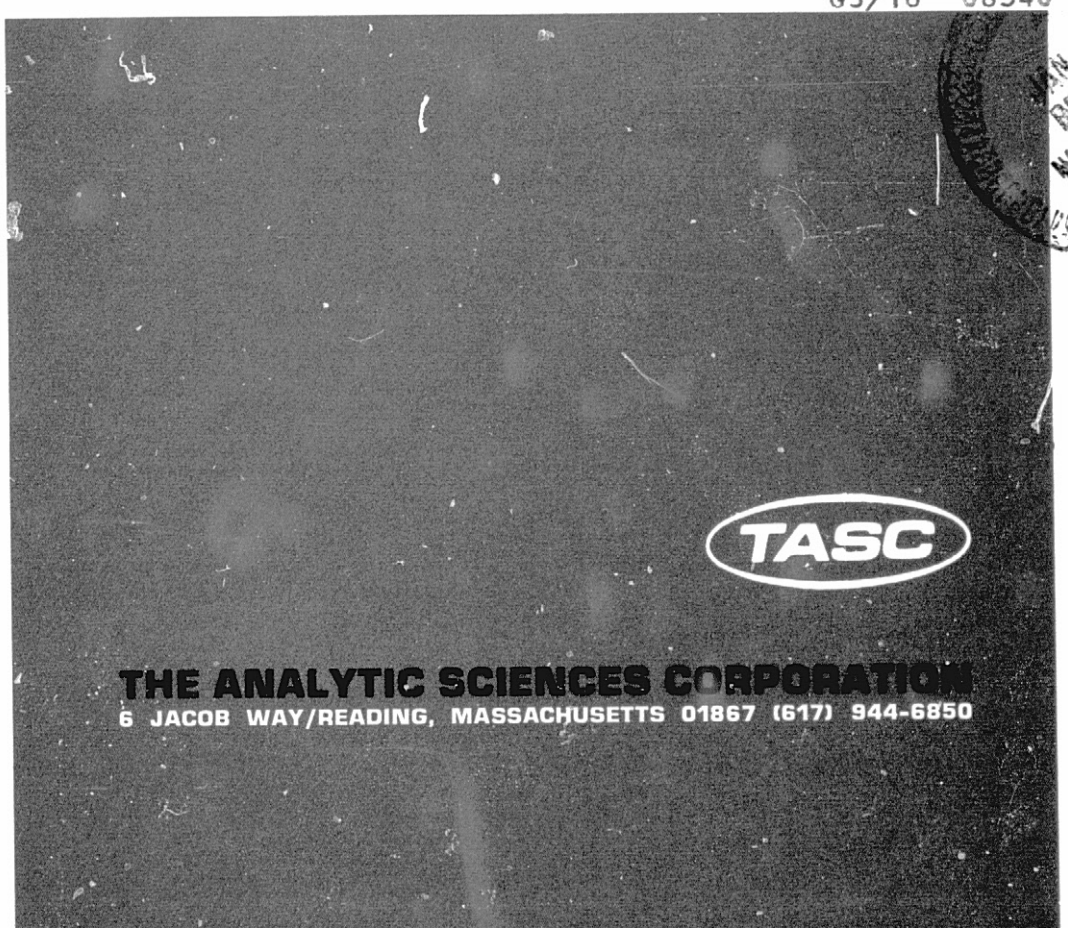

TASC

THE ANALYTIC SCIENCES CORPORATION

6 JACOB WAY/READING, MASSACHUSETTS 01867 (617) 944-6850

TR-302-1

SPACE SHUTTLE POST-ENTRY AND LANDING ANALYSIS

VOLUME I: CANDIDATE SYSTEM EVALUATIONS

20 JULY 1973

Prepared Under:

Contract No. NAS 9-12968

for

NATIONAL AERONAUTICS AND SPACE ADMINISTRATION
Johnson Space Center
Houston, Texas

Prepared by:

Bard S. Crawford
Edward M. Duiven

Approved by:

Arthur A. Sutherland, Jr.
Arthur Gelb

THE ANALYTIC SCIENCES CORPORATION
6 Jacob Way
Reading, Massachusetts 01867

ABSTRACT

Four candidate navigation systems for the Space Shuttle Orbiter approach and landing phase are evaluated in detail. These include three conventional navaid systems and a single-station one-way doppler system. In each case a Kalman filter is assumed to be mechanized in the onboard computer, blending the navaid data with IMU and altimeter data. Filter state dimensions ranging from 6 to 24 are involved in the candidate systems. Comprehensive truth models with state dimensions ranging from 63 to 82 are formulated and used to generate detailed error budgets and sensitivity curves illustrating the effect of variations in the size of individual error sources on touchdown accuracy. The projected overall performance of each system is shown in the form of time histories of position and velocity error components. The detailed results are summarized, compared and interpreted, the filter designs are reviewed and suggestions are made concerning possible software improvements.

ACKNOWLEDGEMENT

The authors acknowledge the guidance and assistance of the Contract Technical Monitors, Messers R.T. Savely and P.T. Pixley of the Mathematical Physics Group of the Mission Planning and Analysis Division of NASA/JSC. Assistance and cooperation were also received from Messers B.F. Cockrell and P.H. Mitchell of the same group. The authors would also like to thank Mr. M.F. D'Avanzo of TASC for his assistance in the programming portion of this work.

TABLE OF CONTENTS

VOLUME I

		Page No.
ABSTRACT		iii
ACKNOWLEDGEMENT		iv
LIST OF FIGURES		viii
LIST OF TABLES		ix
1.	INTRODUCTION	
	1.1 Objectives and Scope	1-1
	1.2 Relationship to Other Efforts	1-4
	1.3 Approach	1-7
	1.4 Organization of the Report	1-9
2.	TRAJECTORY, MEASUREMENT SCHEDULES AND METHODOLOGY	
	2.1 Nominal Trajectory	2-1
	2.2 Measurement Schedules	2-2
	2.3 Trajectory Modification for System D Study	2-6
	2.4 Covariance Equations	2-8
3.	TRUTH MODELS	
	3.1 System A Truth Model	3-1
	3.1.1 States and Error Sources	3-2
	3.1.2 Truth Model Equations	3-2
	3.1.3 Truth Model Data Base	3-18
	3.2 System B Truth Model	3-25
	3.2.1 States and Error Sources	3-26
	3.2.2 Truth Model Equations	3-29
	3.2.3 Truth Model Data Base	3-34
	3.3 System C Truth Model	3-34
	3.3.1 States and Error Sources	3-34
	3.3.2 Truth Model Equations	3-37
	3.3.3 Truth Model Data Base	3-42
	3.4 System D Truth Model	3-46
	3.4.1 States and Error Sources	3-47
	3.4.2 Truth Model Equations	3-50
	3.4.3 Truth Model Data Base	3-56

TABLE OF CONTENTS (Continued)

		Page No.
4.	FILTER COVARIANCE AND GAIN CALCULATIONS	
	4.1 System A Filter	4-1
	4.2 System B Filter	4-10
	4.3 System C Filter	4-16
	4.4 System D Filter	4-21
5.	RESULTS	
	5.1 System A Evaluation	5-1
	5.1.1 Overall System Performance	5-2
	5.1.2 Detailed Error Budget	5-5
	5.1.3 Sensitivity Curves: System A	5-9
	5.2 System B Evaluation	5-16
	5.2.1 Overall System Performance	5-16
	5.2.2 Detailed Error Budget	5-19
	5.2.3 Sensitivity Curves: System B	5-28
	5.3 System C Evaluation	5-29
	5.3.1 Overall System Performance	5-29
	5.3.2 Detailed Error Budget	5-31
	5.3.3 Sensitivity Curves: System C	5-35
	5.4 System D Evaluation	5-44
	5.4.1 Overall System Performance	5-44
	5.4.2 Detailed Error Budget	5-46
	5.4.3 Sensitivity Curves: System D	5-50
6.	SUMMARY COMPARISON AND DISCUSSION	
	6.1 Overall Performance Comparison	6-1
	6.2 Comparative Individual Contributions	6-8
	6.2.1 IMU Errors	6-8
	6.2.2 Conventional Navaids	6-12
	6.2.3 One-Way Doppler Errors	6-14
	6.2.4 Altimeter Errors	6-15
	6.2.5 Survey Errors	6-15
	6.3 Filter Design	6-16

TABLE OF CONTENTS (Continued)

		Page No.
7.	CONCLUSION	
	7.1 Summary of Findings	7-1
	7.2 Recommended Future Studies	7-3
REFERENCES		R-1

VOLUME II

APPENDIX A	COORDINATE FRAMES AND TRANSFORMATIONS	A-1
APPENDIX B	COMPUTATION OF SPECIAL OUTPUT QUANTITIES	B-1
APPENDIX C	ERROR CONTRIBUTION TIME HISTORIES	C-1

LIST OF FIGURES

Figure No.		Page No.
1.1-1	A Candidate Shuttle Orbiter Landing System	1-2
1.3-1	Aided Inertial Navigation with a Feedback Filter	1-7
1.3-2	Realistic System Performance Projections	1-9
2.1-1	Trajectory Ground Trace	2-2
2.2-1	External Aid Locations	2-7
2.3-1	System D Trajectory Altitude Profile	2-8
2.4-1	Truth Model Structure	2-10
3.1-1	System A Truth Model Structure	3-6
3.1-2	Orientation of Gyro Axes	3-11
3.1-3	Localizer-Shuttle Geometry	3-16
3.1-4	Glide Slope-Shuttle Geometry	3-16
3.2-1	System B Truth Model Structure	3-30
3.3-1	System C Truth Model Structure	3-38
3.4-1	System D Truth Model Structure	3-51
3.4-2	VOR/DME - Shuttle Geometry	3-54
4.1-1	Filter Covariance Program Flow Chart (System A and System B)	4-2
5.1-1	System A Overall Performance: Position	5-3
5.1-2	System A Overall Performance: Velocity	5-3
5.1-3	Sensitivity of Downrange Position and Velocity Errors at Touchdown to Gyro Bias Drift: System A	5-11
5.1-4	Sensitivity of Vertical Position and Velocity Errors at Touchdown to Accelerometer Misalignment: System A	5-12

LIST OF FIGURES (Continued)

Figure No.		Page No.
5.1-5	Sensitivity of Vertical Position Error at Touchdown to Radar Altimeter Markov Error: System A	5-13
5.1-6	Sensitivity of Crossrange Position Error at Touchdown to Localizer Markov Error: System A	5-14
5.1-7	Sensitivity of Crossrange Position Error at Touchdown to Localizer Bias Error: System A	5-14
5.1-8	Sensitivity of Crossrange Position and Velocity Errors at Touchdown to Accelerometer Scale Factor Errors: System A	5-15
5.2-1	System B Overall Performance: Position	5-17
5.2-2	System B Overall Performance: Velocity	5-17
5.2-3	Sensitivity of Downrange Position and Velocity Errors at Touchdown to DME Bias Errors: System B	5-24
5.2-4	Sensitivity of Downrange Position and Velocity Errors at Touchdown to Gyro Bias Drift: System B	5-25
5.2-5	Sensitivity of Vertical Position and Velocity Errors at Touchdown to Radar Altimeter Markov Error: System B	5-26
5.2-6	Sensitivity of Vertical Velocity Error at Touchdown to DME Scale Factor Error: System B	5-27
5.2-7	Sensitivity of Crossrange Position Error at Touchdown to Localizer Markov Error: System B	5-28
5.2-8	Sensitivity of Crossrange Position Error at Touchdown to Gyro Bias Drift: System B	5-28
5.3-1	System C Overall Performance: Position	5-30
5.3-2	System C Overall Performance: Velocity	5-30
5.3-3	System C Final Approach Performance	5-32
5.3-4	Sensitivity of Vertical Position and Velocity Errors at Touchdown to Accelerometer Misalignment: System C	5-38
5.3-5	Sensitivity of Vertical Position and Velocity Error at Touchdown to Radar Altimeter Markov Error: System C	5-39

LIST OF FIGURES (Continued)

Figure No.		Page No.
5.3-6	Sensitivity of Vertical Position and Velocity Errors at Touchdown to Onboard Doppler Rate Bias Error: System C	5-40
5.3-7	Sensitivity of Crossrange Position and Velocity Errors at Touchdown to Antenna Motion Compensation Error: System C	5-41
5.3-8	Sensitivity of Crossrange Position and Velocity Error at Touchdown to Accelerometer Scale Factor Errors: System C	5-42
5.3-9	Sensitivity of Crossrange Position and Velocity Errors at Touchdown to Gyro Bias Drift: System C	5-43
5.4-1	System D Overall Performance: Position	5-45
5.4-2	System D Overall Performance: Velocity	5-45
5.4-3	Sensitivity of Downrange Position Error at Touchdown to DME Bias Error: System D	5-52
5.4-4	Sensitivity of Downrange Position Error at Touchdown to Localizer Markov Error: System D	5-52
5.4-5	Sensitivity of Vertical Position and Velocity at Touchdown to Accelerometer Misalignment: System D	5-53
5.4-6	Sensitivity of Vertical Position and Velocity Errors at Touchdown to Radar Altimeter Markov Error: System D	5-54
5.4-7	Sensitivity of Crossrange Position and Velocity Errors at Touchdown to Localizer Markov Error: System D	5-56
5.4-8	Sensitivity of Crossrange Position and Velocity Errors at Touchdown to Localizer Bias Error: System D	5-57

LIST OF TABLES

Table No.		Page No.
1.1-1	Candidate Systems	1-3
1.1-2	Landing Navigation Specifications	1-4
2.1-1	Key Event Data	2-3
3.1-1	System A Truth Model States and Error Sources	3-3/3-4
3.1-2	System A Truth Model Data Base	3-20/3-21
3.2-1	System B Truth Model States and Error Sources	3-27/3-28
3.3-1	System C Truth Model States and Error Sources	3-35/3-36
3.3-2	System C Truth Model Data Base	3-43/3-44
3.4-1	System D Truth Model States and Error Sources	3-48/3-49
3.4-2	System D Truth Model Data Base (Where Different from System A)	3-58
4.1-1	Filter State Measurement Error Statistics: System A	4-4
4.1-2	System A Filter-Indicated Performance	4-9
4.2-1	System B Filter-Indicated Performance	4-16
4.3-1	Filter State Measurement Error Statistics: System C	4-17
4.3-2	System C Filter-Indicated Performance	4-21
4.4-1	Filter State Measurement Error Statistics: System D	4-22
4.4-2	System D Filter-Indicated Performance	4-24
5.1-1	System A Baseline Error Budget	5-6
5.1-2	System A Alternative Contributions	5-7
5.2-1	System B Baseline Error Budget	5-20
5.2-2	System B Alternative Contributions	5-21

LIST OF TABLES (Continued)

Table No.		Page No.
5.3-1	System C Baseline Error Budget	5-33
5.3-2	System C Alternative Contributions	5-36
5.4-1	System D Baseline Error Budget	5-47
5.4-2	System D Alternative Contributions	5-51
6.1-1	Comparison of Projected System Accuracy at Touchdown	6-2

1. INTRODUCTION

The reusable Space Shuttle Orbiter will be required to navigate accurately in multiple mission phases, based on data received from a variety of sources. Considerable effort is underway within NASA and among NASA contractors, aimed at producing reasonable solutions to the various multi-sensor navigation problems involved. A best overall solution is likely to involve a commonalty of navigation hardware elements and software modules. This document describes the results of a program of research which is one element in that overall effort.

1.1 OBJECTIVES AND SCOPE

The general purpose of this study is to aid in the evaluation and design of multi-sensor navigation schemes proposed for the Orbiter. The scope of the effort described herein is limited to the post-entry, energy management and approach and landing mission phases. Figure 1.1-1 illustrates one candidate system based on conventional navigation aids, including two DME (Distance Measuring Equipment) stations and ILS (Instrument Landing System) glide slope and localizer antennae. Some key elements of the system not shown in the figure are the onboard IMUs (Inertial Measurement Units), altimeters and a computer. The latter is programmed to mix together (filter) the IMU data and the externally-derived data. A completely automatic, all-weather landing capability is required. Since no air-breathing engines will be carried on orbital flights, there will be no chance to "go around" and try again following a missed approach.

R-8447

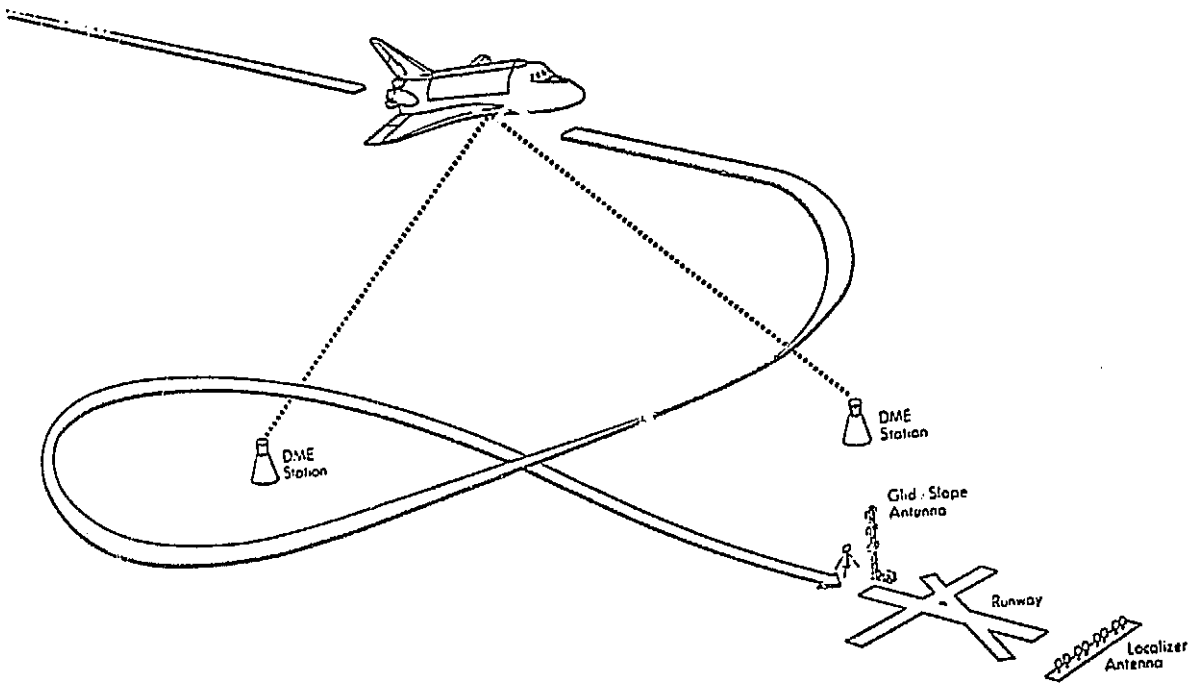

Figure 1.1-1 A Candidate Shuttle Orbiter Landing System

Specific objectives of this effort are:

- Define and develop mathematical models describ- all potentially significant sources of error for each candidate navigation system considered.
- Develop a detailed, quantitative understanding of the contributions of individual error sources to overall system performance.
- Present results in a form which will help NASA choose or specify hardware elements (IMU, navaids) or their characteristics.
- Evaluate alternative software approaches to the navigation filter design problem.

Table 1.1-1 summarizes the main features of four candidate systems which have been evaluated in detail. The first two, Systems A and B, consist of identical sets of hardware elements, but very different filters.

TABLE 1.1-1

CANDIDATE SYSTEMS

	IMU	External Aids	Filter	Use of Drag Updating
System A	KT-70	2 DMEs Baro Altimeter ILS (3 deg) Radar Altimeter	24-State Multi-Phase Filter	No
System B	KT-70	2 DMEs Baro Altimeter ILS (3 deg) Radar Altimeter	6-State Square-Root Filter	No
System C	KT-70	One-Way Doppler Baro Altimeter Radar Altimeter	22-State Multi-Phase Filter	No
System D	KT-70	1 DME 1 VOR ILS (Localizer Only) Baro Altimeter Radar Altimeter	23-State Multi-Phase Filter	Yes

The key hardware elements are the DME and ILS navaids pictured in Fig. 1.1-1. System C substitutes a one-way doppler beacon for the conventional navaids used in Systems A and B. System D is similar to System A except that a single VOR/DME (VHF Omnidirectional Range/Distance Measuring Equipment) station is used instead of 2 DME stations and the glide slope portion of the ILS system is omitted. The principle computational results of this study are the error budget tables given in Section 5, one for each of these four candidate systems.

The projected system navigation accuracies are compared in Section 5 with the specification values summarized in Table 1.1-2. These values are taken from Schiesser (Ref. 1), who states that they

are preliminary numbers and are a function of vehicle dynamics, structure, runway size and braking. A basic groundrule, which defines allowable navigation error to be some fraction of allowable total error, is also involved. Although the values tabulated are likely to change, they provide a useful standard of comparison.

TABLE 1.1-2

LANDING NAVIGATION SPECIFICATIONS

	Allowable RMS Navigation Errors at Touchdown		
	Vertical	Downrange	Crossrange
Position (ft)	3.0	80.0	4.7
Velocity (ft/sec)	0.2	3.0	2.0

1.2 RELATIONSHIP TO OTHER EFFORTS

An important foundation of this study is a family of computer programs (and the associated experience in using them) generated by TASC in connection with two Air Force sponsored programs. The first was a CIRIS (Completely Integrated Reference Instrumentation System) study in which TASC performed an independent evaluation (Ref. 2) of two filter designs. This called for the generation of system performance projections and detailed error budgets for each candidate system over a common trajectory and measurement geometry with respect to a network of precision ranging transponders. The second was a CLASS

(Close Air Support System) weapon delivery system evaluation (Ref. 3). In both studies a high-dimensional mathematical truth model was formulated and the linear covariance technique outlined in Section 1.3 was used to obtain the desired results. In the latter case (Ref. 3) it was possible to make detailed comparisons of computer-generated covariance results with actual flight test results. Good agreement was was noted, leading to high confidence in the truth model and methodology employed.

Major inputs to this study have come from three types of efforts conducted by others.

- Filter Design Studies
- IMU Error Propagation Studies
- Error Model Developments

A number of Space Shuttle Landing navigation filter studies have been conducted or supported by NASA/JSC. Two which have directly impacted this effort are the continuing activities of TRW (Refs. 4, 5 and 10) and MIT Draper Laboratory (Refs. 6 and 18). Both of these have roots in previous work on the Apollo program. The filters evaluated as part of Systems A, C and D of this study are specializations of the 28-state "multi-phase" filter described by Lear in Ref. 4. The 6-state filter of System B is based on the square-root filter algorithms employed in the MIT Draper Laboratory studies.

The starting point of the candidate system evaluations reported nerein is the end-of-blackout point, which occurs at an altitude of 130,000 ft along a nominal reentry trajectory. Considerable use has

been made of data generated by Clark and Mitchell (Ref. 7). This data represents initial navigation state errors and their correlations with basic IMU error sources, based on a shuttle "one-rev" mission with pure inertial navigation prior to entry. That effort made use of previously developed programs, notably the GEAP (General Error Analysis Program) described in Ref. 19.

Error models representing the performance of IMUs and the various navigation aids considered have been the subject of numerous reports. A number of these are cited as references in the "truth model data base" tables of Section 3. A particularly useful NASA document, for our purposes, has been Ref. 9, which pulls together much data from a broad variety of sources and presents it in readily usable form. That document has in turn drawn much from Ref. 20 prepared by the Lockheed Electronics Company.

The impact which this study is expected to have on other efforts involves both software and hardware decisions to be made by NASA or its major contractors. The software decisions involve methods for mixing inertial data with externally-derived data -- choice of filter states, filter update algorithms, etc. The hardware decisions involve the selection of an IMU and the devices needed to obtain the external data, as well as the specification of particular hardware characteristics, required survey accuracy, etc. The detailed, quantitative results and their interpretation provide valuable insights which are a useful input to the decision-making process.

1.3 APPROACH

Figure 1.3-1 is a generalized representation of all candidate navigation systems evaluated in this study. The hardware elements are an inertial measurement unit (IMU), a computer and a collection of devices (some airborne, some on the ground) needed to make external measurements. The computer function is divided into two parts, as shown. First, there is a standard set of algorithms needed to mechanize an inertial navigation system (INS). Second, there is a set of filter algorithms needed to blend in the external data. The filter is of the "feedback" variety, in which updated state estimates are used, after each measurement incorporation, to immediately correct appropriate variables of the INS routine and the measurement routine. (The latter corrections take place only if the filter states include estimates of correlated measurement errors.)

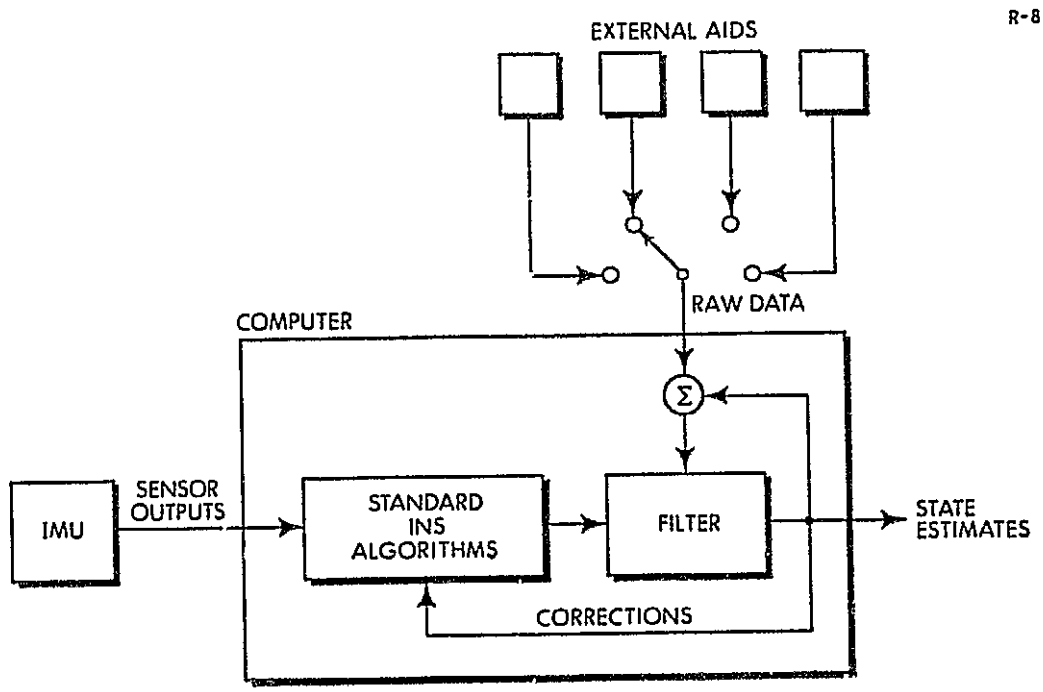

Figure 1.3-1 Aided Inertial Navigation with a Feedback Filter

The overall methodology used in each candidate system evaluation is summarized in Fig. 1.3-2. The upper half of the diagram represents the recursive solution of the filter covariance propagate and update equations. These are solved once for a given trajectory and measurement schedule. Certain elements of the filter dynamics and measurement matrices are functions of the Shuttle position and velocity vectors and the relative geometry between the Shuttle and the ground-navaid antenna locations. The outputs are the time histories of the filter-indicated performance and the Kalman filter gain matrices. The latter are stored on tape and called a "gain file". The lower half of the diagram represents the recursive solution of the linear system covariance equations, given in Section 2.4. These are solved repeatedly to produce an error budget, the same gain file being used each time. The trajectory dependent matrices, describing the real-world error model are of much higher dimension than the corresponding filter matrices. In individual error budget runs specific elements of input matrices, corresponding to specific error sources, are set to non-zero values, with all other elements set to zero. The output time history of the system error covariance matrix is then a statistical measure of the effect of that particular error source or small group of error sources, and generates one row of the error budget table. When the entire table is filled in, an overall system performance projection can be calculated from the detailed error-source-by-error-source breakdown.

It should be mentioned that while the methodology outlined above is conceptually very simple, considerable complication could arise in the detailed computer programming involved, for two reasons. First, there is often a requirement to work with multiple coordinate frames and to transform various vectors and matrices from one frame to another in the course of accepting inputs, making calculations and expressing outputs.

The detailed mathematics given in Appendix A and Appendix B of this report are a good example of this type of complication. Second, the desire to hold down the cost of computer running time has led to numerous complexities and program options which take advantage of special properties of the system truth models. It is not necessary, for example, to work with 80 x 80 matrices when the truth model state vector is 80-dimensional. Because TASC had developed a considerable amount of software to do these calculations prior to the start of this study, the computer-running-time cost of the error budgets generated in this report is at least an order of magnitude less than would be the case if the most straight-forward approach to the methodology outlined above were followed.

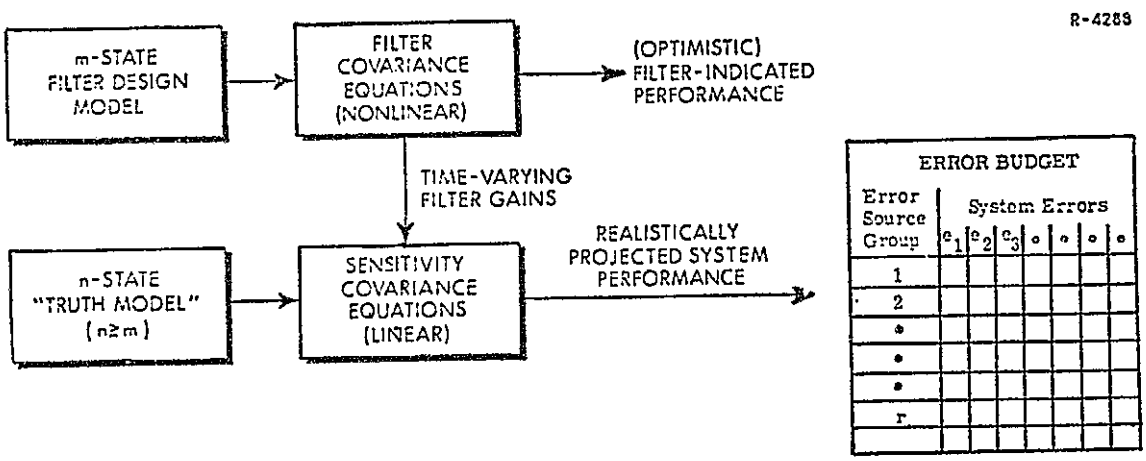

Figure 1.3-2 Realistic System Performance Projections

1.4 ORGANIZATION OF THE REPORT

Section 2 describes the trajectory and measurement schedules used in evaluating the four candidate systems. Systems A, B and C were evaluated using identical trajectories. The same ground track was used in the System D study, but a different descent rate time history was used

during final approach. This modification reflects recent changes in the Orbiter aerodynamic configuration. Some basic terminology and the linear covariance equations used in evaluating candidates systems are also presented in this section.

Section 3 presents the truth models used in evaluating the four systems. In each case the states and error sources are listed first; then the mathematical structure of the model is defined. Finally, the data base listing rms magnitudes, correlation times and data sources is given.

Section 4 defines the filter states and algorithms used to compute filter-indicated performance and to generate the filter gain sequences, which were filed on magnetic tape.

Section 5 presents the major results of the study. For each candidate system a detailed error budget table is given, listing the contributions of individual error sources, or small groups of error sources, to navigation errors at touchdown. Overall system performance projections, expressed as rms position and velocity component errors, are plotted from end-of-blackout to touchdown. Sensitivity curves showing the effects of variations in the size of major error sources are presented.

In Section 6 the results of the candidate system evaluations are summarized, compared and interpreted, and possibilities for improvement through software modifications are discussed.

Section 7 provides a brief summary of major conclusions and recommendations for further study. The appendices (Volume II) contain mathematical details involving coordinate frames and transformations and detailed computer print-outs generated in the course of producing the system error budgets.

2. TRAJECTORY, MEASUREMENT SCHEDULES AND METHODOLOGY

This section describes the approach and landing trajectory, measurement geometry and measurement schedules used in evaluating the four candidate systems. A modified final-approach descent-rate history was used for System D, reflecting recent changes in the Orbiter aerodynamic configuration. Section 2.4 defines the basic terminology and states the linear covariance equations used in evaluating candidate systems.

2.1 NOMINAL TRAJECTORY

At the outset of the study JSC furnished a magnetic tape with position, velocity and other data representing a typical shuttle reentry and landing trajectory, starting at an altitude of 400,000 ft and ending at touchdown. A new tape was created covering the portion below 130,000 ft and including just that data needed for our purposes. Figure 2.1-1 shows the ground trace of the trajectory portion of interest and indicates several key events, such as the time of the first DME measurement, T_{DME}, the time of the first baro altimeter measurement, T_{BA}, etc. One-minute time marks, indicating time elapsed after the first post-blackout measurement are included in the figure. Table 2.1-1 defines the other symbols used in Fig. 2.1-1 and provides further details, such as altitudes and relative velocity magnitudes at various times of interest.

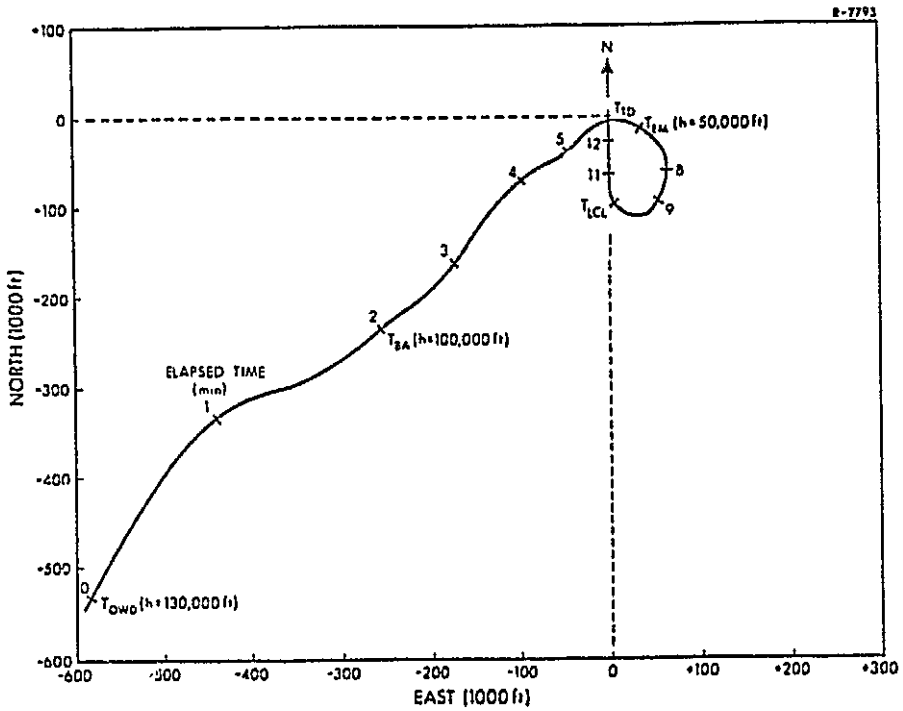

Figure 2.1-1 Trajectory Ground Trace

2.2 MEASUREMENT SCHEDULES

Both the System A and System B evaluations are based on the assumption that filter updates occur every 2 seconds for the first 750 seconds and every 0.5 seconds for the last 46 seconds (after T_{SW}). At each update time a sequence of scalar measurements are incorporated according to the following order.

1. DME Station 1
2. DME Station 2
3. Baro Altimeter ($t \geq T_{BA}$)*
4. ILS Localizer ($t \geq T_{LCL}$)

*The baro altimeter measurements are inhibited in the interval $950 < V_{REL} < 1020$ ft/sec (near Mach 1).

TABLE 2.1-1

KEY EVENT DATA

Event	System	Time		Altitude	Relative Velocity
		Trajectory Tape (sec)	Elapsed (sec)	(ft)	(ft/sec)
T_{DME} or T_{OWD}, First DME or OWD Measurement	ABCD	1636	0	130,000	4,990
T_{BA}, First Baro Altimeter Measurement	ABCD	1806	120	100,000	2,700
T_{EM}, Energy Management Initiation	ABCD	2092	386	50,000	889
T_{LCL}, First Localizer Measurement	AB	2292	606	18,100	696
	D	2292	606	24,000	687
T_{SW}, Switch from 2 sec Update Rate to 0.5 sec Update Rate	C	2406	720	4,690	495
	AB	2436	750	1,870	453
	D	2436	750	4,958	480
T_{RA}, First Radar Altimeter Measurement	ABC	2430	744	2,450	459
	D	2450	763	2,530	465
T_{GLS}, First Glide Slope Measurement	AB	2449.5	762.5	741	440
T_{STOP}, Stop Glide Slope Measurement	AB	2474	788	85	310
T_{TD}, Touchdown	ABCD	2482	796	0	302

5. Radar Altimeter ($t \geq T_{RA}$)
6. ILS Glide Slope ($T_{GLS} \leq t \leq T_{STOP}$)

Therefore the measurement sequences are:

Measurement Number	Time
1, 2	($T_{DME} \leq t < T_{BA}$)
1, 2, 3	($T_{BA} \leq t < T_{LCL}$)* (except near Mach 1)
1, 2, 3, 4	($T_{LCL} \leq t < T_{RA}$)
1, 2, 3, 4, 5	($T_{RA} \leq t < T_{GLS}$)
1, 2, 3, 4, 5, 6	($T_{GLS} \leq t \leq T_{STOP}$)
1, 2, 3, 4, 5	($T_{STOP} < t < T_{TD}$)

The update rate changes after radar altimeter measurements have begun, but before the glide slope measurements begin. This is well before overflight of the first DME station occurs.

The System C measurement schedule includes filter updates every 2 seconds for the first 720 seconds and every 0.5 seconds for the last 76 seconds (after T_{SW}). At each update time a sequence of scalar measurements are incorporated according to the following order:

1. One-Way Doppler
2. Baro Altimeter ($t \geq T_{BA}$) (except near Mach 1)
3. Radar Altimeter ($t \geq T_{RA}$)

Therefore the measurement sequences are:

Measurement Number	Time
1	$(T_{OWD} \leq t < T_{BA})$
1, 2	$(T_{BA} \leq t < T_{RA})$ (except as noted above)
1, 2, 3	$(T_{RA} \leq t < T_{TD})$

The update rate changes before radar altimeter measurements begin and well before the Shuttle overflies the one-way doppler station.

The System D measurement schedule is very similar to that of Systems A and B. Updates occur every 2 seconds for the first 750 seconds and every 0.5 seconds for the last 46 seconds. At each update time a sequence of scalar measurements is incorporated according to the following order.

1. DME
2. VOR*
3. Baro Altimeter $(t \geq T_{BA})$ (except near Mach 1)
4. ILS Localizer $(t \geq T_{LCL})$
5. Radar Altimeter $(t \geq T_{RA})$

Therefore the measurement sequences are:

Measurement Number	Time
1, 2	$(T_{DME} \leq t < T_{BA})$*
1, 2, 3	$(T_{BA} \leq t < T_{LCL})$ (except as noted above)
1, 2, 3, 4	$(T_{LCL} \leq t < T_{RA})$
1, 2, 3, 4, 5	$(T_{RA} \leq t < T_{TD})$

*The VOR measurements are inhibited in two regions when the elevation angle from the station to the vehicle is greater than 60 degrees -- at the beginning of the spiral and during final approach.

Figure 2.2-1 indicates the ground locations of the external aid devices. The values tabulated are incorporated in both the filter covariance programs and the truth model subroutines.

2.3 TRAJECTORY MODIFICATION FOR SYSTEM D STUDY

The trajectory used to evaluate System D has exactly the same ground trace as that used in the earlier studies and pictured in Fig. 2.1-1. A modified altitude history covering the final five minutes prior to touchdown has been employed in the System D study. The difference between the original trajectory and the System D trajectory is sketched in Fig. 2.3-1. A computer-generated listing describing the descent over the final minute was received from NASA. This corresponds to the performance of the new Orbiter configuration and appears as the solid-line portion of the System D curve in the figure. The dashed-line portion was constructed to match the original trajectory at 5 minutes before touchdown and the new trajectory at 1 minute before touchdown, using the following algorithm:

$$\Delta h = k_2 \tau^2 - k_3 \tau^3 \qquad (2.3\text{-}1)$$

where Δh is the difference between the new and the old altitude in Fig. 2.3-1, and

$$\tau = t - t_5 \qquad (2.3\text{-}2)$$

where t_5 is the time at five minutes prior to touchdown, and the parameters k_2 and k_3 are chosen such that

$$\left.\begin{aligned} \Delta h &= 0 \\ \Delta \dot{h} &= 0 \end{aligned}\right\} \text{at } \tau = 0$$

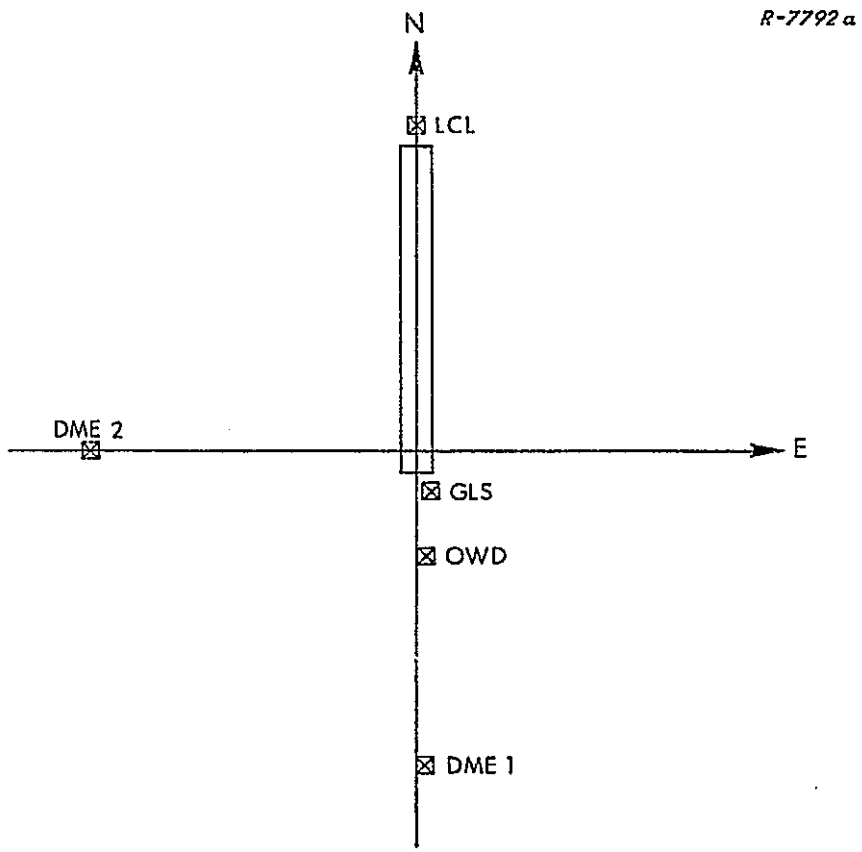

	UP	EAST (ft)	NORTH (ft)
DME 1 and VOR	R_{LP}	200	-9840
DME 2	R_{LP}	-9840	0
LOCALIZER ANTENNA	R_{LP}	0	10,000
GLIDE SLOPE ANTENNA	R_{LP}	500	-1300
OWD BEACON	R_{LP}	115	-3280

R_{LP} = 6373.3116 km
= 20,909,773 ft

Figure 2.2-1 External Aid Locations

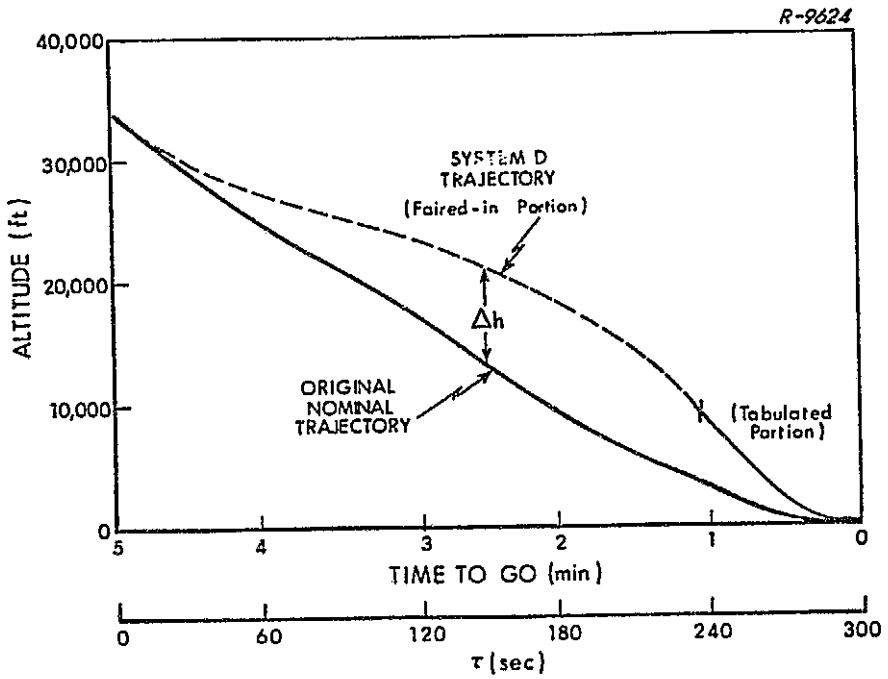

Figure 2.3-1 System D Trajectory Altitude Profile

$$\left.\begin{aligned} \Delta h &= 5174 \text{ ft} \\ \Delta \dot{h} &= -134 \text{ ft/sec} \end{aligned}\right\} \text{at } \tau = 240 \text{ sec}$$

That is, coefficients of the polynomial of Eq. (2.3-1) were chosen to make the new trajectory match the desired altitude and altitude rate at both ends of the faired-in position.

2.4 COVARIANCE EQUATIONS

Detailed system error budgets are generated by repeated solution of just two equations, the system covariance propagation and update equations, given at the end of this section.

Figure 2.4-1 is a conceptual representation of the mathematical structure of all truth models used in this study. An m-dimensional system error state vector, $\delta\underline{x}_S$, propagates between measurement times according to the linear, time-varying differential equation

$$\delta\dot{\underline{x}}_S(t) = F_S(t)\,\delta\underline{x}_S(t) + \underline{w}_S(t) \qquad (2.4\text{-}1)$$

where F_S is the "system error dynamics matrix" and $\underline{w}_S$ is a zero mean, gaussian noise process with

$$E\left[\underline{w}_S(t)\,\underline{w}_S(t-\tau)^T\right] = Q_S\,\delta(t-\tau) \qquad (2.4\text{-}2)$$

At discrete measurement times, t_k, a measurement residual vector, $\delta\underline{z}_S$, is formed by

$$\delta\underline{z}_{S_k} = H_{S_k}\,\delta\underline{x}_{S_k} + \underline{v}_{S_k} \qquad (2.4\text{-}3)$$

where H_S is the "measurement matrix" and $\underline{v}_S$ is a zero mean, gaussian white sequence with

$$E\left[\underline{v}_{S_k}\,\underline{v}_{S_k}^T\right] = R_{S_k} \qquad (2.4\text{-}4)$$

Filter corrections or updates are then given by

$$\underline{c}_{S_k} = K_{S_k}\,\delta\underline{z}_{S_k} \qquad (2.4\text{-}5)$$

where K_S is a gain matrix with m rows.

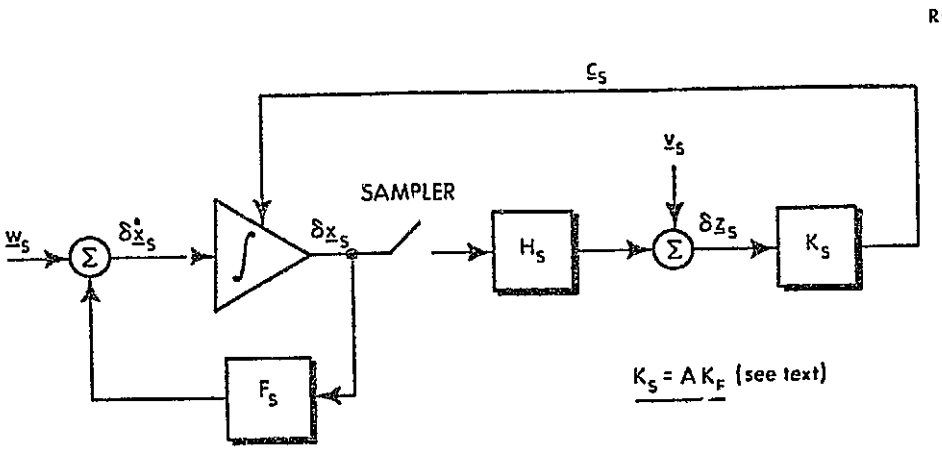

Figure 2.4-1 Truth Model Structure

$$K_S = AK_F = \begin{bmatrix} A' \\ \hline 0 \end{bmatrix} K_F = \left.\begin{bmatrix} A'K_F \\ \hline 0 \end{bmatrix}\right\}\begin{pmatrix}\text{m-n rows} \\ \text{of zeroes}\end{pmatrix} \qquad (2.4\text{-}6)$$

A is an m x n matrix linearly relating the n filter states to the m real-world states, and K_F is the Kalman filter gain matrix (of n rows) produced in the filter covariance calculation. The latter is based on the simplified n-dimensional model of system error propagation adopted by the filter designer. This model is defined by the filter matrices F_F, Q_F, H_F and R_F, which are analogous to the real-world or "system" matrices, F_S, Q_S, H_S and R_S, discussed above. The filter and system error covariance matrices are defined, respectively, as

$$P_F(t) = E\left[\delta\underline{x}_F(t)\ \delta\underline{x}_F(t)^T\right] \qquad (2.4\text{-}7)$$

and

$$P_S(t) = E\left[\delta\underline{x}_S(t)\ \delta\underline{x}_S(t)^T\right] \qquad (2.4\text{-}8)$$

The error budget results given in Section 5 summarize system covariance calculations of the elements of $P_S(t)$. The major inputs to these calculations are the initial value, $P_S(0)$, and time-varying elements of F_S, Q_S, H_S, R_S and K_S. Calculation of the non-zero elements of K_S requires a solution for K_F (see Eq. (2.4-6), which implies a filter covariance calculation. The major inputs to the latter are the initial value, $P_F(0)$, and the time-varying elements of F_F, Q_F, H_F and R_F.

The filter covariance equations used to generate the gain matrices, K_F, can take one of a number of forms, such as the Joseph form, the square-root form, etc. The choice is made by the filter designer. Section 4 describes the specific forms used in this study.

The system or truth model covariance equations are as follows: For propagation between measurements

$$\boxed{P_S(t_{k+1}^-) = \Phi_k P_S(t_k^+) \Phi_k^T + Q_{S_k}} \qquad (2.4\text{-}9)$$

where

$$\Phi_k = \exp\left[F_{S_k} \Delta t\right]$$

the transition matrix relating conditions just after the update at time t_k to conditions just before the update at time $t_{k+1} = t_k + \Delta t$. (F_S is assumed constant over the interval.)

$$Q_{S_k} = \int_0^{\Delta t} \exp\left[F_{S_k}(\Delta t - \tau)\right] Q_S \exp\left[F_{S_k}(\Delta t - \tau)\right]^T d\tau$$

the "discrete noise matrix" representing the integrated effect of system process noise Q_S over the time interval from t_k to t_{k+1}.

Truncated matrix exponential series' are used in evaluating the transition and discrete noise matrices defined above. For update of the system covariance matrix at the k^{th} measurement time

$$P_S(t_k^+) = \left[I - K_{S_k} H_{S_k}\right] P_S(t_k^-) \left[I - K_{S_k} H_{S_k}\right]^T + K_{S_k} R_{S_k} K_{S_k}^T \qquad (2.4\text{-}10)$$

The above is the Joseph form sometimes used in updating the filter covariance matrix. This form is appropriate for any linear filter update and is therefore useful in sub-optimal filter evaluations.

Equations (2.4-9) and (2.4-10) are time-varying, linear equations in the system error covariance, P_S. This fact allows easy computation of overall system performance by root-sum-squaring separate contributions and easy development of the sensitivity curves.

3. TRUTH MODELS

This section describes the "truth models" used in evaluating Systems A, B, C and D.* Each truth model description includes a list of error sources, a detailed mathematical structure and a data base. The overall mathematical structure is a set of linear differential and algebraic equations describing system error propagation, as in Eqs. (2.4-1), (2.4-3) and (2.4-5). Most of the detailed structure is given in terms of sub-matrices of F_S and H_S, the system error dynamics matrix and measurement matrices, defined in Section 2.4. The data base is the set of numerical values, such as rms values and correlation times, used to represent real-world error source statistics.

3.1 SYSTEM A TRUTH MODEL

The hardware elements of System A include a KT-70 IMU, a computer and the equipment needed for six external measurements: range to two DME stations, baro altitude, radar altitude and ILS localizer and glide slope measurements. The ground station locations and the specific measurement sequence are given in Section 2. The computer navigation program includes a 24-state Kalman filter, called herein the JSC/TRW filter. The filter states and algorithms are defined in detail in Section 4.1 and Ref. 4.

*By "truth model", we mean a mathematical model of all potentially significant sources of error and the way they affect system performance in the real world.

3.1.1 States and Error Sources

The truth model states and other error sources used in evaluating System A are listed in Table 3.1-1, which divides them into three major categories:

- The 24 estimated states and uncorrelated measurement and process noises.
- Non-estimated states related to the inertial system.
- Non-estimated states related to the external aids

Error budget results corresponding to the first category above are generated using a truth model structure (F_S, H_S), which corresponds almost exactly to the filter error model structure (F_F, H_F). Results corresponding to the other two categories are generated using a higher-dimensional truth model, which contains the basic 24-state structure plus other states representing time-correlated error sources not modeled explicitly in the filter design. These additional error sources are divided into 16 groups as indicated in Table 3.1-1. (The same group numbers are used in the Baseline Error Budget table in Section 5.1 and in the detailed results tabulated in Appendix C.)

3.1.2 Truth Model Equations

The System A truth model requires a 24 x 24 filter dynamics matrix, F_F, and an 82 x 82 system dynamics matrix, F_S. The filter mechanization treats external data as a sequence of scalar measurements, rather than as components of vector measurements. Up to six separate

TABLE 3.1-1

SYSTEM A TRUTH MODEL STATES AND ERROR SOURCES

Error Source Names	Number of States	Number of Error Sources
I. ESTIMATED STATES AND UNCORRELATED NOISES (Group 1)		
Position Errors	3	3
Velocity Errors	3	3
Platform Misalignments	3	3
Gyro Drifts (First-Order Markovs)	3	3
Accelerometer Scale Factor Errors (First-Order Markovs)	3	3
Accelerometer 'Biases' (First-Order Markovs	3	3
Correlated Measurement Errors (First-Order Markovs)		
2 DMEs	2	2
Baro and Radar Altimeters	2	2
ILS Localizer and Glide Slope	2	2
Uncorrelated Measurement Noise		
2 DMEs	-	2
Baro and Radar Altimeters	-	2
ILS Localizer and Glide Slope	-	2
INS Quantization Noise	-	3
II. NON-ESTIMATED, IMU-RELATED STATES		
Group 2. Accelerometer True Biases	3	3
Group 3. Accelerometer Constant Scale Factor Errors	3	3
Group 4. Accelerometer Misalignments	6	6
Group 5. Accelerometer Nonlinearities	3	3

TABLE 3.1-1 (Continued)

SYSTEM A TRUTH MODEL STATES AND ERROR SOURCES

Error Source Names	Number of States	Number of Error Sources
II. NON-ESTIMATED, IMU-RELATED STATES (Continued)		
Group 6. Gravitational Deflections and Anomalies	3	3
Group 7. Gyro True Bias Drifts	3	3
Group 8. Gyro Mass Unbalances	6	6
Group 9. Gyro Anisoelasticity	3	3
III. NON-ESTIMATED, EXTERNAL-AID RELATED STATES		
Group 10. DME Bias Errors	2	2
Group 11. DME Scale Factor Errors	2	2
Group 12. Baro Altimeter Errors		
Bias	1	1
Scale Factor	1	1
First-Order Markov	1	1
Static Defect	1	1
Group 13. ILS Bias Errors		
Localizer	1	1
Glide Slope	1	1
Group 14. ILS Second-Order Markov Errors		
Localizer	2	1
Glide Slope	2	1
Group 15. Radar Altimeter Errors		
Scale Factor Error	1	1
Bias Error	1	1
Group 16. DME Survey Errors	6	6
Group 17. ILS Survey Errors	6	6
Totals	82	89

scalars may be incorporated at one update time. Therefore, there are six distinct filter measurement matrices, H_{F_1} through H_{F_6} -- each is a 24 dimensional row vector. There are six corresponding system measurement matrices, H_{S_1} through H_{S_6} -- each of these is an 82 dimensional row vector.

Figure 3.1-1 presents the overall structure of the F_S and H_S matrices for System A. The upper-left partition of F_S is the 24 x 24 matrix $F_{1,1}$, whose elements define the dynamic interaction between the Group 1 error states. This sub-matrix of F_S corresponds* to the filter matrix, F_F. The horizontal row of sub-matrices, $F_{1,2}$ through $F_{1,9}$, defines the effects of the non-estimated, IMU-related error sources (Groups 2-9) on the velocity errors (states 4-6) and the platform misalignment (states 7-9). The sub-matrices along the main diagonal, $F_{2,2}$ through $F_{17,17}$, define the dynamics of all non-estimated, correlated error sources. For a group of random-constant error sources this sub-matrix is zero. The six system measurement matrices (row vectors) are outlined in the lower half of Fig. 3.1-1. In each case the first 24 elements are the same as those of the corresponding filter measurement matrix. Other non-zero sub-matrices, $H_{i,j}$, define the effects of the correlated error sources (Group j) in question on the measurement error (δz_i) in question.

The sub-matrices $F_{i,j}$ and $H_{i,j}$ are defined in detail below, using the group-number designations given in Table 3.1-1.

*$F_{1,1}$ and F_F are identical except for the presence of a 3 x 3 coordinate transformation. See $T_{I/P}$ in Eq. (3.1-1).

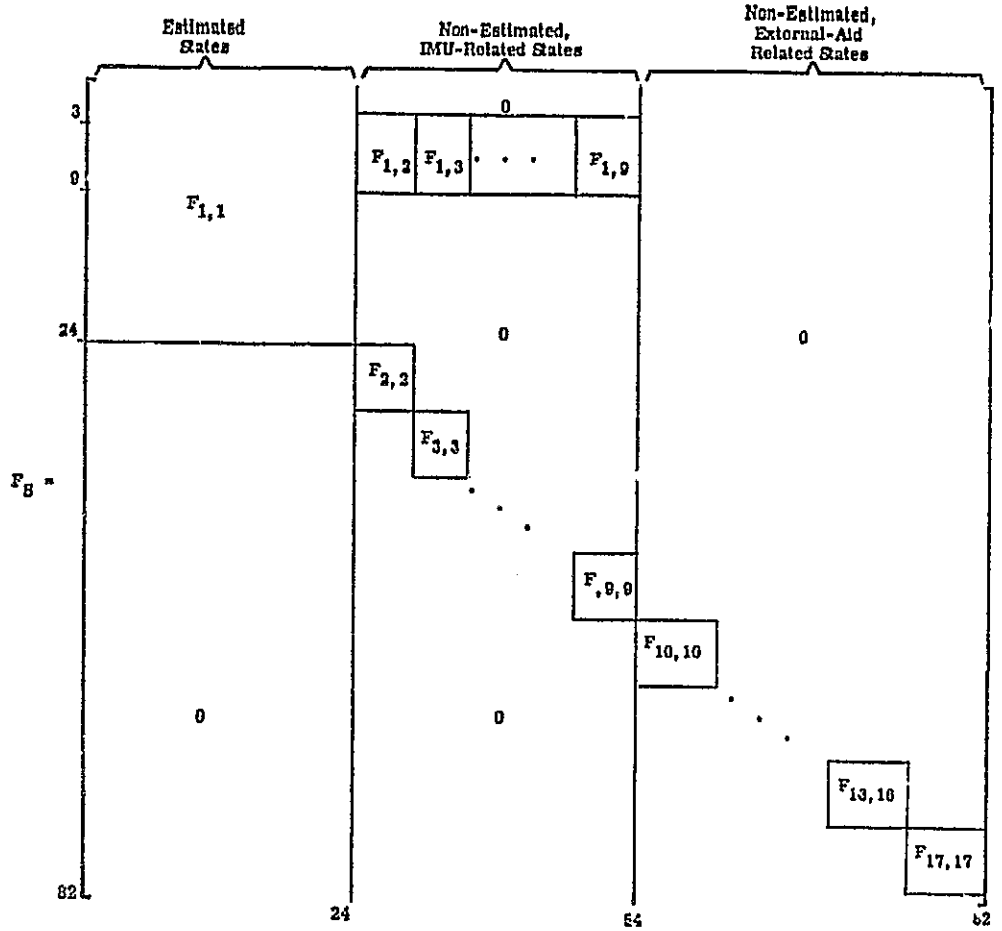

a) State Dynamics Matrix

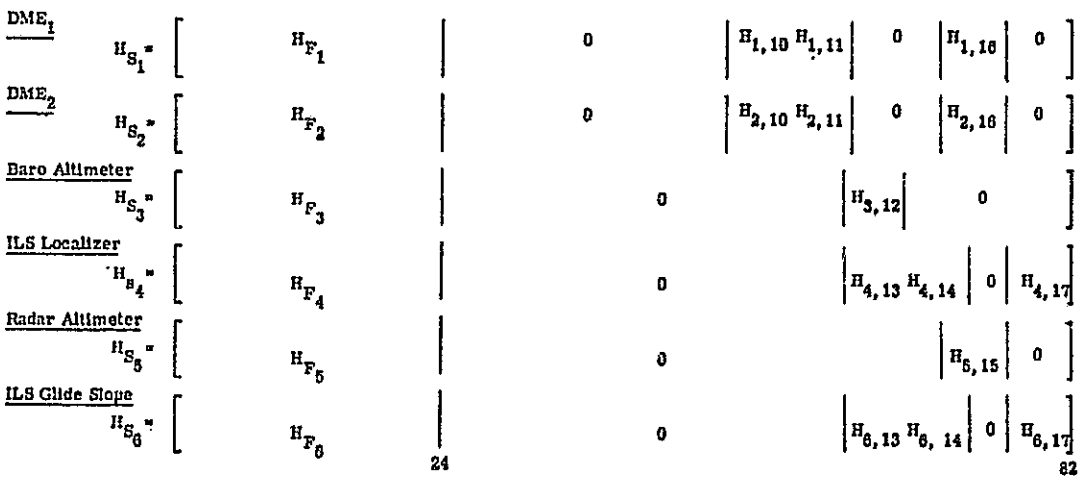

b) Measurement Matrices

Figure 3.1-1 System A Truth Model Structure

Group 1 — Estimated States (See also, Section 4.1)

$$F_{1,1} = \begin{array}{c|cccccc|c} & \text{Position Errors} & \text{Velocity Errors} & \text{Misalignments} & \text{Gyro Drift} & \text{Accelerometer Scale Factor} & \text{Accelerometer Bias} & \text{Measurement Errors} \\ 3 & 0 & I & 0 & 0 & 0 & 0 & \\ 6 & G_r & 0 & T_{I/P}\, F_P & 0 & f_x\ f_y\ f_z & I & 0 \\ 9 & 0 & 0 & 0 & I & 0 & 0 & \\ & & & & & & & \\ & \multicolumn{2}{c}{0} & & \multicolumn{3}{c}{D_\tau} & \\ & & & & & & & \\ 18 & \multicolumn{2}{c}{0} & & & & & \\ 24 & & & & & & & \end{array} \qquad (3.1\text{-}1)$$

where

$$D_\tau = 15 \times 15 \text{ diagonal matrix with } D_{\tau_{ii}} = -1/\tau_i \qquad (3.1\text{-}2)$$

$$G_r = -\frac{\mu}{r^3}\left[I - \frac{3}{r^2}\underline{r}\,\underline{r}^T\right] \qquad (3.1\text{-}3)$$

μ = gravitational constant

I = 3 x 3 identity matrix

$\underline{r}$ = position vector (in I frame; see Appendix A)

$\begin{pmatrix} f_x \\ f_y \\ f_z \end{pmatrix}$ = specific force vector in the I frame

$$F_P = \begin{bmatrix} 0 & -f_3 & f_2 \\ f_3 & 0 & -f_1 \\ -f_2 & f_1 & 0 \end{bmatrix} \qquad (3.1\text{-}4)$$

$\begin{pmatrix} f_1 \\ f_2 \\ f_3 \end{pmatrix}$ = specific force vector in the P frame

$T_{I/P}$ = 3 x 3 matrix which transforms vector in the P (platform) frame to the I(navigation error analysis) frame; see Appendix A. See also, the discussion of the A matrix, at the end of Section 3.1.2.

Group 2 — Accelerometer True Biases, (3 sensors, 1 state each)

$$F_{1,2} = \left[\frac{T_{I/P}}{0}\right]_{6 \times 3} \quad ; \quad F_{2,2} = \left[\ 0\ \right]_{3 \times 3} \qquad (3.1\text{-}5)$$

Group 3 — Accelerometer Constant Scale Factor Errors, (3 sensors, 1 state each)

$$F_{1,3} = \left[\frac{T_{I/P}\ F_3}{0}\right]_{6 \times 3} \quad ; \quad F_{3,3} = \left[\ 0\ \right]_{3 \times 3} \qquad (3.1\text{-}6)$$

where

$$F_3 = \begin{bmatrix} f_1 & 0 & 0 \\ 0 & f_2 & 0 \\ 0 & 0 & f_3 \end{bmatrix} \qquad (3.1\text{-}7)$$

Group 4 — Accelerometer Misalignments, (3 sensors, 2 states each)

$$F_{1,4} = \begin{bmatrix} T_{I/P} F_4 \\ 0 \end{bmatrix}_{6 \times 6} \quad ; \quad F_{4,4} = \begin{bmatrix} 0 \end{bmatrix}_{6 \times 6} \qquad (3.1\text{-}8)$$

where

$$F_4 = \begin{bmatrix} f_2 & f_3 & 0 & 0 & 0 & 0 \\ 0 & 0 & f_1 & f_3 & 0 & 0 \\ 0 & 0 & 0 & 0 & f_1 & f_2 \end{bmatrix} \qquad (3.1\text{-}9)$$

Group 5 — Accelerometer Nonlinearities, (3 sensors, 1 state each)

$$F_{1,5} = \begin{bmatrix} T_{I/P} F_5 \\ 0 \end{bmatrix}_{6 \times 3} \quad ; \quad F_{5,5} = \begin{bmatrix} 0 \end{bmatrix}_{3 \times 3} \qquad (3.1\text{-}10)$$

where

$$F_5 = \begin{bmatrix} f_1^2 & 0 & 0 \\ 0 & f_2^2 & 0 \\ 0 & 0 & f_3^2 \end{bmatrix} \qquad (3.1\text{-}11)$$

Group 6 — Gravity Deflections and Anomaly, (up, east and north components)

$$F_{1,6} = \left[\frac{T_{I/L}}{0}\right]_{6 \times 3} \quad ; \quad F_{6,6} = \begin{bmatrix} -1/\tau_u & 0 & 0 \\ 0 & -1/\tau_e & 0 \\ 0 & 0 & -1/\tau_n \end{bmatrix} \qquad (3.1\text{-}12)$$

where

$$\tau_u = d_u/V_{rel}$$

$$\tau_e = d_e/V_{rel}$$

$$\tau_n = d_n/V_{rel}$$

and d_u, d_e, d_n are correlation distances

Group 7 — Gyro Bias Drifts, (3 sensors, 1 state each)

$$F_{1,7} = \left[\frac{0}{I}\right]_{6 \times 3} \quad ; \quad F_{7,7} = \left[0\right]_{3 \times 3} \qquad (3.1\text{-}13)$$

Group 8 — Gyro Mass Unbalances, (3 sensors, 2 states each)

$$F_{1,8} = \begin{bmatrix} & & & 0 & & \\ \hline f_1 & f_2 & 0 & 0 & 0 & 0 \\ 0 & 0 & f_2 & f_3 & 0 & 0 \\ 0 & 0 & 0 & 0 & f_3 & f_2 \end{bmatrix}_{6 \times 6} \quad ; \quad F_{8,8} = \begin{bmatrix} 0 \end{bmatrix}_{6 \times 6}$$

(3.1-14)

The elements of $F_{1,8}$ and $F_{1,9}$, below, are determined by the gyro input and spin axis directions shown in Fig. 3.1-2.

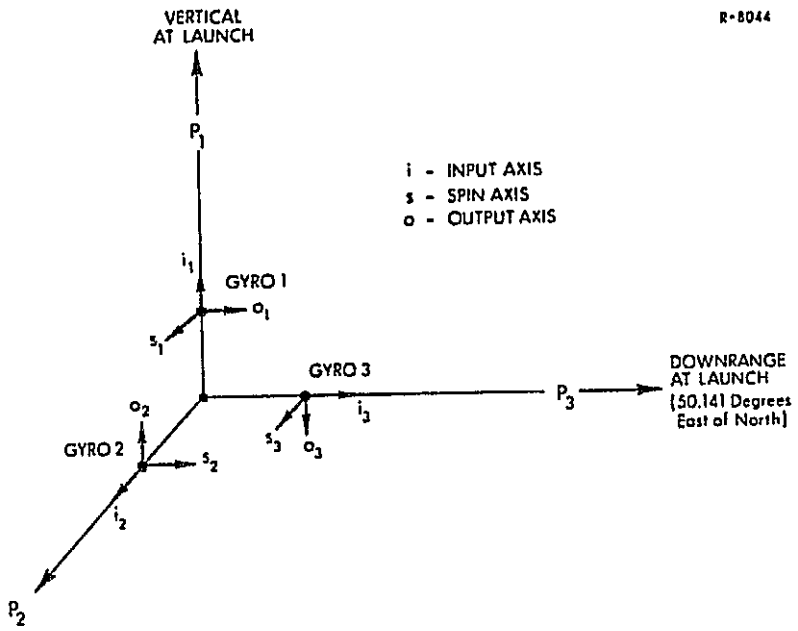

Figure 3.1-2 Orientation of Gyro Axes

Group 9 — Gyro Anisoelasticity, (3 sensors, 1 state each)

$$F_{1,9} = \begin{bmatrix} & 0 & \\ \hline f_1 f_2 & 0 & 0 \\ 0 & f_2 f_3 & 0 \\ 0 & 0 & f_2 f_3 \end{bmatrix}_{6 \times 3} \quad ; \quad F_{9,9} = \begin{bmatrix} 0 \end{bmatrix}_{6 \times 6} \tag{3.1-15}$$

Group 10 — DME Bias Errors, (2 stations, 1 state each)

$$F_{10,10} = \begin{bmatrix} 0 \end{bmatrix}_{2 \times 2} \tag{3.1-16}$$

$$H_{1,10} = 1 \tag{3.1-17}$$

$$H_{2,11} = 1 \tag{3.1-18}$$

Group 11 — DME Scale Factor Errors, (2 stations, 1 state each)

$$F_{11,11} = \begin{bmatrix} -1/\tau_{sf} & 0 \\ 0 & -1/\tau_{sf} \end{bmatrix}_{2 \times 2} \tag{3.1-19}$$

$$H_{1,11} = \rho_1 \tag{3.1-20}$$

$$H_{2,11} = \rho_2 \tag{3.1-21}$$

where ρ_1 and ρ_2 are the distances from the vehicle to DME stations 1 and 2, respectively

Group 12 — Baro Altimeter Errors, (4 states)

$$F_{12,12} = \begin{bmatrix} 0 & 0 & 0 & 0 \\ 0 & 0 & 0 & 0 \\ 0 & 0 & -1/\tau_a & 0 \\ 0 & 0 & 0 & 0 \end{bmatrix} \begin{matrix} \text{bias} \\ \text{scale factor} \\ \text{markov} \\ \text{static defect} \end{matrix} \qquad (3.1\text{-}22)$$

$$H_{3,12} = \begin{bmatrix} 1 & h & 1 & V_{vel}^2 \end{bmatrix} \qquad (3.1\text{-}23)$$

where

h = altitude

V_{rel} = relative velocity

Group 13 — ILS Bias Errors, (2 states: localizer and glide slope)

$$F_{13,13} = \begin{bmatrix} 0 \end{bmatrix}_{2 \times 2} \qquad (3.1\text{-}24)$$

$$H_{4,13} = 1 \qquad (3.1\text{-}25)$$

$$H_{6,13} = 1 \qquad (3.1\text{-}26)$$

Group 14 — ILS Second Order Markov Errors, (4 states: 2 localizer, 2 glide slope)

$$F_{14,14} = \left[\begin{array}{cc|cc} -1/\tau_{LCL} & -1/\tau_{LCL}^2 & \multicolumn{2}{c}{0} \\ 0 & -1/\tau_{LCL} & & \\ \hline \multicolumn{2}{c|}{} & -1/\tau_{GLS} & -1/\tau_{GLS}^2 \\ \multicolumn{2}{c|}{0} & & \\ \multicolumn{2}{c|}{} & 0 & -1/\tau_{GLS} \end{array}\right]_{4 \times 4} \tag{3.1-27}$$

$$H_{4,14} = [1 \quad 0 \quad 0 \quad 0] \tag{3.1-28}$$

$$H_{6,14} = [0 \quad 0 \quad 1 \quad 0] \tag{3.1-29}$$

Group 15 — Radar Altimeter, (2 states: bias, scale factor)

$$F_{15,15} = \left[\begin{array}{c} 0 \end{array}\right]_{2 \times 2} \tag{3.1-30}$$

$$H_{5,15} = [1 \quad h] \tag{3.1-31}$$

Group 16 — DME Survey Errors, (2 stations, 3 components each)

$$F_{16,16} = \left[\begin{array}{c} 0 \end{array}\right]_{6 \times 6} \tag{3.1-32}$$

$$H_{1,16} = \left[-\rho_{1_R}/\rho_1 \quad -\rho_{1_C}/\rho_1 \quad -\rho_{1_D}/\rho_1 \quad 0 \quad 0 \quad 0\right] \tag{3.1-33}$$

$$H_{2,16} = \begin{bmatrix} 0 & 0 & 0 & -\rho_{2_R}/\rho_2 & -\rho_{2_C}/\rho_2 & -\rho_{2_D}/\rho_2 \end{bmatrix} \quad (3.1\text{-}34)$$

where

$\underline{\rho}_1$ = relative positive vector: station 1 to vehicle

$\rho_{1_R}, \rho_{1_C}, \rho_{1_D}$ = components of $\underline{\rho}_1$ in R frame

$\underline{\rho}_2$ = relative position vector: station 2 to vehicle

$\rho_{2_R}, \rho_{2_C}, \rho_{2_D}$ = components of $\underline{\rho}_2$ in R frame

Group 17 — ILS Survey Errors, (2 antenna locations, 3 components each)

$$F_{17,17} = \begin{bmatrix} 0 \end{bmatrix}_{6 \times 6} \quad (3.1\text{-}35)$$

$$H_{4,17} = \begin{bmatrix} -u_{e_R}/\rho_{s_4} & -u_{e_C}/\rho_{s_4} & -u_{e_D}/\rho_{s_4} & 0 & 0 & 0 \end{bmatrix} \quad (3.1\text{-}36)$$

$$H_{6,17} = \begin{bmatrix} 0 & 0 & 0 & -u_{p_R}/\rho_6 & -u_{p_C}/\rho_6 & -u_{p_D}/\rho_6 \end{bmatrix} \quad (3.1\text{-}37)$$

where

$u_{e_R}, u_{e_C}, u_{e_D}$ = components of a cross-runway unit vector; see Figure 3.1-3.

ρ_{s_4} = projection onto the horizontal plane of $\underline{\rho}_4$, the relative position vector from localizer antenna to the vehicle; see Figure 3.1-3.

R-7804

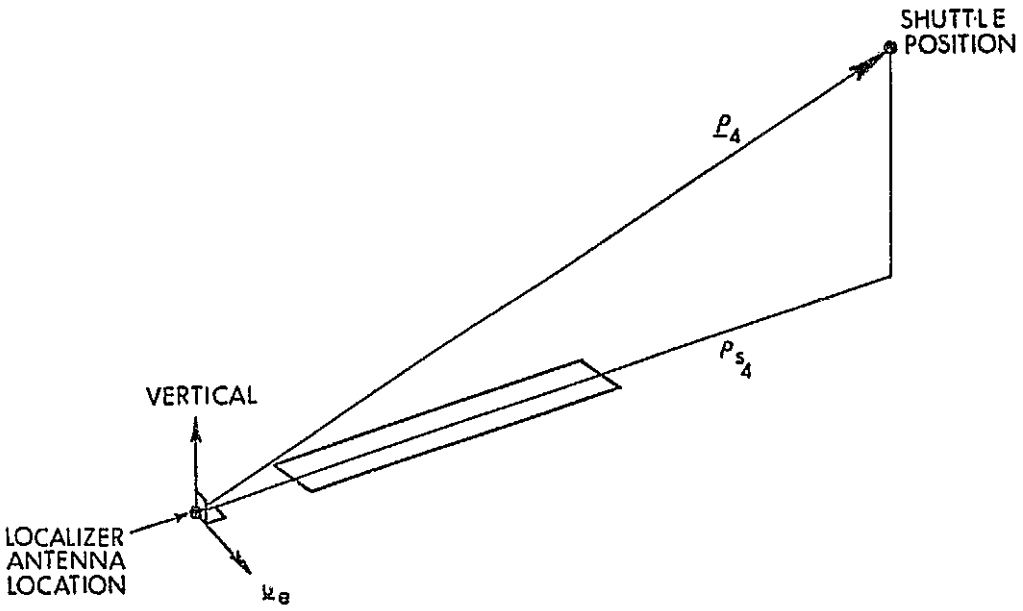

Figure 3.1-3 Localizer-Shuttle Geometry

R-7805

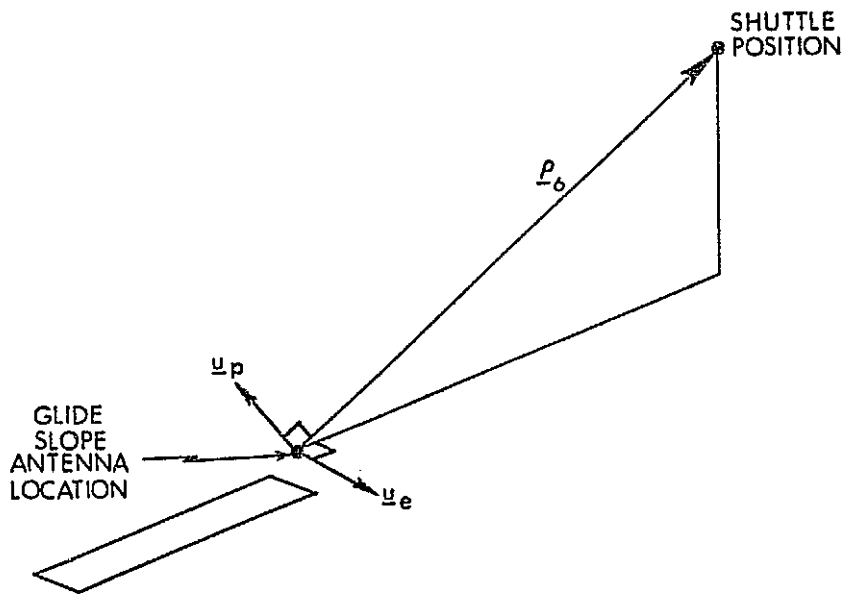

Figure 3.1-4 Glide Slope-Shuttle Geometry

u_{p_R}, u_{p_C}, u_{p_D} = components of a unit vector defined in Figure 3.1-4.

ρ_6 = length of $\underline{\rho}_6$, the relative position vector from glide slope antenna to the vehicle; see Figure 3.1-4.

A Matrix

The 82 x 24 matrix relating the filter states to the truth model states has the form:

$$A = \begin{bmatrix} A'_{24 \times 24} \\ \hline 0 \end{bmatrix} \tag{3.1-38}$$

where

$$A' = \left[\begin{array}{c|c|ccc|c|c} I_{6 \times 6} & & & 0 & & 0 & \\ \hline 0 & T_{P/I} & & & & & \\ \hline & & T_{P/I} & 0 & 0 & & \\ \cline{3-5} 0 & & 0 & T_{P/I} & 0 & 0 & \\ \cline{3-5} & & 0 & 0 & T_{P/I} & & \\ \hline 0 & & & 0 & & I_{6 \times 6} & \end{array}\right] \begin{matrix} \\ \\ \\ \\ \\ \\ \\ \end{matrix} \begin{matrix} \\ \\ \\ \\ \\ \\ \\ \end{matrix} \begin{matrix} \\ \\ \\ \\ \\ \\ \\ \end{matrix} \begin{matrix} \\ \\ \\ \\ \\ \\ \\ \end{matrix} \begin{matrix} \\ \\ \\ \\ \\ \\ \\ \end{matrix} \begin{matrix} \\ \\ \\ \\ \\ \\ \\ \end{matrix} \begin{matrix} \\ \\ \\ \\ \\ \\ \\ \end{matrix} \tag{3.1-39}$$

$$\begin{matrix} & & 6 & 9 & & & 18 & 24 \end{matrix}$$

The filter states 7 through 18, corresponding to platform misalignments, gyro drifts; accelerometer scale factor errors and accelerometer biases, are

defined in the I frame. The corresponding truth model states are defined in the platform (P) frame because a considerable amount of useful input data (from Ref. 7) represents the initial (h = 130,000 ft) contributions of individual sensors in the particular orientations pictured in Fig. 3.1-2. Thus, the transformation $T_{P/I}$, from I to P coordinates, appears four times in the A matrix.

The mathematical structure of the 82-state System A truth model and its relation to the 24 filter states has been completely defined in this section. The filter model is described in Section 4.1.

3.1.3 Truth Model Data Base

In this section numerical values are assigned to the System A truth model matrix elements describing error source statistics. Most of these values are elements of the following matrices:

$P_S(0)$ – the initial system (real world) error covariance matrix

Q_S – the system process noise matrix

$R_{S_i}(i=1,\ldots,6)$ – the system measurement error variances, σ_i^2 (in this case each R_{S_i} is a 1 x 1 matrix, or scalar).

In addition to the above, some elements of F_S, left unspecified in the previous section, are needed to complete the truth model. These are main-diagonal elements, such as the elements of $F_{6,6}$, which involve correlation times of markov processes associated with various error source groups. These elements of F_S and corresponding elements of $P_S(0)$ and Q_S are normally chosen together to define random processes with desired properties. Frequently, a first-order markov process (exponentially correlated random process) is modeled with a specified

rms value, σ_i, and correlation time, τ_i. In this case the relevant truth model matrix elements are:

$$P_{S_{ii}}(0) = \sigma_i^2 \tag{3.1-40}$$

$$F_{S_{ii}} = -1/\tau_i \tag{3.1-41}$$

$$Q_{S_{ii}} = 2\sigma_i^2/\tau_i \tag{3.1-42}$$

A constant error source can be considered a special case of the above with $\tau_i = \infty$ and $F_{S_{ii}} = Q_{S_{ii}} = 0$.

Table 3.1-2 summarizes the truth model rms values and correlation times used in evaluating System A. The data is organized according to the three major categories and 17 groups of error sources already used in Table 3.1-1. The final column in the table indicates the pricipal references or sources of data.

The 9 x 9 initial condition error covariance matrix is taken directly from page 203 of Ref. 7 (Table D-III-c). This matrix represents error statistics at an altitude of 130,000 ft, following a "one-rev" mission in which pure inertial navigation is used from launch to the 130,000 ft point. The assumed error sources correspond to KT-70 IMU performance, and are exactly those given in Table 3.1-2 for groups 2, 3, 4, 5, 7, 8 and 9. The assumed prelaunch alignment technique consists of gyrocompassing for azimuth alignment and accelerometer tilt leveling. This matrix is used in Section 5.1 to produce one row in the "Alternative Error Contributions" table, showing how the initial errors, considered independent of root causes, propagate through the approach and landing

TABLE 3.1-2

SYSTEM A TRUTH MODEL DATA BASE

Error Source	Value	Correlation Time (sec)	Data Source
I. ESTIMATED STATES AND UNCORRELATED NOISE (Group 1)			
Initial Condition Errors: Position, Velocity, Misalignment	9 x 9 Covariance Matrix (see text)	—	Ref. 7
IMU Quantization Errors	$Q_{S_{ii}} = 4.48 \times 10^{-4} \frac{(ft/sec)^2}{sec}$ (i = 4, 5, 6 -- see text)	—	Ref. 8
DME Measurement White Noise	σ = 24 ft	—	Ref. 9
Baro Altimeter Measurement White Noise	σ = 5 ft	—	Ref. 3
Radar Altimeter Measurement White Noise	σ = 3.28 ft	—	Ref. 11
Radar Altimeter First Order Markov Error	see Eq. (3.1-43)	4.0	Ref. 11
ILS First Order Markov Errors: Localizer	see Eq. (3.1-44)	0.55	Ref. 5
ILS First Order Markov Errors: Glide Slope	see Eq. (3.1-45)	0.55	Ref. 5
II. NON-ESTIMATED, IMU-RELATED STATES			
Group 2. Accelerometer Biases	σ = 60 μg	∞	Ref. 9
Group 3. Accelerometer Scale Factor Errors	σ = 34 ppm	∞	Ref. 9
Group 4. Accelerometer Misalignments	σ = 40 $\widehat{sec}$	∞	Ref. 9
Group 5. Accelerometer Nonlinearities	σ = 3.5 $\mu g/g^2$	∞	Ref. 9

TABLE 3.1-2 (Continued)

SYSTEM A TRUTH MODEL DATA BASE

Error Source	Value	Correlation Time (sec)	Data Source
II. (Continued)			
Group 6. Gravity Anomaly	$\sigma = 13.3 \times 10^{-4}$ ft/sec^2	$492{,}000/V_{rel}$	Ref. 12
Deflection about East	$\sigma = 5.1$ sec	$144{,}000/V_{rel}$	
Deflection about North	$\sigma = 6.5$ sec	$98{,}500/V_{rel}$	
Group 7. Gyro Bias Drifts	$\sigma = 0.01$ deg/hr	∞	Ref. 9
Group 8. Gyro Mass Unbalances	$\sigma = 0.015$ deg/hr/g	∞	Ref. 9
Group 9. Gyro Anisoelasticity	$\sigma = 0.005$ deg/hr/g^2	∞	Ref. 9
III. NON-ESTIMATED, EXTERNAL-AID RELATED STATES			
Group 10. DME Bias Errors	$\sigma = 295$ ft	∞	Ref. 9
Group 11. DME Scale Factor Errors	$\sigma = 100$ ppm	3600	Ref. 13
Group 12. Baro Altimeter Errors			
Bias	$\sigma = 100$ ft	∞	Ref. 3
Markov	$\sigma = 20$ ft	100	
Scale Factor	$\sigma = 0.03$	∞	Ref. 14
Static Defect	$\sigma = 1.52 \times 10^{-4}$ ft/V$^2_{rel}$	∞	
Group 13. ILS Bias Errors			see text
Localizer	$\sigma = 0.5$ mrad	∞	
Glide Slope	$\sigma = 0.5$ mrad	∞	
Group 14. ILS Second Order Markov Errors			Ref. 9
Localizer	see Eq. (3.1-44)	1.5*	
Glide Slope	see Eq. (3.1-45)	1.5*	
Group 15. Radar Altimeter Errors			see text
Bias	$\sigma = 1$ ft	∞	
Scale Factor	$\sigma = 0.025$	∞	
Group 16. DME Survey Errors	$\sigma = 1$ ft	∞	Ref. 15
Group 17. ILS Survey Errors	$\sigma = 1$ ft	∞	Ref. 15

*These are values for τ_{LCL} and τ_{GLS} in Eq. (3.1-27)

phase. In the "Baseline Error Budget" initial position, velocity and alignment errors are taken into account implicitly by proper treatment of accelerometer (Groups 2, 3, 4, 5)and gyro (Groups 7, 8, 9) errors. This is done by inserting the contributions to the initial errors of individual error sources, along with the error sources themselves. These contributions are taken from the "1 sigma error tables" of Ref. 7.

The most convenient way to express the effect of IMU quantization errors is in terms of the forcing function Q_S of the velocity estimation error variances between updates. The value given in Table 3.1-2 is based on the following typical values taken from Ref. 8, describing a current KT-70 application.

$$\text{One } \Delta V \text{ pulse} = 1 \text{ cm/sec}$$
$$\text{Navigation cycle time} = 0.2 \text{ sec.}$$

Assuming that each ΔV count has a random error selected from a uniform distribution ranging from -0.5 cm/sec to +0.5 cm/sec, the rms error is

$$\sigma_{\Delta V} = 1/\sqrt{12} \text{ cm/sec}$$
$$= 0.00945 \text{ ft/sec}$$

Assuming, further, that successive errors are uncorrelated, the addition of five such errors per second causes a navigation error growth rate of

$$Q_{S_{ii}} = 5(0.00945)^2 \quad (i = 4, 5, 6)$$
$$= 4.48 \times 10^{-4} \text{ (ft/sec)}^2/\text{sec}$$

as given in the table.

Table 3.1-2 does not list values for some of the Group 1

(estimated) first-order markov states, which are included in the truth model mathematical structure. These are the gyro, accelerometer, DME and baro altimeter first-order states. The error budget given in Section 5.1 is based on the assumption the gyro and accelerometer errors are random constants, as assumed in Ref. 7 and for Groups 2, 3, 4, 5, 7, 8 and 9, and that DME and baro altimeter errors are represented by a more complicated structure, as in Groups 10, 11, 12 and 16.

More complicated models are also used to represent ILS and radar altimeter errors, as in Groups 13, 14, 15 and 17. However, Group 1 states are included in Table 3.1-2 for these categories since the filter models are thought to be equally valid--results based on alternative models are given in Section 5.1. The filter model for the radar altimeter correlated error takes the rms value to be the following function of altitude (units in feet):

$$\sigma_{RA} = \begin{cases} 0.05\ \text{Alt} & (\text{Alt} > 500) \\ 0.02\ \text{Alt} & (500 \geq \text{Alt} > 100) \\ 2.0 & (100 \geq \text{Alt}) \end{cases} \qquad (3.1\text{-}43)$$

The filter models for the ILS correlated errors are based on (σ in milliradians, ρ in feet)

$$\sigma_{LCL} = \begin{cases} 5.6 & (\rho > 27300) \\ 1.4 + 4.2\left(\dfrac{\rho - 3500}{23800}\right) & (27300 \geq \rho > 3500) \\ 1.4 & (3500 > \rho) \end{cases} \qquad (3.1\text{-}44)$$

$$\sigma_{GLS} = \begin{cases} 2.5 & (\rho > 27300) \\ 1.4 + 1.1 \left(\frac{\rho - 3500}{23800}\right) & (27300 \geq \rho > 3500) \\ 1.4 & (3500 \geq \rho) \end{cases} \qquad (3.1\text{-}45)$$

where ρ is the slant range from the antenna in question to the vehicle.

Gravity deflections and anomalies are adequately modeled as first-order markov processes (Ref. 12) with fixed correlation distances. These are converted to equivalent correlation times by dividing by earth relative velocity, as shown in Table 3.1-2, Group 6.

DME correlated errors are separated into bias, scale factor and survey errors -- Groups 10, 11 and 16, respectively. The bias components represent the combined errors in calibrating both the airborne and ground equipment. The scale factor components represent the inaccuracies in calibrating the index of refraction. Values ranging from 10 parts per million to 100 parts per million have been mentioned in the literature, varying with the extent to which knowledge of local atmospheric conditions and measurement geometry is used in the calibration procedure. Survey errors represent inaccuracies in knowledge of the ground transponder locations relative to the runway. Since, in this case, the devices are nearby, small survey errors are expected.

Baro Altimeter correlated errors (Group 12) are separated into bias, markov, scale factor and static defect components. Values for the bias and markov components are taken from Ref. 3, which treats a baro-inertial-transponder system involving overflight of a transponder. In that case (the CLASS filter evaluation study) it was found to be important to include the markov state to account for moderately rapid changes in local weather conditions. Values for the scale factor and static defect

components are taken from Ref. 14, which discussed them in the context of of the Shuttle landing problem.

It is not possible to cite references for the values used to represent ILS bias errors (Group 13) and radar altimeter bias and scale factor error (Group 15). These components were included simply to gain insight into the problem -- that is, to discover the effect of such error sources, should they exist. The ILS second-order markov errors (Group 14) are modeled using the same rms values as given for the first-order components (Eqs. (3.1-44) and (3.1-45)). The process noise elements driving these states are computed using

$$Q_{S_{i,i}} = 4\sigma_i^2/\tau_i$$

$$Q_{S_{i,i+1}} = Q_{S_{i+1,i}} = 4\sigma_i^2$$

$$Q_{S_{i+1,i+1}} = 4\sigma_i^2\tau_i \qquad (3.1\text{-}46)$$

The data given in this section, together with the equations given in the previous section, completely define the System A truth model.

3.2 SYSTEM B TRUTH MODEL

The hardware elements of System B are the same as those of System A; namely, a KT-70 IMU, a computer and the equipment needed for six external measurements: range to two DME stations, baro altitude, radar altitude and ILS localizer and glide-slope measurements. The ground station locations and the specific measurement sequence are given in Section 2.

The computer navigation program includes a 6-state Kalman filter called herein the MIT-type filter. The filter states and algorithms are defined in detail in Section 4.2 and Ref. 6.

3.2.1 States and Error Sources

The truth model states and other error sources used in evaluating System B are listed in Table 3.2-1, which divides them into three major categories:

- The six estimated states (position and velocity errors), platform misalignments and uncorrelated measurement and process noises.
- Non-estimated error source states related to the inertial system.
- Non-estimated states related to the external aids.

Error budget results corresponding to the first category above are generated using a 9-dimensional truth model structure (F_S, H_S), whose first six states correspond exactly to the 6-dimensional filter error model structure (F_F, H_F). Results corresponding to the other two categories are generated using a higher dimensional model, which contains the basic 9-dimensional structure plus other states representing time-correlated error sources. These additional error sources are divided into 17 groups as indicated in Table 3.2-1. The group numbering system follows that used in the System A evaluation, and is used in the Baseline Error Budget table in Section 5.2 and in the detailed results tabulated in Appendix C.

TABLE 3.2-1

SYSTEM B TRUTH MODEL STATES AND ERROR SOURCES

Error Source Names	Number of States	Number of Error Sources
I. ESTIMATES STATES, MISALIGNMENTS AND UNCORRELATED NOISES (Group 1)		
Position Errors	3	3
Velocity Errors	3	3
Platform Misalignments	3	3
Uncorrelated Measurement Noise		
2 DMEs	-	2
Baro and Radar Altimeters	-	2
ILS Localizer and Glide Slope	-	2
INS Quantization Noise	-	3
II. NON-ESTIMATED, IMU-RELATED STATES		
Group 2. Accelerometer True Biases	3	3
Group 3. Accelerometer Constant Scale Factor Errors	3	3
Group 4. Accelerometer Misalignments	6	6
Group 5. Accelerometer Non-linearities	3	3
Group 6. Gravitational Deflection and Anomalies	3	3
Group 7. Gyro True Bias Drifts	3	3
Group 8. Gyro Mass Unbalances	6	6
Group 9. Gyro Anisoelasticity	3	3

TABLE 3.2-1 (Continued)

SYSTEM B TRUTH MODEL STATES AND ERROR SOURCES

Error Source Names	Number of States	Number of Error Sources
III. NON-ESTIMATED, EXTERNAL-AID RELATED STATES		
Group 10. DME Bias Errors	2	2
Group 11. DME Scale Factor Errors	2	2
Group 12. Baro Altimeter Errors		
Bias	1	1
Scale Factor	1	1
First-Order Markov	1	1
Static Defect	1	1
Group 13. ILS Bias Errors		
Localizer	1	1
Glide Slope	1	1
Group 14. ILS Second-Order Markov Errors		
Localizer	2	1
Glide Slope	2	1
Group 15. Radar Altimeter Errors		
Scale Factor Error	1	1
Bias Error	1	1
First-Order Markov	1	1
Group 16. DME Survey Errors	6	6
Group 17. ILS Survey Errors	6	6
Group 18. ILS First-Order Markov Errors		
Localizer	1	1
Glide Slope	1	1
Totals	70	77

3.2.2 Truth Model Equations

The System B truth model requires a 6 × 6 filter dynamics matrix, F_F, and a 70 × 70 system dynamics matrix, F_S. The filter is mechanized to handle external data as a sequence of scalar measurements. As in System A there are six-distinct filter measurement matrices, H_{F_1} through H_{F_6} -- each is a six dimensional row vector. The six corresponding system measurement matrices, H_{S_1} through H_{S_6}, are 70-dimensional row vectors.

Figure 3.2-1 presents the overall structure of the F_S and H_S matrices for System B. The upper left partition of F_S is the 9 × 9 matrix, $F_{1,1}$, whose elements define the dynamic interaction between the Group 1 error states. The upper left 6 × 6 partition of $F_{1,1}$ is identically equal to the filter matrix, F_F. The horizontal row of sub-matrices, $F_{1,2}$ through $F_{1,9}$, define the effects of the IMU-related error sources (Groups 2-9) on the velocity errors (states 4-6) and the platform misalignments (states 7-9). The sub-matrices along the main diagonal, $F_{2,2}$ through $F_{18,18}$, define the dynamics of all correlated error sources. The six system measurement matrices (row vectors) are outlined in the lower half of Fig. 3.2-1. In each case the first six elements are the same as those of the corresponding filter measurement matrix. Other non-zero sub-matrices, $H_{i,j}$, define the effects of the correlated error sources (Group j) in question of the measurement error (δz_i) in question.

The sub-matrices, $F_{1,1}$, $F_{15,15}$, $F_{18,18}$, $H_{5,15}$, $H_{4,18}$ and $H_{6,18}$ are defined in detail below. All of the others are exactly the same as in System A, and are defined in Section 3.1.2.

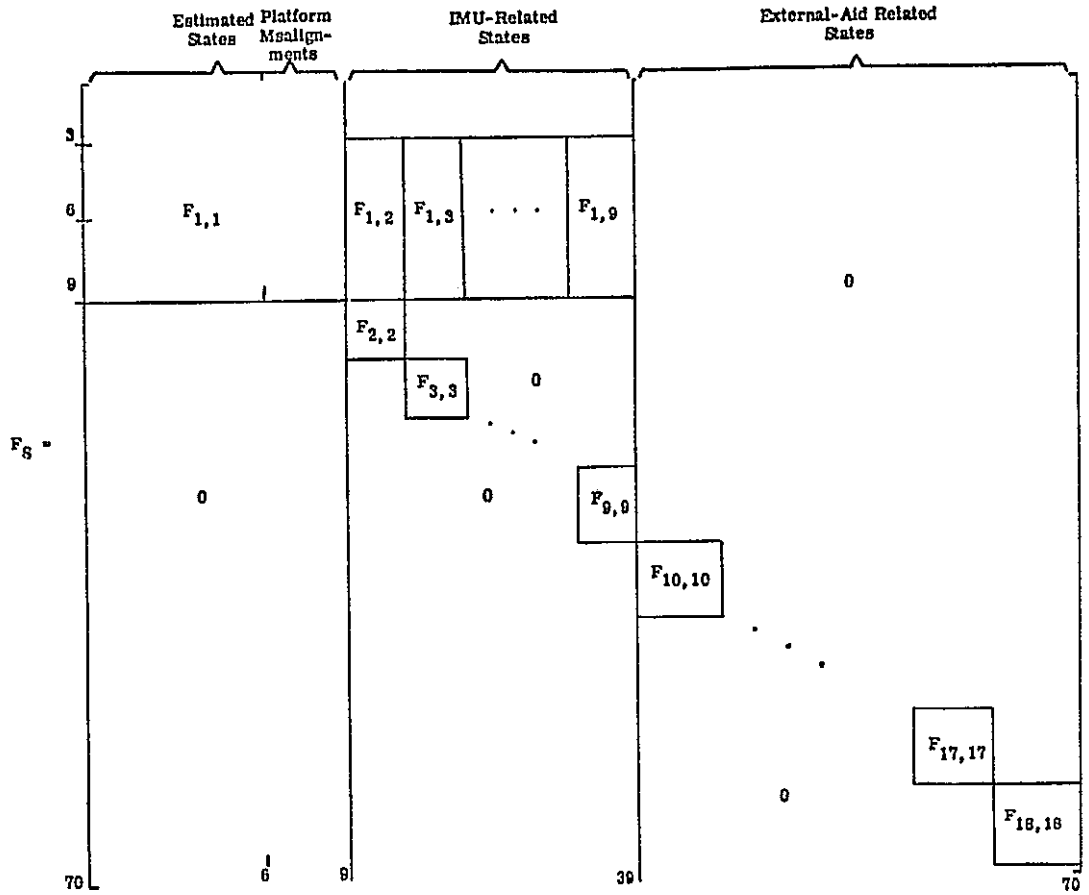

a) State Dynamics Matrix

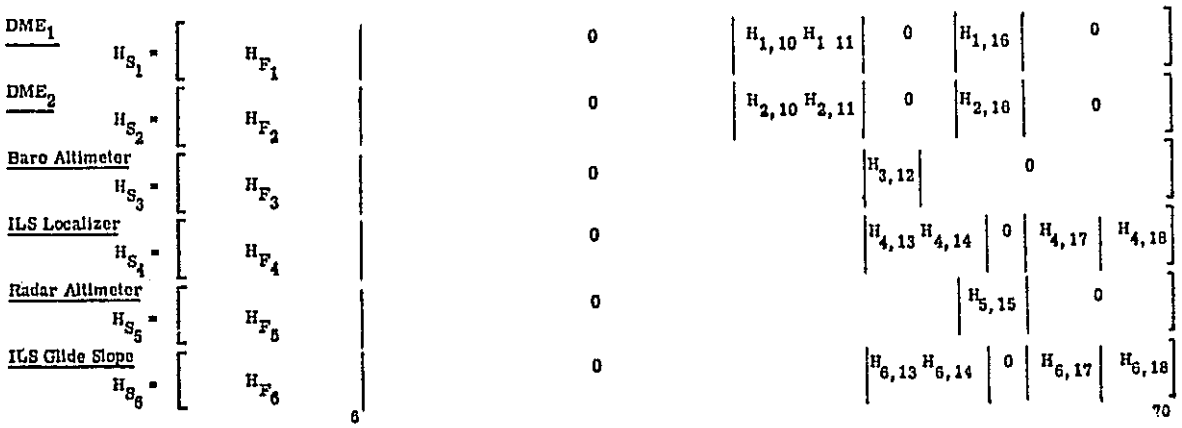

b) Measurement Matrices

Figure 3.2-1 System B Truth Model Structure

Group 1 — Position, Velocity and Alignment Errors

$$F_{1,1} = \begin{array}{c} \text{Position Errors} \quad \text{Velocity Errors} \quad \text{Misalignments} \\ \left[\begin{array}{c|c|c} 0 & I & 0 \\ \hline G_r & 0 & T_{I/P}\, F_P \\ \hline 0 & 0 & 0 \end{array}\right] \end{array} \tag{3.2-1}$$

where

$$G_r = -\frac{\mu}{r^3}\left[I - \frac{3}{r^2}\,\underline{r}\,\underline{r}^T\right] \tag{3.2-2}$$

μ = gravitational constant

I = 3×3 identity matrix

$\underline{r}$ = position vector (in I frame; see Appendix A)

$$F_P = \begin{bmatrix} 0 & -f_3 & f_2 \\ f_3 & 0 & -f_1 \\ -f_2 & f_1 & 0 \end{bmatrix} \tag{3.2-3}$$

$\begin{pmatrix} f_1 \\ f_2 \\ f_3 \end{pmatrix}$ = specific force vector in the P frame

$T_{I/P}$ = 3 x 3 matrix which transforms vector in the P (platform) frame to the I (navigation error analysis) frame; see Appendix A.

Groups 2-14, 16, 17 — See Section 3.1.2 -- Systems A and B are the same.

Group 15 — Radar Altimeter, (3 states: bias, scale factor, markov). In the System A truth model the markov state is included in Group 1 since it is estimated by the filter.

$$F_{15,15} = \begin{bmatrix} 0 & 0 & 0 \\ 0 & 0 & 0 \\ 0 & 0 & -1/\tau_5 \end{bmatrix}_{3 \times 3} \qquad (3.2\text{-}4)$$

$$H_{5,15} = \begin{bmatrix} 1 & h & 1 \end{bmatrix} \qquad (3.2\text{-}5)$$

Group 18 — ILS First-Order Markov Errors (2 states: 1 localizer, 1 glide slope). In the System A truth model these states are included in group 1 since they are estimated by the filter.

$$F_{18,18} = \begin{bmatrix} -1/\tau_4 & 0 \\ 0 & -1/\tau_6 \end{bmatrix} \tag{3.2-6}$$

$$H_{4,18} = \begin{bmatrix} 1 & 0 \end{bmatrix} \tag{3.2-7}$$

$$H_{6,18} = \begin{bmatrix} 0 & 1 \end{bmatrix} \tag{3.2-8}$$

A Matrix

The 70 x 6 matrix relating the filter states to the truth model states has the form:

$$A = \begin{bmatrix} I_{6 \times 6} \\ \hline 0 \end{bmatrix} \tag{3.2-9}$$

The material of this section, augmented by the definitions of most of the F and H sub-matrices given in Section 3.1.2, completely defines the mathematical structure of the 70-state System B truth model.

3.2.3 Truth Model Data Base

The numerical values assigned to the System B truth model are exactly the same as those given in Table 3.1-2.for System A. The values and expressions, Eq. (3.1-43), (3.1-44) and (3.1-45), given for the radar altimeter, localizer and glide slope first-order markov errors, which are listed under Group 1 in the table, are properly considered part of Groups 15 and 18 in the System B truth model. With these minor book-keeping changes Table 3.1-2 is the System B data base.

3.3 SYSTEM C TRUTH MODEL

The hardware elements of System C include a KT-70 IMU, a computer and the equipment needed for three external measurements: a cycle count indicating the integral of doppler shift over measurement intervals, baro altitude and radar altitude. The ground doppler beacon location is given in Section 2. The computer navigation program includes a 22-state version of the JSC/TRW multi-phase filter. The filter states and algorithms are defined in detail in Section 4.3 and Ref. 10.

3.3.1 States and Error Sources

The truth model states and other error sources used in evaluating System C are listed in Table 3.3-1, which divides them into three major categories:

- The 22 estimated states and uncorrelated measurement and process noises.
- Non-estimated states related tc the inertial system.
- Non-estimated states related to the external aids.

TABLE 3.3-1

SYSTEM C TRUTH MODEL STATES AND ERROR SOURCES

Error Source Names	Number of States	Number of Error Sources
I. ESTIMATED STATES AND UNCORRELATED NOISES (Group 1)		
Position Errors	3	3
Velocity Errors	3	3
Platform Misalignments	3	3
Gyro Drifts (First-Order Markovs)	3	3
Accelerometer Scale Factor Errors (First-Order Markovs)	3	3
Accelerometer "Biases" (First-Order Markovs)	3	3
Correlated Measurement Errors (First-Order Markovs)		
Doppler Rate Bias Errors	2	2
Baro and Radar Altimeters	2	2
Uncorrelated Measurement Noise		
Doppler cycle quantization	-	1
Baro and Radar Altimeters	-	2
INS Quantization Noise	-	3
II. NON-ESTIMATED, IMU-RELATED STATES		
Group 2. Accelerometer True Biases	3	3
Group 3. Accelerometer Constant Scale Factor Errors	3	3
Group 4. Accelerometer Misalignments	6	6
Group 5. Accelerometer Nonlinearities	3	3
Group 6. Gravitational Deflections and Anomalies	3	3
Group 7. Gyro True Bias Drifts	3	3
Group 8. Gyro Mass Unbalances	6	6
Group 9. Gyro Anisoelasticity	3	3

TABLE 3.3-1 (Continued)

SYSTEM C TRUTH MODEL STATES AND ERROR SOURCES

Error Sources Names	Number of States	Number of Error Sources
III. NON-ESTIMATED, EXTERNAL-AID RELATED STATES		
Group 10. Doppler Errors		
Rapid Shift Errors	1	1
Antenna Motion Compensation Error	1	1
Group 12. Baro Altimeter Errors		
Bias	1	1
Scale Factor	1	1
First-Order Markov	1	1
Static Defect	1	1
Group 15. Radar Altimeter Errors		
Scale Factor Error	1	1
Bias Error	1	1
Group 16. Doppler Beacon Survey Errors	3	3
Totals	63	69

Error budget results corresponding to the first category above are generated using a truth model structure (F_S, H_S), which corresponds almost exactly to the filter error model structure (F_F, H_F). Results corresponding to the other two categories are generated using a higher-dimensional truth model, which contains the basic 22-state structure plus other states representing time-correlated error sources not modeled explicitly in the filter design. These additional error sources are divided into 12 groups as indicated in Table 3.3-1. (The group numbering system is consistent with that used in the System A evaluation, and is used in the Baseline Error Budget table in Section 5.3. Groups 11, 13, 14 and 17 have been deleted.)

3.3.2 Truth Model Equations

The System C truth model requires a 22 × 22 filter dynamics matrix, F_F, and a 63 × 63 system dynamics matrix, F_S. The filter mechanization treats external data as a sequence of scalar measurements, rather than as components of vector measurements. Up to three separate scalars may be incorporated at one update time. Therefore, there are three distinct filter measurement matrices, H_{F_1} through H_{F_3} -- each is a 22 dimensional row vector. There are three corresponding system measurement matrices, H_{S_1} through H_{S_3} -- each of these is an 63-dimensional row vector.

Figure 3.3-1 presents the overall structure of the F_S and H_S matrices for System C. The upper-left partition of F_S is the 22 × 22 matrix $F_{1,1}$, whose elements define the dynamic interaction between the Group 1 error states. This sub-matrix of F_S corresponds* to the filter matrix, F_F. The horizontal row of sub-matrices, $F_{1,2}$ through $F_{1,9}$, defines the effects of the non-estimated, IMU-related error sources (Groups 2-9) on the velocity errors (states 4-6) and the platform misalignments (states 7-9). The sub-matrices along the main diagonal, $F_{2,2}$ through $F_{16,16}$, define the dynamics of all non-estimated, correlated error sources. For a group of random constant error sources this sub-matrix is zero. The three system measurement matrices (row vectors) are outlined in the lower half of Fig. 3.3-1. In each case the first 22 elements are the same as those of the corresponding filter measurement matrix. Other non-zero sub-matrices, $H_{i,j}$, define the effects of the correlated error sources (Group j) in question on the measurement error (δz_i) in question.

*$F_{1,1}$ and F_F are identical except for the presence of a 3 × 3 coordinate transformation. See $T_{I/P}$ in Eq. (3.1-1).

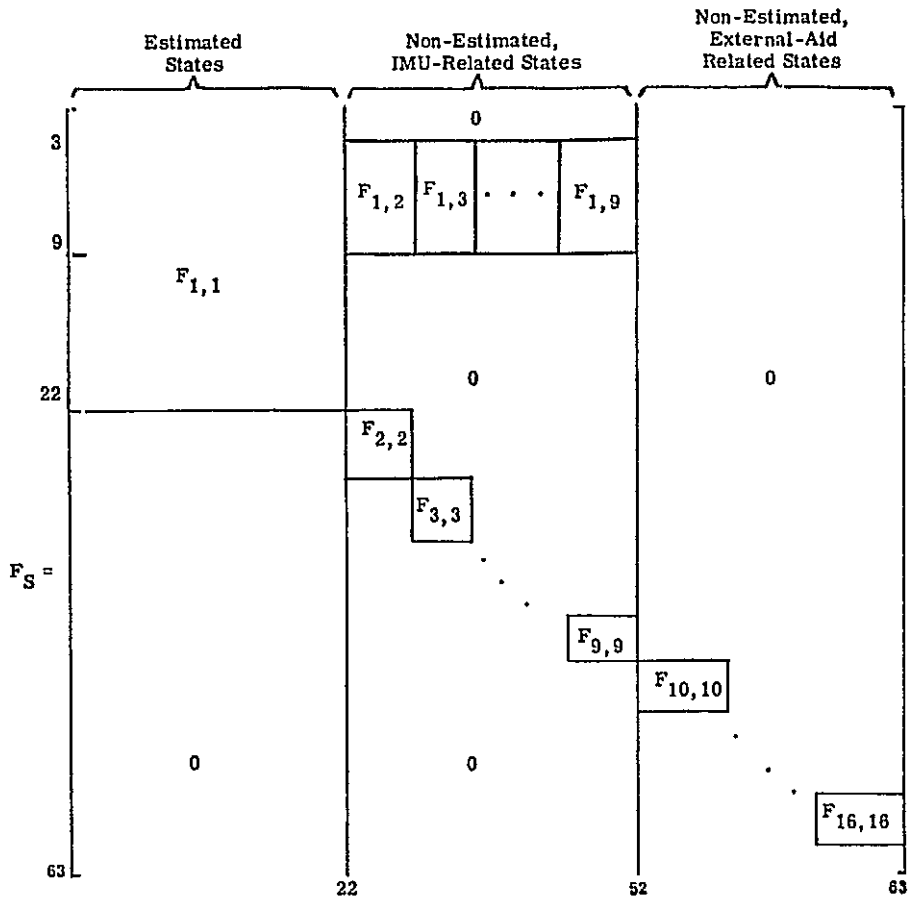

a) State Dynamics Matrix

One-Way Doppler:

$$H_{S_1} = \left[\begin{array}{c|c|c|c|c} H_{F_1} & 0 & H_{1,10} & 0 & H_{1,16} \end{array}\right]$$

Laro Altimeter:

$$H_{S_2} = \left[\begin{array}{c|c|c|c} H_{F_2} & 0 & H_{2,12} & 0 \end{array}\right]$$

Radar Altimeter:

$$H_{S_3} = \left[\begin{array}{c|c|c|c} H_{F_3} & 0 & H_{3,15} & 0 \end{array}\right]$$

(22 | 52 | 63)

b) Measurement Matrices

Figure 3.3-1 System C Truth Model Structure

The sub-matrices, $F_{1,1}$, $F_{10,10}$, $F_{16,16}$, $H_{1,10}$, $H_{1,16}$, $H_{2,12}$ and $H_{3,15}$ are defined in detail below. All of the others are exactly the same as in System A, and are defined in Section 3.1.2.

Group 1 — Estimated States (See also Section 4.3)

$$F_{1,1} = \begin{array}{c|cccccc} & \text{Position Errors} & \text{Velocity Errors} & \text{Misalignments} & \text{Gyro Drift} & \text{Accelerometer Scale Factor} & \text{Accelerometer Bias} \\ 3 & 0 & I & 0 & 0 & 0 & 0 \\ 6 & G_r & 0 & T_{I/P} F_P & 0 & \begin{matrix} f_x & & \\ & f_y & \\ & & f_z \end{matrix} & I \\ 9 & 0 & 0 & 0 & I & 0 & 0 \\ 18 & 0 & & & D_\tau & & \\ 22 & 0 & & & & & \end{array} \qquad \begin{array}{c} \text{Measurement Errors} \\ \\ 0 \\ \\ \\ \end{array} \qquad (3.3\text{-}1)$$

where

$$D_\tau = 13 \times 13 \text{ diagonal matrix with } D_{\tau_{ii}} = -1/\tau_i \qquad (3.3\text{-}2)$$

G_r and the other elements appearing in Eq. (3.3-1) are defined in Eqs. (3.1-3) and (3.1-4).

Groups 2 through 9 - See Section 3.1.2 -- Systems A and C are the same.

Group 10 - Doppler Errors (2 states: rapidly shifting rate bias error and antenna motion compensation error).

$$F_{10,10} = \begin{bmatrix} -1/\tau_r & 0 \\ 0 & -1/\tau_A \end{bmatrix} \qquad (3.3\text{-}3)$$

$$H_{1,10} = [\Delta t \qquad 1] \qquad (3.3\text{-}4)$$

(See discussion of doppler errors in Section 3.3.3).

Group 11 - Not in the System C truth model.

Group 12 - Baro-Altimeter Errors - See Section 3.1.2 -- Systems A and C are the same, except that the measurement sub-matrix is $H_{2,12}$ instead of $H_{3,12}$.

Groups 13 and 14. - Not in the System C truth model.

Groups 15 - Radar Altimeter Errors - See Section 3.1.2 Systems A and C are the same, except that the measurement sub-matrix is $H_{3,15}$ instead of $H_{5,15}$.

Group 16 - Doppler Beacon Survey Errors (3 states: up, east, north).

$$F_{16,16} = [0]_{3\times 3} \tag{3.3-5}$$

$$H_{1,16} = \begin{bmatrix} h_{F_R} & h_{F_C} & h_{F_D} \end{bmatrix} \tag{3.3-6}$$

where h_{F_R}, h_{F_C} and h_{F_D} are the R frame components of a vector defined in the I frame by h_1, h_2, h_3, the first three components of the filter matrix given in Eq. (4.3-6). (Survey errors are input in the R frame.)

A Matrix - The 63 x 22 matrix relating the filter states to the truth model states has the form:

$$A = \begin{bmatrix} A'_{22 \times 22} \\ \hline 0 \end{bmatrix} \tag{3.3-7}$$

where

$$A' = \left[\begin{array}{cc|ccc|c} I_{6\times 6} & & & 0 & & 0 \\ \hline 0 & T_{P/I} & & & & \\ & & T_{P/I} & 0 & 0 & \\ & 0 & 0 & T_{P/I} & 0 & 0 \\ & & 0 & 0 & T_{P/I} & \\ \hline 0 & & & 0 & & I_{4\times 4} \end{array}\right] \tag{3.3-8}$$

The role of the transformation $T_{P/I}$ in Eq. (3.3-8) is discussed at Eq. (3.1-39).

The material of this section, augmented by the definitions of many of the F and H sub-matrices given in Section 3.1.2, completely defines the mathematical structure of the 63-state System C truth model.

3.3.3 Truth Model Data Base

The general discussion of Section 3.1.3, pertaining to the System A data base, applies just as well to System C and is not repeated here. Also, most of the specific error sources, such as gyro and accelerometer errors, IMU quantization, baro altimeter and radar altimeter errors, are modeled the same way again; so those discussions are not repeated either. Table 3.3-2 summarizes the truth model rms values and correlation times used in evaluating System C. As indicated above, most of the values and references are exactly the same as those previously listed in Table 3.1-2. The error sources unique to System C are all associated with the one-way doppler measurements; these are discussed below.

Altogether there are eight error sources associated with doppler measurements in the System C truth model. Three of them correspond directly to error sources modeled in the filter; these three are covered under Group 1 in Table 3.3-2. They are measurement noise (treated as uncorrelated) due to the doppler cycle quantization and the two correlated rate bias errors associated with shifts in the onboard and ground beacon frequency standards. The baseline rms values and correlation times for these processes are taken to be the same as those assumed by the filter. The value given for the onboard rate bias error corresponds to a clock error of 1 part in 10^{10} -- see Ref. 10.

TABLE 3.3-2

SYSTEM C TRUTH MODEL DATA BASE

Error Source	Value	Correlation Time (sec)	Data Source
I. ESTIMATED STATES AND UNCORELATED NOISE (Group 1)			
Initial Condition Errors Position Velocity Misalignment	9 x 9 Covariance Matrix (see text)	—	Ref. 7
IMU Quantization Errors	$Q_{S_{ii}} = 4.48 \times 10^{-4} \frac{(ft/sec)^2}{sec}$ (i = 4, 5, 6 -- see text)	—	Ref. 8
Doppler Cycle Quantization	σ = 0.0357 ft	—	Ref. 10
Baro Altimeter Measurement White Noise	σ = 5 ft	—	Ref. 3
Radar Altimeter Measurement White Noise	σ = 3.28 ft	—	Ref. 11
Doppler Rate Bias Errors Onboard Frequency Standard Ground Frequency Standard	σ = 0.0876 ft/sec σ = 0.0044 ft/sec	800 400	Ref. 10
Radar Altimeter First-Order Markov Error	see Eq. (3.1-43)	4.0	Ref. 11
II. NON-ESTIMATED, IMU-RELATED STATES			
Group 2. Accelerometer Biases	σ = 60 µg	∞	Ref. 9
Group 3. Accelerometer Scale Factor Errors	σ = 34 ppm	∞	Ref. 9
Group 4. Accelerometer Misalignments	σ = 40 $\widehat{sec}$	∞	Ref. 9
Group 5. Accelerometer Nonlinearities	σ = 3.5 $\mu g/g^2$	∞	Ref. 9

TABLE 3.3-2 (Continued)

SYSTEM C TRUTH MODEL DATA BASE

Error Source	Value	Correlation Time (sec)	Data Source
II. (Continued)			
Group 6. Gravity			
Anomaly	$\sigma = 13.3 \times 10^{-4}$ ft/sec^2	492,000/Vrel	Ref. 12
Deflection about East	$\sigma = 5.1$ sec	144,000/Vrel	
Deflection about North	$\sigma = 6.5$ sec	98,500/Vrel	
Group 7. Gyro Bias Drifts	$\sigma = 0.01$ deg/hr	∞	Ref. 9
Group 8. Gyro Mass Unbalances	$\sigma = 0.015$ deg/hr/g	∞	Ref. 9
Group 9. Gyro Anisoelasticity	$\sigma = 0.005$ deg/hr/g^2	∞	Ref. 9
III. NON-ESTIMATED, EXTERNAL-AID RELATED STATES			
Group 10. Doppler Errors			
Fast Varying Frequency Standard Error	$\sigma = 0.01$ ft/sec	30	See text
Antenna Motion Compensation Error	$p\ell = 0.5$ ft, see Eq. (3.3-9)	Δt	
Group 12. Baro Altimeter Errors			
Bias	$\sigma = 100$ ft	∞	Ref. 3
Markov	$\sigma = 20$ ft	100	
Scale Factor	$\sigma = 0.03$	∞	Ref. 14
Static Defect	$\sigma = 1.52 \times 10^{-4}$ ft/V$^2_{rel}$	∞	
Group 15. Radar Altimeter Errors			
Bias	$\sigma = 1$ ft	∞	See text
Scale Factor	$\sigma = 0.025$	∞	
Group 16. Doppler Beacon Survey Errors	$\sigma = 1$ ft	∞	Ref. 15

Two other doppler measurement error sources are covered under Group 10 in Table 3.3-2. The first is a rapidly-varying rate bias error assigned a correlation time of 30 seconds. No reference can be cited for this error source. It was included to gain insight into the problem -- that is, to discover the effect of such an error source should it exist. (We know, for example, that a crystal frequency source might be subject to g-sensitive shifts. On the other hand, the rubidium device suggested in Ref. 10 is not expected to be subject to such errors.) The other source under Group 10 represents an error in compensating for antenna motion due to vehicle angular motion over the doppler measurement intervals. It is clear that compensation (via software) is required to account for the fact that the onboard doppler antenna is not located at the IMU, and will not experience the same relative motion with respect to the ground antenna whenever there is angular motion during a measurement interval. The inputs to the compensation calculation must include a pre-stored moment arm value, gimbal angle changes over the interval and a description of the geometrical relationship between the relative range vector (to the ground beacon) and the IMU axes. For error analysis purposes we use the following expression for the forcing function of this doppler measurement error source.

$$Q_S = (p\ell)^2 \Delta\theta_T^2 / \Delta t \qquad (3.3\text{-}9)$$

where

p = a percentage error in compensation

ℓ = IMU-antenna moment arm

Δt = measurement interval

$$\Delta\theta_T^2 = \Delta\theta_1^2 + \Delta\theta_2^2 + \Delta\theta_3^2 \qquad (3.3\text{-}10)$$

$\Delta\theta_1$, $\Delta\theta_2$, $\Delta\theta_3$ = the three gimbal angle changes during the interval, Δt.

The value, $p\ell = 0.5$ ft, given in Table 3.3-2 corresponds, for example, to a compensation error of 5 percent with a 10 ft moment arm. With the correlation time chosen as Δt, the effect of this model is to produce an rms error of $p\ell\Delta\theta_T$ for the first time interval after the beginning of an angular motion. If the motion continues over successive intervals, the successive errors will be correlated to some extent. After the motion ceases the error will die out quickly.

Finally, three survey errors, representing inaccurate knowledge of the ground beacon location relative to the runway, are included in Group 16. Since the devices are nearby, small survey errors are expected.

The data given in this section, together with that given in Section 3.1, completely define the System C truth model.

3.4 SYSTEM D TRUTH MODEL

The hardware elements of System D include a KT-70 IMU, a computer and the equipment needed for five external measurements: range and azimuth to a single VOR/DME station, baro altitude, radar altitude and ILS localizer measurements. The ground station locations and the specific measurement sequence are given in Section 2. The computer navigation program includes a 23-state version of the JSC/TRW multi-phase Kalman filter. The filter states and algorithms are defined in detail in Section 4.4 and Ref. 4.

Initial condition errors are treated somewhat differently in the System D evaluation than they were in the preceeding three cases. The difference arises from the assumption, for System D, that drag acceleration is used to update the navigation state prior to the "initial" point at an altitude of 130,000 feet. This has no effect on the structure of the truth model, but does alter the details of the data base, as discussed in Section 3.4.3.

3.4.1 States and Error Sources

The truth model states and other error sources used in evaluating System D are listed in Table 3.4-1, which divides them into three major categories:

- The 23 estimated states and uncorrelated measurement and process noises.
- Non-estimated states related to the inertial system.
- Non-estimated states related to the external aids.

Error budget results corresponding to the first category above are generated using a truth model structure (F_S, H_S), which corresponds almost exactly to the filter error model structure (F_F, H_F). Results corresponding to the other two categories are generated using a higher-dimensional truth model, which contains the basic 23-state structure plus other states representing time-correlated error sources not modeled explicitly in the filter design. These additional error sources are divided into 17 groups as indicated in Table 3.4-1. (The same group numbers are

TABLE 3.4-1

SYSTEM D TRUTH MODEL STATES AND ERROR SOURCES

Error Source Names	Number of States	Number of Error Sources
I. ESTIMATED STATES AND UNCORRELATED NOISES (Group 1)		
Position Errors	3	3
Velocity Errors	3	3
Platform Misalignments	3	3
Gyro Drifts (First-Order Markovs)	3	3
Accelerometer Scale Factor Errors (First-Order Markovs)	3	3
Accelerometer 'Biases' (First-Order Markovs)	3	3
Correlated Measurement Errors (First-Order Markovs)		
DME	1	1
VOR	1	1
Baro and Radar Altimeters	2	2
ILS Localizer	1	1
Uncorrelated Measurement Noise		
DME	-	1
VOR	-	1
Baro and Radar Altimeters	-	2
ILS Localizer	-	1
INS Quantization Noise	-	3
II. NON-ESTIMATED, IMU-RELATED STATES		
Group 2. Accelerometer True Biases	3	3
Group 3. Accelerometer Constant Scale Factor Errors	3	3
Group 4. Accelerometer Misalignments	6	6
Group 5. Accelerometer Nonlinearities	3	3
Group 6. Gravitational Deflections and Anomalies	3	3
Group 7. Gyro True Bias Drifts	3	3
Group 8. Gyro Mass Unbalances	6	6
Group 9. Gyro Anisoelasticity	3	3

TABLE 3.4-1 (Continued)

SYSTEM D TRUTH MODEL STATES AND ERROR SOURCES

Error Sources Names	Number of States	Number of Error Sources
III. NOT-ESTIMATED, EXTERNAL-AID RELATED STATES		
Group 10. DME Bias Error	1	1
Group 11. DME Scale Factor Error	1	1
Group 12. Baro Altimeter Errors		
Bias	1	1
Scale Factor	1	1
First-Order Markov	1	1
Static Defect	1	1
Group 13. ILS Bias Error		
Localizer	1	1
Group 14. ILS Second-Order Markov Error		
Localizer	2	1
Group 15. Radar Altimeter Errors		
Scale Factor Error	1	1
Bias Error	1	1
Group 16. VOR/DME Survey Errors	6	6
Group 17. ILS Survey Errors	3	3
Group 19. VOR Bias Error	1	1
Totals	74	81

used in the Baseline Error Budget table in Section 5.4 and in the detailed results tabulated in Appendix C. There is no group 18 in the System D truth model.)

3.4.2 Truth Model Equations

The System D truth model requires a 23 x 23 filter dynamics matrix, F_F, and a 74 x 74 system dynamics matrix, F_S. The filter mechanization treats external data as a sequence of scalar measurements, rather than as components of vector measurements. Up to five separate scalars may be incorporated at one update time. Therefore, there are five distinct filter measurement matrices, H_{F_1} through H_{F_5} -- each is a 23-dimensional row vector. There are five corresponding system measurement matrices, H_{S_1} through H_{S_5} -- each of these is a 74-dimensional row vector.

Figure 3.4-1 presents the overall structure of the F_S and H_S matrices for System D. The upper-left partition of F_S is the 23 x 23 matrix $F_{1,1}$, whose elements define the dynamic interaction between the Group 1 error states. This sub-matrix of F_S corresponds* to the filter matrix, F_F. The horizontal row of sub-matrices, $F_{1,2}$ through $F_{1,9}$, define the effects of the non-estimated, IMU-related error sources (Groups 2-9) on the velocity errors (states 4-6) and the platform misalignments (states 7-9). The sub-matrices along the main diagonal, $F_{2,2}$ through $F_{19,19}$, define the dynamics of all non-estimated, correlated error sources. For a group of random-constant error sources this sub-matrix is zero. The six system measurement matrices (row vectors) are outlined in the lower half of Fig. 3.4-1. In each case the first 23 elements are the same as those of the corresponding filter measurement matrix. Other non-zero sub-matrices, $H_{i,j}$, define the effects of the correlated error sources (Group j) in question on the measurement error (δz_i) in question.

*$F_{1,1}$ and F_F are identical except for the presence of a 3 x 3 coordinate transformation. See $T_{I/P}$ in Eq. (3.1-1).

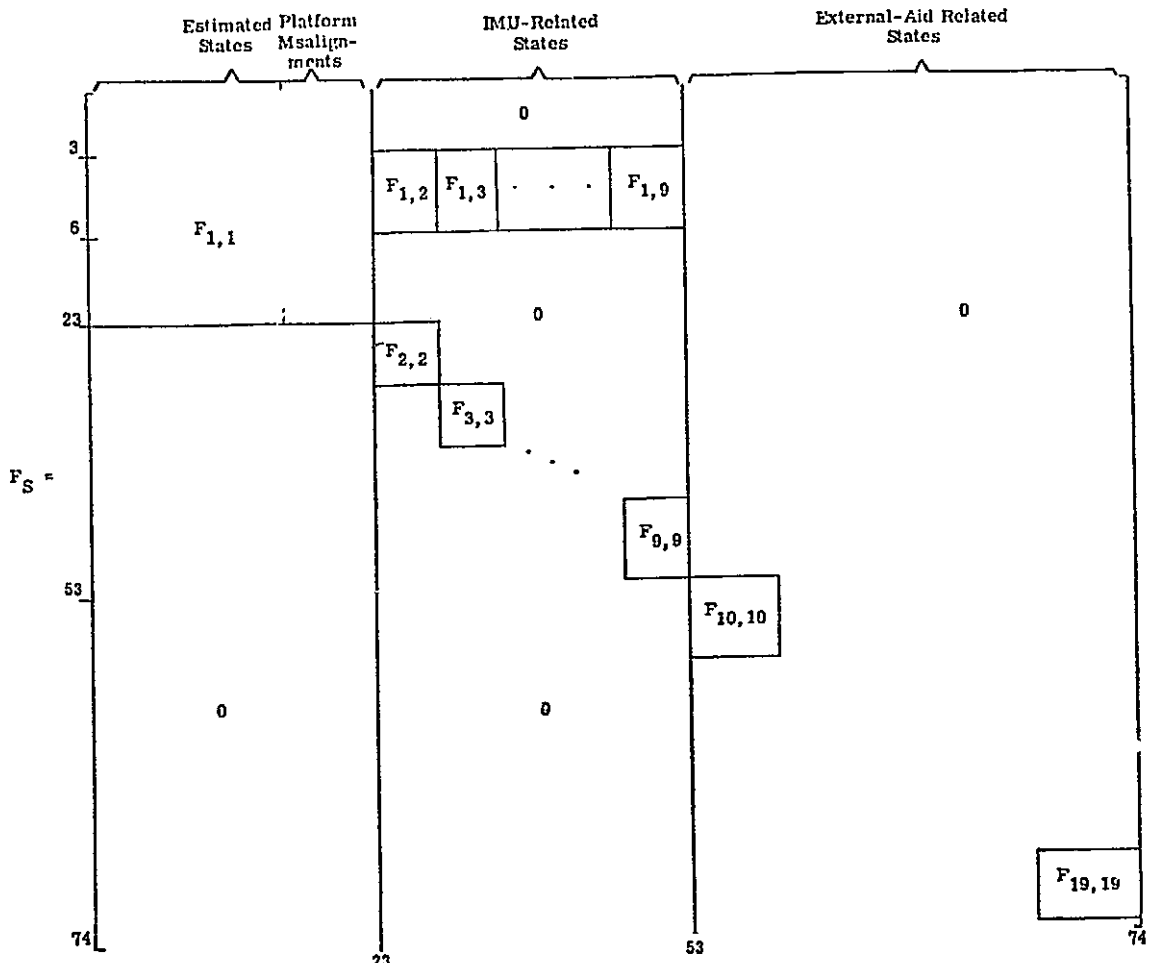

a) State Dynamics Matrix

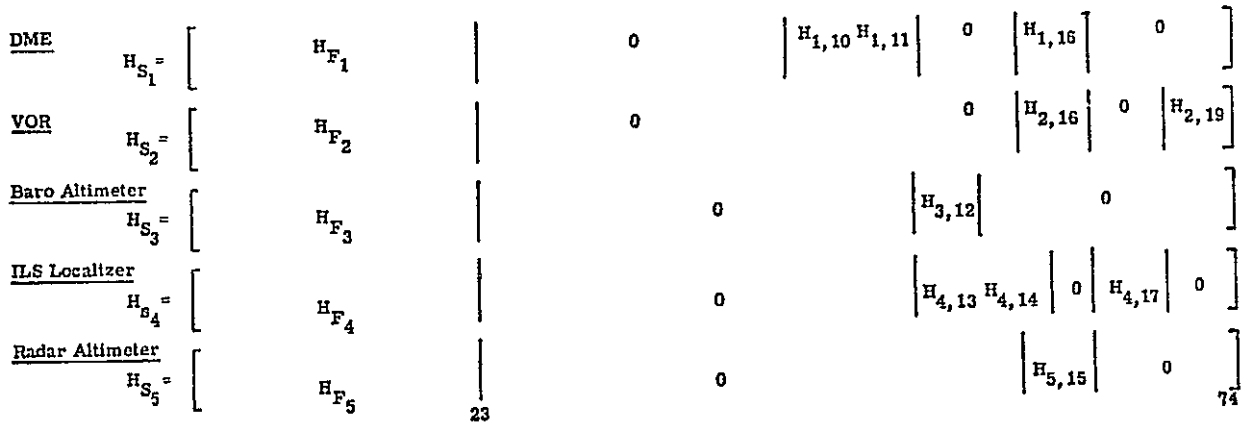

b) Measurement Matrices

Figure 3.4-1 System D Truth Model Structure

The sub-matrix $F_{1,1}$ is identical to that given by Eq. (3.1-1) for System A except that the 24th row and column are omitted -- since there is no glide slope measurement in System D. The sub-matrices $F_{10,10}$, $F_{11,11}$, $F_{13,13}$, $F_{14,14}$, $F_{16,16}$, $F_{17,17}$, $F_{19,19}$, $H_{1,10}$, $H_{1,11}$, $H_{1,16}$, $H_{2,16}$, $H_{2,19}$, $H_{4,13}$, $H_{4,14}$, $H_{4,17}$, $H_{5,16}$, and $H_{5,19}$ are defined in detail below. All of the others are exactly the same as in System A, and are defined in Section 3.1-2.

Groups 2-9, 12, 15 — See Section 3.1-2 -- Systems A and D are the same.

Group 10 — DME Bias Error (1 station, 1 state)

$$F_{10,10} = 0 \tag{3.4-1}$$

$$H_{1,10} = 1 \tag{3.4-2}$$

Group 11 — DME Scale Factor Error (1 station, 1 state)

$$F_{11,11} = -1/\tau_{sf} \tag{3.4-3}$$

$$H_{1,11} = \rho_1 \tag{3.4-4}$$

where ρ_1 is the distance from the vehicle to the DME station.

Group 13 — ILS Localizer Bias (1 state)

$$F_{13,13} = 0 \tag{3.4-5}$$

$$H_{4,13} = 1 \tag{3.4-6}$$

Group 14 — ILS Localizer Second-Order Markov Error (2 states)

$$F_{14,14} = \begin{bmatrix} -1/\tau_{LCL} & -1/\tau_{LCL}^2 \\ 0 & -1/\tau_{LCL} \end{bmatrix}_{2 \times 2} \tag{3.4-7}$$

$$H_{4,14} = \begin{bmatrix} 1 & 0 \end{bmatrix} \tag{3.4-8}$$

Group 16 — DME and VOR Survey Errors (2 antennae, 3 components each)

$$F_{16,16} = [0]_{6 \times 6} \tag{3.4-9}$$

$$H_{1,16} = \begin{bmatrix} -\rho_{1_R}/\rho_1 & -\rho_{1_C}/\rho_1 & -\rho_{1_D}/\rho_1 & 0 & 0 & 0 \end{bmatrix} \tag{3.4-10}$$

$$H_{2,16} = \begin{bmatrix} 0 & 0 & 0 & -u_{2_R}/\rho_{s_1} & -u_{2_C}/\rho_{s_1} & -u_{2_D}/\rho_{s_1} \end{bmatrix} \tag{3.4-11}$$

where

$\underline{\rho}_1$ = relative position vector: VOR/DME station to vehicle; see Fig. 3.4-2.

$\rho_{1_R}, \rho_{1_C}, \rho_{1_D}$ = components of $\underline{\rho}_1$ in R frame

$u_{2_R}, u_{2_C}, u_{2_D}$ = components of unit vector $\underline{u}_2$, perpendicular to $\underline{\rho}_1$ and lying in horizontal plane; see Fig. 3.4-2.

ρ_{s_1} = projection of $\underline{\rho}_1$ onto horizontal plane.

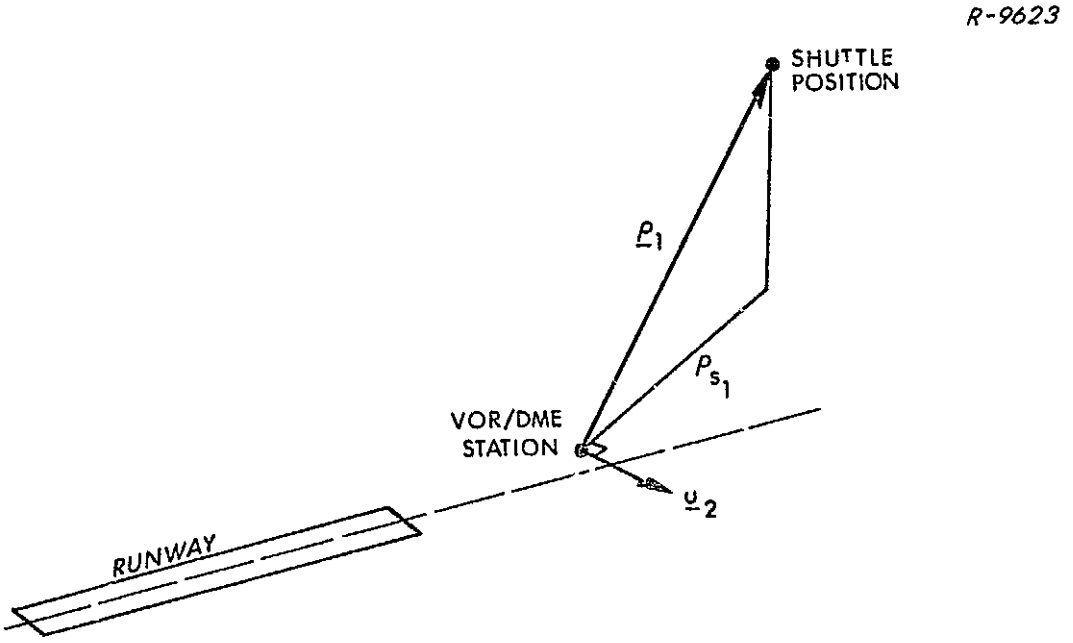

Figure 3.4-2 VOR/DME - Shuttle Geometry

Group 17 — ILS Localizer Survey Errors (3 components)

$$F_{17,17} = [0]_{3 \times 3} \tag{3.4-12}$$

$$H_{4,17} = \begin{bmatrix} -u_{e_{R/\rho_{s_4}}} & -u_{e_{C/\rho_{s_4}}} & -u_{e_{D/\rho_{s_4}}} & 0 & 0 & 0 \end{bmatrix} \tag{3.4-13}$$

where

$u_{e_R}, u_{e_C}, u_{e_D}$ = components of cross-runway unit vector; see Fig. 3.1-3.

ρ_{s_4} = projection onto horizontal plane of $\underline{\rho}_4$ the relative position vector from localizer antenna to the vehicle; see Fig. 3.1-2.

Group 19 — VOR Bias (1 state)

$$F_{19,19} = 0 \tag{3.4-14}$$

$$H_{2,19} = 1 \tag{3.4-15}$$

A Matrix

The 74 x 23 matrix relating filter states to the truth model states has the form:

$$A = \begin{bmatrix} A'_{23 \times 23} \\ \hline 0 \end{bmatrix} \tag{3.4-16}$$

where A' has the same structure given in Eq. (3.1-39) for System A, except that the lower-right-hand corner is a 5 x 5 identity matrix rather than 6 x 6.

The material of this section, augmented by the definitions of common F and H sub-matrices given in Section 3.1.2, completely defines the mathematical structure of the 74-state System D truth model.

3.4.3 Truth Model Data Base

The general discussion of Section 3.1.3, pertaining to the System A data base, applies just as well to System D and is not repeated here. Also, most of the specific error sources, including IMU errors, baro altimeter, radar altimeter, DME and localizer errors are modeled the same way again. Table 3.1-1 represents, therefore, most of the System D truth model data base. There are two ways in which the System D data base is different: in its treatment of initial condition errors and in the inclusion of VOR errors; these are discussed below.

As mentioned earlier it is assumed, for the System D evaluation, that drag-updating is employed prior to end-of-blackout to improve the navigation state estimate. This assumption has significant effects on both the initial filter covariance and the initial truth model errors. (The former is discussed in Section 4.4.) A recent study* at NASA/JSC, involving 30 monte carlo runs through the black-out portion of a typical entry profile, produced a 6 x 6 covariance matrix representing the position and velocity error statistics at end-of-blackout -- assuming the use of a drag-update scheme as proposed by Lear in Ref.16. This covariance matrix represents the combined effects of IMU initial errors (at 400,000 ft, taken from Ref. 7), measurement noise and uncertainties in vehicle aerodynamic coefficients; it is one of the inputs used to generate the System D error budget given in Section 5.4. The same NASA study generated a measure of the effect of a non-standard atmosphere profile by inserting such a profile and holding it constant throughout the 30 monte carlo runs. The result was a non-zero mean vector of position

*Summary results of the study were communicated to TASC by Messers. P. Pixley and P. Michell of NASA.

and velocity errors. This vector is another input to the System D error budget calculations. The initial errors at 400,000 ft, which were used in the study cited, correspond to the one-rev mission analyzed in Ref. 7 with a KT-70 IMU and pre-launch alignment based on accelerometer leveling and optics azimuth alignment. In order to be consistent with the above we have treated the accelerometer errors (Groups 2-5) and gyro errors (Groups 7-9) by inserting the contributions to initial misalignments at 130,000 ft of individual error sources, along with the error sources themselves. These contributions are taken from the "1 σ Error Tables" (Table D-III-b) of Ref. 7. One additional error source is the initial pre-launch azimuth misalignment -- this did not appear in the System A, B or C evaluations because pre-launch gyrocompassing was assumed.

A drawback of the procedure outlined above is that certain initial correlations, such as between position errors and misalignments at 130,000 ft, are not properly accounted for. (In fact there is no way to deduce them based on the information available to us.) Fortunately, however, it happens that the missing correlations cannot have major effects in the case studied. This is shown by the result that the final contributions at touchdown of all initial position and velocity errors are small (Table 5.4-1). Thus, whether or not these quantities are highly correlated with other error sources is of little consequence. (Note that this result may not be the case for every system studied.)

Table 3.4-2 summarizes the features of the System D data base which are different from the System A data base given in Table 3.1-1. Altogether there are six error sources associated with VOR measurements in the System D truth model. Two of them correspond

TABLE 3.4-2

SYSTEM D TRUTH MODEL DATA BASE
(WHERE DIFFERENT FROM SYSTEM A)

Error Source	Value	Correlation Time (sec)	Date Source
Group 1			
Initial Condition Errors			
Position, Velocity	6 x 6 Covariance Matrix, Mean Error Vector	—	see text
Azimuth Misalignment	60 sec	—	Ref. 7
VOR Measurement White Noise	8.5 mrad	—	Ref. 5
VOR First-Order Markov Error	18.67 mrad	800	Ref. 5
Group 16			
VOR Survey Errors	1 ft	—	Ref.15
Group 19			
VOR Bias Error	5.0 mrad	—	Ref. 9
Groups 1, 13, 14, 17			
Glide Slope Errors Omitted	—	—	—

directly to error sources modeled in the filter. These are an exponentially correlated error and an uncorrelated measurement noise; they appear under Group 1 in Table 3.4-1. Three error sources not modeled by the filter are the three VOR survey error components listed under Group 16. These are treated as distinct from the DME survey errors, since different antennae are involved. The rms magnitude is taken to be one foot per component, as assumed for all survey errors considered in this report.

Finally, there is a state representing a VOR bias error. This is not modeled by the filter and is listed as Group 19 in the table.

The data and equations given in this section, augmented by that given in Section 3.1, completely define the System D truth model.

Summary – The four system truth models have been presented using a consistent format. The truth model data bases for Systems A and B are identical (except for minor bookkeeping differences) since these two systems have identical hardware elements. System C has a number of added features, all related to the one-way doppler measurements; the elements related to the DME and ILS measurements are deleted. The System D truth model is very similar to that of Systems A and B, with VOR elements added, glide slope elements deleted and initial condition assumptions altered.

4. FILTER COVARIANCE AND GAIN CALCULATIONS

Two of the preliminary steps required prior to performing error budget calculations are the detailed definition of the filter which forms part of the system and the preparation of a filter covariance program. This program contains the covariance update and propagate algorithms specified by the filter designer and generates a sequence of gain vectors corresponding to a particular trajectory and measurement schedule. This sequence is saved on tape and repeatedly used by the truth model covariance program in generating the system error budget. Presented below are the specific algorithms used to represent the filter gain calculations corresponding to the four candidate systems evaluated in this study. Systems A, C and D employ different versions of the JSC/TRW multi-phase filter. System B employs a low-dimensional square-root filter patterned after those studied by the MIT Draper Laboratory.

4.1 SYSTEM A FILTER

Figure 4.1-1 is a macro flow chart indicating the overall organization of the filter covariance programs used for both System A and System B. The principal inputs are the starting time, T_o, and the initial filter covariance matrix, P_{F_0}.

The principal output is the file of gain vectors, K_1 through K_3 for the first 303 update times (606 seconds) and K_1 through K_6 for the remaining 164 update times (144 seconds with a 2 second interval and

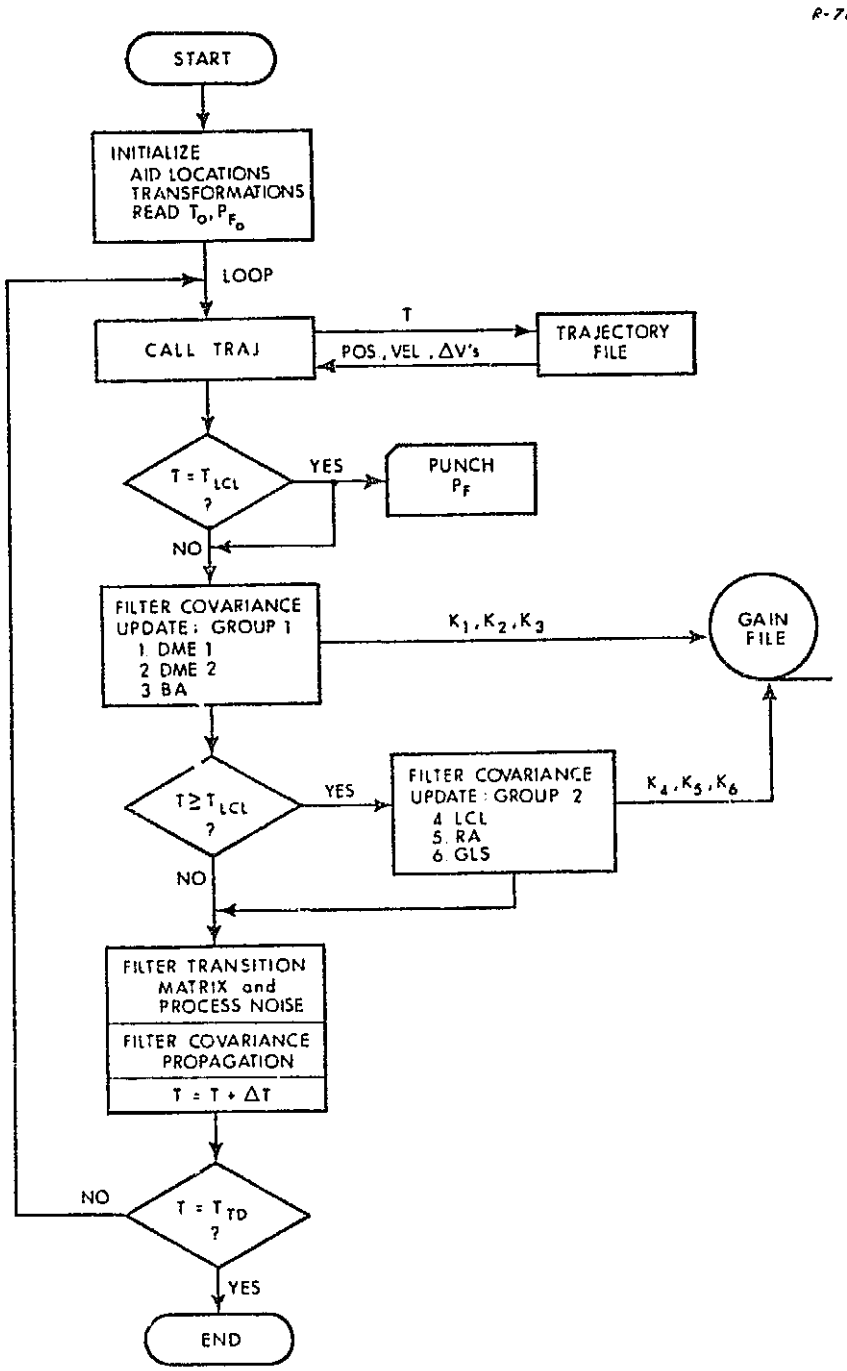

Figure 4.1-1 Filter Covariance Program Flow Chart (System A and System B)

46 seconds with a half second interval). At the time of the first localizer measurement ($T = T_{LCL}$) the current P_F matrix can be punched on cards. This gives us the capability to restart the problem at T_{LCL} using these cards to represent the new P_{F_0}.

The large square blocks in Fig. 4.1-1 contain the detailed covariance update and propagate algorithms. These can vary greatly from one filter design to another, depending on filter state size, state definitions, whether or not a square root formulation is used, reinitializations, process noise treatment, etc.

The JSC/TRW System A filter has been represented as a 24-state filter with the following state definitions.

State Numbers	Variables
1-3	Position Errors
4-6	Velocity Errors
7-9	Platform Misalignments
10-12	Gyro Drifts
13-15	Accelerometer Scale Factor Errors
16-18	Accelerometer Bias Errors
19	DME1 Correlated Error
20	DME2 Correlated Error
21	Baro Altimeter Correlated Error
22	ILS Localizer Correlated Error
23	Radar Altimeter Correlated Error
24	ILS Glide Slope Correlated Error

The upper-left 18 x 18 submatrix of P_{F_0} has been supplied to TASC by JSC; the numbers are not repeated here. The last six rows

and columns are all zeros except for the six diagonal elements. These are the squares of the initial rms values given or indicated in the "σ_c" column in Table 4.1-1. The transition matrix elements are programmed in accordance with the description given in Ref. 4 (see pages 46-53).

TABLE 4.1-1

FILTER STATE MEASUREMENT ERROR STATISTICS: SYSTEM A*

Measurement	Correlated Error (Filter State)		Measurement Noise
	σ_c	τ	σ_m
1. DME1	295 ft	400 sec	48 ft
2. DME2	295 ft	400 sec	48 ft
3. Baro Altimeter	Eq. (4.1-10)	40 sec	Eq. (4.1-11)
4. ILS Localizer	Eq. (4.1-13)	0.55 sec	0
5. Radar Altimeter	Eq. (4.1-12)	4 sec	3.28 ft
6. ILS Glide Slope	Eq. (4.1-14)	0.55 sec	0

The last six diagonal elements of the filter transition matrix have the form:

$$\phi_{F_{ii}} = \frac{1 - \Delta t/(2\,\tau_i)}{1 + \Delta t/(2\,\tau_i)}^{**} \quad ; i = 19, \ldots, 24 \qquad (4.1\text{-}1)$$

*Data from Ref. 5 and personal communication with W. Lear of TRW.

**Except where $2\,\tau_i < \Delta t$; see Eq. (4.89) Ref. 4.

where Δt is the propagation step size. The corresponding discrete process noise elements have the form

$$Q_{F_{ii}} = \sigma_{c_i}^2 \left(1 - \phi_{F_{ii}}^2\right) \tag{4.1-2}$$

where the τ_i are the correlation times given in Table 4.1-1. Each filter covariance propagation employs the following standard formula:

$$P_{F_{k+1}} = \Phi_{F_k} P_{F_k} \Phi_{F_k}^T + Q_{F_k} \tag{4.1-3}$$

At each update time a sequence of covariance updates are calculated, corresponding to a sequence of scalar measurements. In each case a 24 x 1 gain matrix is calculated using

$$K_F = P_F^- H_F^T / (H_F P_F^- H_F^T u_{70} + \sigma_m^2) \tag{4.1-4}$$

where H_F is a 1 x 24 measurement matrix, P_F^- is the covariance just prior to the updating, u_{70} is a scalar measurement underweighting factor,* and σ_m^2 is the assumed measurement noise variance (see the last column of Table 4.1-1). The covariance matrix is then updated in accordance with

$$P_F^+ = (I - K_F H_F) P_F^- \tag{4.1-5}$$

*The scalar u_{70} is normally unity, but has the value 1.2 during the early portion of the trajectory (see Refs. 4 and 17).

C-2

The 1 x 24 H_F matrices can be viewed as 24-dimensional row vectors, $\underline{h}$. The non-zero elements of $\underline{h}$ for each of the six scalar measurements are given below:

DME1	DME2
$h_1 = \rho_x/\rho$	$h_1 = \rho_x/\rho$
$h_2 = \rho_y/\rho$	$h_2 = \rho_y/\rho$
$h_3 = \rho_z/\rho$	$h_3 = \rho_z/\rho$
$h_{19} = 1$	$h_{20} = 1$

(4.1-6)

where ρ is the magnitude of the vector displacement of the vehicle from the DME station in question, and ρ_x, ρ_y and ρ_z are its components in the I frame (see Appendix A).

Baro Altimeter	Radar Altimeter
$h_1 = x/r$	$h_1 = x/r$
$h_2 = y/r$	$h_2 = y/r$
$h_3 = z/r$	$h_3 = z/r$
$h_{21} = 1$	$h_{23} = 1$

(4.1-7)

In the above r is the magnitude of the current position vector from the center of the earth and x, y and z are its components.

ILS Localizer

$$h_1 = u_{e_x}/\rho_{s_4}$$
$$h_2 = u_{e_y}/\rho_{s_4}$$

$$h_3 = u_{e_z}/\rho_{s_4}$$
$$h_{22} = 1 \qquad (4.1\text{-}8)$$

In the above ρ_{s_4} is the magnitude of the projection of the displacement vector $\underline{\rho}_4$ onto the earth's surface, as shown in Fig. 3.1-3. The quantities u_{e_x}, u_{e_y}, and u_{e_z} are components of the unit vector $\underline{u}_e$ shown in the figure.

ILS Glide Slope

$$h_1 = u_{p_x}/\rho_6$$
$$h_2 = u_{p_y}/\rho_6$$
$$h_3 = u_{p_z}/\rho_6$$
$$h_{24} = 1 \qquad (4.1\text{-}9)$$

In the above ρ_6 is the magnitude of the displacement vector shown in Fig. 3.1-3, and u_{p_x}, u_{p_y} and u_{p_z} are components of the unit vector $\underline{u}_p$.

The rms values of the correlated errors associated with the last four external-aid devices are programmed as a function of position and (in one case) relative velocity. The baro altimeter measurement noise 1-sigma value is also given as a function of altitude. These functions are indicated below.

Baro Altimeter, (units in feet and ft/sec)

$$\sigma_c^2 = 17,222 + 3.99 \times 10^{-14}\ \text{Alt}^4 + 3.22 \times 10^{-8}\ V_{rel}^4 \qquad (4.1\text{-}10)$$

$$\sigma_m^2 = 9.84 + (0.00025\ \text{Alt})^2 \qquad (4.1\text{-}11)$$

Radar Altimeter, (units in feet)

$$\sigma_c = \begin{cases} 0.05\ \text{Alt} & (\text{Alt} > 500) \\ 0.02\ \text{Alt} & (500 \geq \text{Alt} > 100) \\ 2.0 & (100 \geq \text{Alt}) \end{cases} \qquad (4.1\text{-}12)$$

ILS Localizer, (σ_c in milliradians, ρ in feet)

$$\sigma_c = \begin{cases} 5.6 & (\rho > 27,300) \\ 1.4 + 4.2\left(\frac{\rho - 3,500}{23,800}\right) & (27,300 \geq \rho > 3,500) \\ 1.4 & (3,500 \geq \rho) \end{cases} \qquad (4.1\text{-}13)$$

ILS Glide Slope, (σ_c in milliradians, ρ in feet)

$$\sigma_c = \begin{cases} 2.5 & (\rho > 27,300) \\ 1.4 + 1.1\left(\frac{\rho - 3,500}{23,800}\right) & (27,300 \geq \rho > 3,500) \\ 1.4 & (3,500 \geq \rho) \end{cases} \qquad (4.1\text{-}14)$$

The filter covariance program based on the 24-state filter outlined above has been exercised over the trajectory and measurement schedule described in Section 2. The time history of the filter-indicated performance is given in Table 4.1-2. RMS values of position and velocity errors in R frame components (runway coordinates; see Appendix A) are given at key times -- just before and just after the first measurement of each type, and at touchdown. At the bottom of the table the filter-indicated rms estimation errors, at touchdown, for the other 18 filter states are also given. The results given in Table 4.1-2 represent what optimal performance would be if this 24-state filter model were a completely accurate

TABLE 4.1-2

SYSTEM A FILTER-INDICATED PERFORMANCE

Event (see Table 2.1-1)	Time (sec)	RMS Position Errors (R frame (ft))			RMS Velocity Errors (R frame (ft/sec))		
		Vertical	Downrange	Crossrange	Vertical	Downrange	Crossrange
T_{DME}	1686^- 1686^+	49,400 15,300	93,100 25,900	25,000 20,200	160 40.8	93.6 57.2	134 64.1
T_{BA}	1806^- 1806^+	2,920 2,080	1,170 1,030	874 817	6.71 5.12	5.79 5.73	7.69 6.94
T_{LCL}	2292^- 2292^+	473 470	208 203	569 416	1.69 1.65	1.98 1.74	3.98 3.03
T_{RA}	2430^- 2430^+	655 122	231 213	53.1 50.4	1.77 0.58	1.26 1.14	0.92 0.89
T_{GLS}	2449.5^- 2449.5^+	43.4 24.8	218 206	16.9 16.3	0.49 0.47	1.15 1.12	0.62 0.62
T_{TD}	2482	1.9	30.6	5.5	0.16	0.90	0.34

OTHER INDICATED ESTIMATION ERRORS AT TOUCHDOWN, T_{TD}

Misalignments (rad)	— 0.287×10^{-3}, 0.079×10^{-3}, 0.123×10^{-3}
Gyro Drift (rad/sec)	— 0.279×10^{-6}, 0.283×10^{-6}, 0.278×10^{-6}
Accelerometer Scale Factors	— 4.94×10^{-5}, 4.55×10^{-5}, 4.90×10^{-5}
Accelerometer Biases (ft/sec^2)	— 5.67×10^{-4}, 5.60×10^{-4}, 5.66×10^{-4}
DME Errors (ft)	— 41.4, 29.2
Baro Altimeter Error (ft)	— 2.5
Localizer Error (rad)	— 1.54×10^{-3}
Radar Altimeter Error (ft)	— 1.8
Glice Slope Error (rad)	— 1.4×10^{-3}

representation of real-world error dynamics. The results given in Section 5.1 are a projection of the performance of this 24-state sub-optimal filter in an 82-state model of the real world.

*The rms misalignment estimation errors are in runway coordinates (Vertical, Downrange, Crossrange); the gyro and accelerometer errors are given in I frame (X, Y, Z) coordinates -- see Appendix A.

4.2 SYSTEM B FILTER

An MIT-type square root filter used in System B has been represented as a 6-state filter with the following state definitions.

State Numbers	Variables
1-3	Position Errors
4-6	Velocity Errors

The square root matrix W is defined by

$$WW^T = P_F$$

For this study the following initial diagonal matrix has been used:

$$W_0 = \left[\begin{array}{ccc|ccc} \sigma_p & & & & & \\ & \sigma_p & & & 0 & \\ & & \sigma_p & & & \\ \hline & & & \sigma_v & & \\ & 0 & & & \sigma_v & \\ & & & & & \sigma_v \end{array}\right] \qquad (4.2\text{-}1)$$

where

$$\sigma_p = 20{,}000 \text{ ft}$$

$$\sigma_v = 20 \text{ ft/sec}$$

The filter error dynamics matrix is

$$F_F = \left[\begin{array}{c|c} 0 & I \\ \hline G_r & 0 \end{array}\right]_{6 \times 6} \qquad (4.2\text{-}2)$$

where G_r is the gravity gradient matrix defined by Eq. (3.1-3). The process noise matrix is

$$Q_F = \left[\begin{array}{c|c} 0 & 0 \\ \hline 0 & Q \end{array}\right]_{6 \times 6} \qquad (4.2\text{-}3)$$

where

$$Q = \begin{bmatrix} q_v & 0 & 0 \\ 0 & q_v & 0 \\ 0 & 0 & q_v \end{bmatrix} \qquad (4.2\text{-}4)$$

$$q_v = 0.01 \text{ (ft/sec)}^2/\text{sec}$$

(See the dicussion of the choice of q_v at the end of this section.)

The propagation of W between measurements is based on the following equation (from Ref. 6).

$$\dot{W} = F_F W + \frac{1}{2} Q_F W_D^{-1} \qquad (4.2\text{-}5)$$

where W_D is a "diagonalized" form of W. The "average G" numerical integration procedure (Ref. 18) is mechanized as follows:

$$W(t+\Delta t) = \left\{ I + \Delta t \left[\begin{array}{c|c} 0 & I \\ \hline G_{avg} & 0 \end{array}\right] + \frac{\Delta t^2}{2} \left[\begin{array}{c|c} G_r(t) & 0 \\ \hline 0 & G_r(t+\Delta t) \end{array}\right] \right\} W(t)$$

$$+ \frac{\Delta t}{2} \left[\begin{array}{c|c} 0 & \frac{\Delta t}{2} Q \\ \hline 0 & Q \end{array}\right] W_D^{-1}(t) \qquad (4.2\text{-}6)$$

where

$$G_{avg} = \frac{G_r(t) + G_r(t+\Delta t)}{2} \qquad (4.2\text{-}7)$$

To update W at the i^{th} scalar measurement incorporation the following equations are used (see Ref. 6).

$$z_i = W^T H_{F_i}^T \quad (i = 1, \ldots, 6) \qquad (4.2\text{-}8)$$

$$D_i = z^T z + R_{F_i} \quad \text{(a scalar)} \qquad (4.2\text{-}9)$$

$$K_i = W z_i / D_i \qquad (4.2\text{-}10)$$

$$W^+ = W^- - \frac{K_i z_i^T}{1 + \sqrt{R_{F_i}/D_i}} \qquad (4.2\text{-}11)$$

The K_i are the 6-dimensional gain vectors making up the gain file shown in Fig. 4.1-1. This file is used to produce the System B error budget results given in Section 5.2. Expressions and values for the measurement matrices H_{F_i} (6-dimensional row vectors) and measurement error variances R_{F_i} are given below. The H_{F_i} have the form

$$H_{F_i} = \begin{bmatrix} h_1 & h_2 & h_3 & 0 & 0 & 0 \end{bmatrix} \qquad (4.2\text{-}12)$$

The three non-zero elements, h_1, h_2 and h_3, are the same as the corresponding System A elements, given in Section 4.1. For the DME measurements (i = 1 and 2):

DME 1	DME 2
$h_1 = \rho_x/\rho$	$h_1 = \rho_x/\rho$
$h_2 = \rho_y/\rho$	$h_2 = \rho_y/\rho$
$h_3 = \rho_z/\rho$	$h_3 = \rho_z/\rho$

(4.2-13)

where ρ is the magnitude of the vector displacement of the vehicle from the DME station in question, and ρ_x, ρ_y, and ρ_z are its I frame components.

For altimeter measurements (i = 3 and 5):

Baro Altimeter	Radar Altimeter
$h_1 = x/r$	$h_1 = x/r$
$h_2 = y/r$	$h_2 = y/r$
$h_3 = z/r$	$h_3 = z/r$

(4.2-14)

where r is the magnitude of the current position vector, from the center of the earth, and x, y and z are its I frame components.

For ILS measurements (i = 4 and 6):

Localizer	Glide Slope
$h_1 = u_{e_x}/\rho_{s_4}$	$h_1 = u_{p_x}/\rho_6$
$h_2 = u_{e_y}/\rho_{s_4}$	$h_2 = u_{p_y}/\rho_6$
$h_3 = u_{e_z}/\rho_{s_4}$	$h_3 = u_{p_z}/\rho_6$

(4.2-15)

The unit vector $\underline{u}_e$ and $\underline{\rho}_{s4}$ are defined in Fig. 3.1-3. The unit vector $\underline{u}_p$ and $\underline{\rho}_6$ are defined in Fig. 3.1-4.

The six filter measurement error variances R_{F_i} (i = 1,...,6), used in the System B filter covariance calculations were computed in the following way: In each case the values used in the System A model for both correlated errors, σ_c, and uncorrelated errors, σ_m, were combined to yield

$$R_{F_i} = \sigma_i^2$$

$$= \sigma_{c_i}^2 + \sigma_{m_i}^2 \qquad (4.2\text{-}16)$$

The values or expressions indicated in Table 4.1-1, for System A, were used in Eq. (4.2-16) for System B.

MIT personnel suggested the following range of possible values for the velocity process noise:

$$q_v = 0.01 \text{ to } 0.10 \text{ (ft/sec)}^2/\text{sec}$$

The minimum and maximum values in this range were tried in the System B filter covariance program. The smaller value produced a significantly better filter-indicated vertical velocity performance at touchdown, so the gain values corresponding to that run were used to generate the System B error budget. The time history of the filter-indicated performance is given in Table 4.2-1. (The final values corresponding to the larger process noise are also given, at the bottom of the table.) These results present what optimal performance would be if this 6-state filter model were a completely accurate representation of real-world error dynamics. The results given in Section 5.2 are a projection of the performance of this 6-state sub-optimal filter in a 70-state model of the real world.

Note on Subsequent MIT Studies — Since the completion of the System B evaluation, MIT personnel have conducted further studies corresponding to similar measurement sequences. These have included trail-and-error procedures to achieve better choices of process noise

TABLE 4.2-1

SYSTEM B FILTER-INDICATED PERFORMANCE

Event (see Table 2.1-1)	Time (sec)	RMS Position Errors (R frame (ft))			RMS Velocity Errors (R frame (ft/sec))		
		Vertical	Downrange	Crossrange	Vertical	Downrange	Crossrange
T_{DME}	1686^- 1686^+	20,000 19,800	20,000 11,500	20,000 10,500	20.0 20.0	20.0 20.0	20.0 20.0
T_{BA}	1806^- 1806^+	10,500 2,200	2,900 1,100	1,790 894	18.4 18.3	14.0 12.5	14.9 10.9
T_{LCL}	2292^- 2292^+	42.5 41.1	70.7 67.2	184 174	0.57 0.55	0.67 0.65	1.14 1.08
T_{RA}	2430^- 2430^+	35.0 32.6	50.3 49.2	50.5 48.4	0.55 0.51	0.66 0.64	0.65 0.63
T_{GLS}	2449.5^- 2449.5^+	11.3 8.4	38.3 37.2	11.8 11.4	0.25 0.19	0.55 0.54	0.36 0.35
T_{TD} ($q_v = 0.01$)	2482	1.4	21.3	4.1	0.19	0.48	0.26
T_{TD} ($q_v = 0.1$)	2482	1.9	29.9	5.4	0.43	1.30	0.64

and measurement noise variances, as well as the use of additional filter states such as level misalignment and DME bias error estimates. One of their conclusions is that better performance is possible with a six-state filter than with the six-state version described above. It is felt that the general comparison and summary discussion given in Section 6 of this report remains valid. In addition, our suggestions concerning the use of additional states seem to be borne out by the results of the MIT experiments along these lines.

4.3 SYSTEM C FILTER

The JSC/TRW System C filter has been represented as a 22-state filter with the following state definitions.

State Numbers	Variables
1-3	Position Errors
4-6	Velocity Errors
7-9	Platform Misalignments
10-12	Gyro Drifts
13-15	Accelerometer Scale Factor Errors
16-18	Accelerometer Bias Errors
19	Onboard Doppler Rate Bias Errors
20	Beacon Doppler Rate Bias Error
21	Baro Altimeter Correlated Error
22	Radar Altimeter Correlated Error

The upper-left 18 x 18 submatrix of P_{F_0} is identical to that used in the System A evaluation. The last four rows and columns are all zeros except for the four diagonal elements. These are the squares of the initial rms values given or indicated in the "σ_c" column in Table 4.3-1.

TABLE 4.3-1

FILTER STATE MEASUREMENT ERROR STATISTICS: SYSTEM C

Measurement	Correlated Error (Filter State)		Measurement Noise
	σ_c	τ	σ_m
1. One-Way Doppler Onboard Rate Bias Beacon Rate Bias	 0.0876 ft/sec 0.0044 ft/sec	 800 sec 400 sec	0.0357 ft
2. Baro Altimeter	Eq. (4.1-10)	40 sec	Eq. (4.1-11)
3. Radar Altimeter	Eq. (4.1-14)	4 sec	3.28 ft

The transition matrix elements are programmed in accordance with the description given in Ref. 4 (see pages 46 and 53) and discussed in Section 4.1.

The filter covariance propagation and update calculations are those given in Eqs. (4.1-3), (4.1-4) and (4.1-5) except for one additional term used to account for measurement nonlinearities. The denominator of the gain equation (4.1-4) is increased by an amount ΔR as follows:

$$K_F = \bar{P}_F H_F^T / (H_F \bar{P}_F H_F^T u_{70} + \sigma_m^2 + \Delta R) \qquad (4.3\text{-}1)$$

The increase is calculated using the second partial derivatives of a non-linear measurement equation which is expanded in a Taylor series about the estimated state. The second partial derivatives with respect to position and velocity make up a 6 x 6 matrix, S_P. Then, a 6 x 6 matrix product is calculated

$$M_P = S_P \tilde{P}_F \qquad (4.3\text{-}2)$$

where $\tilde{P}_F$ is the 6 x 6 upper-left partition of P_F. M_P is used to compute a double-sum term, DSUM, and a quadruple-sum term, QSUM.

$$\text{DSUM} = \text{Trace}\,(M_P) \qquad (4.3\text{-}3)$$

$$\text{QSUM} = \sum_{j=1}^{6} \sum_{j=1}^{6} c_{ij} M_P(i, j)\, M_P(j, i) \qquad (4.3.4)$$

where

$$c_{ij} = \begin{cases} 1: & i = j \\ 2: & i \neq j \end{cases}$$

Then,

$$\Delta R = \frac{1}{2}\,\mathrm{QSUM} + \left(\frac{1}{2}\,\mathrm{DSUM}\right)^2 \qquad (4.3\text{-}5)$$

It is shown in Ref. 10 that $\frac{1}{2}$ DSUM is the expected value of the measurement bias error associated with the second-order terms of the Taylor series. The factor u_{70} in Eq. (4.3-1) is the measurement underweighting factor discussed in Section 4.1.

The 1×22 H_F matrices can be viewed as 22-dimensional row vectors, $\underline{h}$. The non-zero elements of $\underline{h}$ for each of the three scalar measurements are given below.

One-Way Doppler

$$h_1 = \Delta t\left[\frac{\dot\rho_x}{\rho} - \frac{\rho_x \lambda}{\rho^3} - \frac{\Delta t}{2}\left(\frac{\ddot\rho_x}{\rho} - \frac{\rho_x \eta}{\rho^3}\right)\right]$$

$$h_2 = \Delta t\left[\frac{\dot\rho_y}{\rho} - \frac{\rho_y \lambda}{\rho^3} - \frac{\Delta t}{2}\left(\frac{\ddot\rho_y}{\rho} - \frac{\rho_y \eta}{\rho^3}\right)\right]$$

$$h_3 = \Delta t\left[\frac{\dot\rho_z}{\rho} - \frac{\rho_z \lambda}{\rho^3} - \frac{\Delta t}{2}\left(\frac{\ddot\rho_z}{\rho} - \frac{\rho_z \eta}{\rho^3}\right)\right]$$

$$h_4 = \Delta t\,\rho_x/\rho$$

$$h_5 = \Delta t\,\rho_y/\rho$$

$$h_6 = \Delta t\,\rho_z/\rho$$

$$h_{19} = \Delta t$$
$$h_{20} = \Delta t \qquad (4.3\text{-}6)$$

Where the ρ_x, ρ_y, ρ_z, $\dot{\rho}_x$, etc. are I frame components of the displacement vector, $\underline{\rho}$, from beacon to shuttle, and its derivatives $\underline{\dot{\rho}}$ and $\underline{\ddot{\rho}}$. The other parameters appearing above are defined as follows:

$$\rho = \sqrt{\underline{\rho} \cdot \underline{\rho}}$$
$$\lambda = \underline{\rho} \cdot \underline{\dot{\rho}}$$
$$\eta = \underline{\rho} \cdot \underline{\ddot{\rho}}$$
$$\Delta t = \text{update interval} \qquad (4.3\text{-}7)$$

Baro Altimeter	Radar Altimeter
$h_1 = x/r$	$h_1 = x/r$
$h_2 = y/r$	$h_2 = y/r$
$h_3 = z/r$	$h_3 = z/r$
$h_{21} = 1$	$h_{22} = 1$

(4.3-8)

In the above r is the magnitude of the current position, from the center of the earth, and x, y and z are its I frame components.

The filter covariance program based on the 22-state filter outlined above has been exercised over the trajectory and measurement schedule described in Section 2. The time history of the filter-indicated performance is given in Table 4.3-2. RMS values of position and velocity errors in R frame components are given just before and after the first measurement of each type and at a few other times, including touchdown. The results given in Table 4.3-2 represent what optimal performance

TABLE 4.3-2

SYSTEM C FILTER-INDICATED PERFORMANCE

Event (see Table 2.1-1)	Time (sec)	RMS Position Errors (R frame (ft))			RMS Velocity Errors (R frame (ft/sec))		
		Vertical	Downrange	Crossrange	Vertical	Downrange	Crossrange
T_{OWD}	1686^-	49,400	93,100	25,000	160	93.6	134
	1686^+	34,300	54,100	24,900	110	49.6	70.8
T_{BA}	1806^-	10,300	15,400	19,100	34.2	16.0	9.77
	1806^+	4,910	9,610	11,200	17.0	10.6	9.02
	2292	140	63.4	88.2	0.87	0.31	0.85
T_{RA}	2430^-	35.8	65.8	77.6	0.32	0.11	0.84
	2430^+	33.7	65.7	77.5	0.31	0.11	0.83
T_{TD}	2482	2.1	0.7	3.6	0.22	0.07	0.33

OTHER INDICATED ESTIMATION ERRORS AT TOUCHDOWN, T_{TD}

Misalignments (rad)	0.266×10^{-3}, 0.066×10^{-3}, 0.056×10^{-3}
Gyro Drift (rad/sec)	0.256×10^{-6}, 0.281×10^{-6}, 0.276×10^{-6}
Accelerometer Scale Factors	4.91×10^{-5}, 4.48×10^{-5}, 4.84×10^{-5}
Accelerometer Biases (ft/sec^2)	5.67×10^{-4}, 5.60×10^{-4}, 5.64×10^{-4}
Onboard Rate Bias (ft/sec)	0.051
Ground Rate Bias (ft/sec)	0.007
Baro Altimeter Error (ft)	9.53
Radar Altimeter Error (ft)	1.89

would be if this 22-state filter model were a completely accurate representation of real-world error dynamics. The results given in Section 5.3 are a projection of the performance of this 22 state sub-optimal filter in a 63-state model of the real world.

4.4 SYSTEM D FILTER

The JSC/TRW System D filter has been represented as a 23-state filter with the following state definitions.

*The rms misalignment estimation errors are in runway coordinates (Vertical, Downrange, Crossrange); the gyro and accelerometer errors are given in I frame (X, Y, Z) coordinates -- see Appendix A.

State Numbers	Variables
1-3	Position Errors
4-6	Velocity Errors
7-9	Platform Misalignments
10-12	Gyro Drifts
13-15	Accelerometer Scale Factor Errors
16-18	Accelerometer Bias Errors
19	DME Correlated Error
20	VOR Correlated Error
21	Baro Altimeter Correlated Error
22	ILS Localizer Correlated Error
23	Radar Altimeter Correlated Error

The upper left 18×18 submatrix of P_{F_0} has been supplied by NASA (a different set from that used in the System A and C evaluations). The last five rows and columns are all zeros except for the five diagonal elements. These are the initial rms values given or indicated in the "σ_c" column of Table 4.4-1.

TABLE 4.4-1

FILTER STATE MEASUREMENT ERROR STATISTICS: SYSTEM D

Measurement	Correlated Error (Filter State)		Measurement Noise
	σ_c	τ	σ_m
1. DME	295 ft	400 sec	48 ft
2. VOR	18.67 mrad	800 sec	8.5 mrad
3. Baro Altimeter	Eq. (4.1-10)	40 sec	Eq. (4.1-11)
4. ILS Localizer	Eq. (4.1-13)	0.55 sec	0
5. Radar Altimeter	Eq. (4.1-12)	4 sec	3.28 ft

The transition matrix elements are programmed in accordance with the description given in Ref. 4 and discussed in Section 4.1. The filter covariance propagation and update calculations are those given in Eqs. (4.1-3), (4.1-4) and (4.1-5)

The 1 x 23 H_F matrices can be viewed as 23-dimensional row vectors, $\underline{h}$. The non-zero elements of $\underline{h}$ for the first two scalar measurements are given below:

DME		VOR	
h_1	$= \rho_x/\rho_1$	h_1	$= u_{2_x}/\rho_{s_1}$
h_2	$= \rho_y/\rho_1$	h_2	$= u_{2_y}/\rho_{s_1}$
h_3	$= \rho_2/\rho_1$	h_3	$= u_{2_z}/\rho_{s_1}$
h_{19}	$= 1$	h_{20}	$= 1$

where ρ_1 is the magnitude of the vector displacement $\underline{\rho}_1$ of the vehicle from the VOR/DME station, ρ_x, ρ_y and ρ_z are is I frame components, ρ_{s_1} is the magnitude of the projection of $\underline{\rho}_1$ onto the earth's surface, and u_{2_x}, u_{2_y} and u_{2_z} are the I frame components of the unit vector $\underline{u}_2$ shown in Fig. 3.4-2.

The non-zero elements of the $\underline{h}$ vectors associated with baro altimeter, radar altimeter, and ILS localizer measurements are the same as in the System A filter; see Eqs. (4.1-7) and (4.1-8).

The filter covariance program based on the 23-state filter outlined above has been exercised over the trajectory and measurement schedule described in Section 2. The time history of the filter-indicated performance is given in Table 4.4-2. RMS values of position and velocity errors in R frame components (runway coordinates; see Appendix A) are

TABLE 4.4-2

SYSTEM D FILTER-INDICATED PERFORMANCE

Event (see Table 2.1-1)	Time (sec)	RMS Position Errors (R frame (ft))			RMS Velocity Errors (R frame (ft/sec))		
		Vertical	Downrange	Crossrange	Vertical	Downrange	Crossrange
T_{DME}	1686^- 1686^+	4,600 4,580	27,200 14,200	22,600 12,800	22.8 17.6	36.9 35.5	16.6 15.9
T_{BA}	1806^- 1806^+	5,060 3,120	2,120 1,590	1,050 999	14.8 10.5	14.7 13.7	12.4 11.8
T_{LCL}	2292^- 2292^+	780 773	290 285	580 421	2.82 2.78	2.52 2.38	3.55 2.81
T_{RA}	2450^- 2450^+	277 113	284 270	12.3 11.6	0.98 0.78	1.71 1.62	0.65 0.64
T_{TD}	2482	2.5	54.2	5.7	0.50	1.33	0.30
T_{TD} (old trajectory)	2482	2.3	43.4	5.6	0.31	1.29	0.29

OTHER INDICATED ESTIMATION ERRORS AT TOUCHDOWN, T_{TD}

Misalignments (rad)	—	0.545×10^{-3}, 0.122×10^{-3}, 0.211×10^{-3} *
Gyro Drift (rad/sec)	—	0.543×10^{-6}, 0.546×10^{-6}, 0.526×10^{-6} *
Accelerometer Scale Factors	—	9.97×10^{-5}, 9.21×10^{-5}, 9.91×10^{-5} *
Accelerometer Biases (ft/sec^2)	—	1.59×10^{-3}, 1.56×10^{-3}, 1.59×10^{-3} *
DME Error (ft)	—	2.48
VOR Error (rad)	—	2.38×10^{-3}
Baro Altimeter Error (ft)	—	9.61
Localizer Error (rad)	—	0.54×10^{-3}
Radar Altimeter Error (ft)	—	2.04

given at key times--just before and just after the first measurement of each type, and at touchdown. At the bottom of the table the filter-indicated rms estimation errors, at touchdown, for the other 17 filter states are also given.

The added row of position and velocity errors at touchdown, labeled "T_{TD}(old trajectory)", corresponds to an additional run through the System D filter covariance program with the trajectory tape which had been used in the System A, B and C evaluations. This extra run was motivated by the observation that the System D filter-indicated touchdown performance (with the new trajectory) is very similar to the System A

*The rms misalignment estimation errors are in runway coordinates (Vertical, Downrange, Crossrange); the gyro and accelerometer errors are given in I frame (X,Y,Z) coordinates -- see Appendix A.

filter-indicated performance (Table 4.1-2) in every component except vertical velocity -- 0.50 ft/sec compared with the System A value of 0.16 ft/sec. The added run, in which the terminal rms vertical velocity error is 0.31 ft/sec, shows that a major part of the difference between the System A and System D results is caused by the steeper approach path for System D. This point is discussed further in Section 6.1.

The results given in Table 4.4-2 represent what optimal performance would be if this 23-state filter model were a completely accurate representation of real-world error dynamics. The results given in Section 5.4 are a projection of the performance of this 23-state suboptimal filter in a 74-state model of the real world.

5. RESULTS

This section presents detailed results for the four candidate systems. Overall performance curves are given for each system, showing time histories of position and velocity errors due to all sources combined. In each case a "Baseline Error Budget" table is given, showing the contributions of individual error sources, or small groups of error sources, at touchdown. Smaller tables of "Alternative Contributions" are provided, allowing the reader to see the effects of different truth model assumptions. Sensitivity curves illustrating the effect of variations in the rms value of a given major error source (or group of error sources) on overall system performance are also given. Section 6 provides a general summary and comparison of the four sets of results, including discussions of how particular groups of error sources contribute differently to different systems and of filter states which might be safely deleted or usefully added.

5.1 SYSTEM A EVALUATION

The results presented below correspond to the trajectory segment, lasting 796 seconds, pictured in Fig. 2.1-1. The measurement schedule is described in Section 2.1; it employs a 2 second interval between updates for 750 seconds, followed by a 0.5 second update interval for the final 46 seconds. A file of gain values, generated using the filter covariance program outlined in Section 4.1, has been used repeatedly to

compute detailed error contributions corresponding to this trajectory and measurement schedule.

5.1.1 Overall System Performance

Figures 5.1-1 and 5.1-2 present overall performance curves for System A, showing position error components and velocity error components, respectively. The curves plotted represent rms errors due to the combined effects of all error source groups in the baseline error budget. They were generated by root-sum-squaring individual contributions at one minute intervals (tabulated in Appendix C). At T_{DME}, when the first DME measurements are made, and at other key times, such as T_{BA}, T_{LCL}, T_{RA} and T_{GLS}, the root-sum-square calculation was performed both before and after update. Thus, the large jumps in certain component errors, which occur at these times, are accurately shown. Otherwise, the curves are faired-in over the one-minute intervals between the calculated points.

At the time of the first DME measurements, T_{DME}, some of the component errors increase -- notably, the crossrange position and velocity errors. This reflects the fact that the initial filter covariance matrix does not accurately represent the assumed real world covariance, resulting in non-optimal performance. Clearly, if the filter were "tuned" for the particular case considered, it could do better at the first update time. Navigation errors then decrease rapidly over the several minutes following the first update. Note, especially, the large decrease in vertical position and velocity errors at the time of the first baroaltimeter update. The exception is the increase in crossrange velocity error during the first minute. Examination of individual contributions

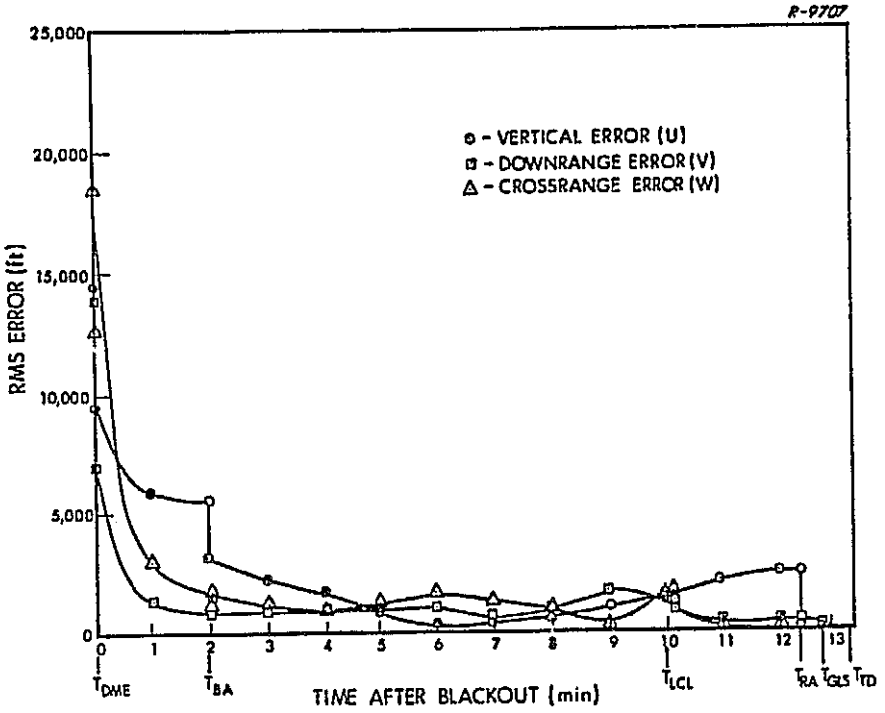

Figure 5.1-1 System A Overall Performance: Position

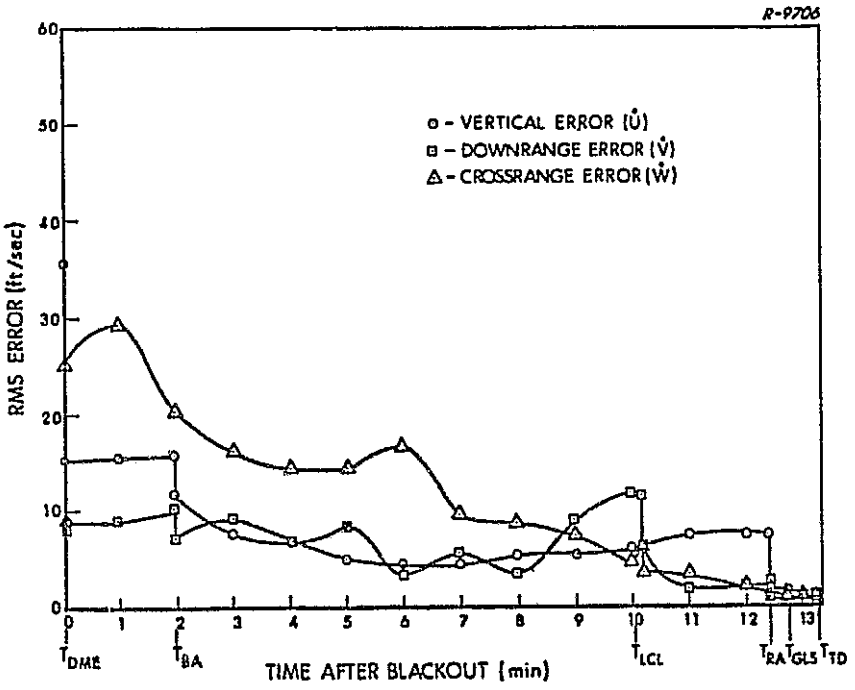

Figure 5.1-2 System A Overall Performance: Velocity

(as tabulated in Appendix C) shows that the major cause of this increase is the group of accelerometer scale factor errors (Group 3). This group is also the major cause of the increase at the first update. The effect is associated more with initial correlations caused by the accelerometer scale factor errors during boost than with the accelerometer errors occurring in the time interval plotted.

An interesting feature of the velocity performance curves of Fig. 5.1-2 is the sharp decrease in the downrange velocity error at the time of the first localizer measurement, T_{LCL}. Clearly, the crossrange and downrange position and velocity errors must be highly correlated at this time. We note in passing that a filter scheme which automatically re-initialized to a diagonal filter covariance matrix at this point in time would lose the benefit illustrated.

A potentially serious problem for System A is illustrated in Figs. 5.1-1 and 5.1-2 by the large vertical errors just prior to the time of the first radar altimeter measurements, T_{RA}. This occurs less than one minute prior to touchdown, and the projected rms vertical position error of more than 2000 feet is probably unacceptable -- despite the fact that the performance is quite good after the radar altimeter comes into use. The large rms vertical position error prior to T_{RA} is caused by the large vertical velocity error integrated over time. The major contributors to vertical velocity errors are the gyro bias and mass unbalance drifts (Groups 7 and 8). Evidently, the filter "believes" it has accurate estimates of platform alignment and vertical velocity information, and is making heavy use of mis-resolved accelerometer outputs. The problem illustrated here is <u>not inherent</u> to the type of conventional navaids under investigation (since it does not occur in the System B or D studies). It is a filter design problem and is, thus, subject to fixing by software modification.

Section 6 contains further discussions of the implications of the performance curves presented in this section.

5.1.2 Detailed Error Budget

System error covariances have been calculated for each group of error sources over the entire 796 second trajectory (t = 1686 sec to 2482 sec). The total amount of data produced is therefore quite large, since rms values of all significant quantities, before and after each measurement, have been generated. In order to summarize important results in one table of manageable size, a "snapshot" view of conditions at the nominal touchdown time (2482 sec) is presented in Tables 5.1-1 and 5.1-2. Table 5.1-1 is the System A Baseline Error Budget showing rms estimation errors in position, velocity and platform alignment components at touchdown. Each value is the rms contribution of the error source or sources indicated in the left hand column; it comes from a computer run in which the elements of $P_S(0)$, Q_S or R_S, corresponding to those errors alone, are set at truth-model values -- and all others are zero. The overall System A performance, or root-sum-square values, are given at the bottom of the table and compared, first with the filter's own estimate of performance based on its simplified 24-state model of system error dynamics, and second with the Shuttle landing navigation specification given in Ref. 1. Table 5.1-2 lists the System A Alternative Contributions showing how different assumptions or additional error sources would produce other contributions to position, velocity and alignment errors at touchdown.

Particular numbers have been circled in the position and velocity error columns of Table 5.1-1 to focus attention on major

TABLE 5.1-1

SYSTEM A BASELINE ERROR BUDGET

Error Source	Value	RMS Navigation Errors at Touchdown								
		Position (ft)			Velocity (ft/sec)			Misalignment (mrad)		
		Vertical	Downrange	Crossrange	Vertical	Downrange	Crossrange	Vertical	Downrange	Crossrange
ESTIMATED STATES AND NOISES										
Group 1. IMU Quantization Noise	One Pulse - 1 cm/sec	0.3	5.6	0.7	0.07	0.24	0.09	0.048	0.032	0.034
Measurement Noises										
DME's	24 ft	0.1	4.2	0.1	0.01	0.05	—	0.008	0.002	0.006
Radar Altimeter	3.28 ft	0.8	4.6	—	0.05	0.09	—	0.004	—	0.008
Radar Altimeter Markov	Eq. (3.1-43)	1.0	8.6	—	0.05	0.13	—	0.006	—	0.012
IMU-RELATED STATES										
Group 2. Accelerometer Biases	60 μg	0.2	8.2	0.9	0.05	0.31	0.11	0.541	0.075	0.078
Group 3. Accelerometer Scale Factor Errors	34 ppm	0.3	4.9	1.8	0.03	0.24	0.26	1.608	0.114	0.013
Group 4. Accelerometer Misalignments	40 sec	0.6	8.7	0.6	0.10	0.27	0.06	0.178	0.172	0.201
Group 5. Accelerometer Nonlinearities	$3.5\ \mu g/g^2$	—	0.3	—	—	0.01	—	—	—	—
Group 6. Gravity Anomalies and Deflections	see Table 3.1-2	0.2	3.9	0.3	0.04	0.13	0.03	0.025	0.021	0.021
Group 7. Gyro Bias Drifts	0.01 deg/hr	0.2	17.8	0.6	0.05	0.85	0.07	0.739	0.043	0.018
Group 8. Gyro Mass Unbalances	0.015 deg/hr/g	0.4	3.6	0.6	0.04	0.07	0.06	0.266	0.012	0.036
Group 9. Gyro Anisoelasticity	$0.005\ deg/hr/g^2$	—	0.1	—	—	—	—	0.005	0.001	0.001
EXTERNAL-AID RELATED STATES										
Group 10. DME Bias Errors	295 ft	0.2	1.7	0.2	0.01	0.14	0.02	0.010	0.004	0.004
Group 11. DME Scale Factor Errors	100 ppm	—	0.8	0.1	—	0.04	0.01	0.005	0.002	0.007
Group 12. Baro Altimeter Errors										
Bias and Scale Factor	100 ft 0.03	—	0.1	—	—	0.01	—	—	0.001	0.002
Markov and Measurement Noise	20 ft 5 ft	—	—	—	—	—	—	—	—	—
Static Defect	1.52×10^{-4} ft/(ft/sec)^2	—	0.1	—	—	0.01	—	—	—	0.001
GGroup 13. ILS Bias Errors										
Localizer	0.5 mrad	—	1.2	4.7	—	0.07	0.21	0.050	0.025	0.014
Glide Slope	0.5 mrad	0.5	4.7	0.1	0.13	0.07	0.01	0.003	0.001	0.004
Group 14. ILS 2nd Order Markovs										
Localizer	Eq. (3.1-44)	0.1	2.4	5.9	—	0.09	0.30	0.049	0.038	0.017
Glide Slope	Eq. (3.1-45)	0.7	9.2	0.1	0.01	0.15	—	0.007	0.001	0.016
Group 15. (Not included in Baseline Error Budget)										
Group 16. DME Survey Errors	1 ft	—	0.6	—	—	0.01	—	0.001	—	0.001
Group 17. ILS Survey Errors										
Localizer	1 ft	—	—	1.0	—	—	—	0.001	—	—
Glide Slope	1 ft	0.2	7.1	—	0.03	0.11	—	0.005	—	0.011
Total Projected Performance (root-sum-square)		1.9	28.7	8.0	0.22	1.07	0.49	1.860	0.232	0.226
Filter-Indicated Performance		1.9	30.6	5.5	0.16	0.90	0.34	0.287	0.079	0.123
Specification (Ref. 6)		3.0	80.0	4.7	0.20	3.00	2.00	Not Specified		

A "—" entry refers to a negligibly small contribution.

TABLE 5.1-2

SYSTEM A ALTERNATIVE CONTRIBUTIONS

Error Source	Value	RMS Navigation Errors at Touchdown								
		Position (ft)			Velocity (ft/sec)			Misalignment (mrad)		
		Vertical	Downrange	Crossrange	Vertical	Downrange	Crossrange	Vertical	Downrange	Crossrange
Group 1. Initial 9 × 9 Covariance Matrix (Position, Velocity and Alignment)	See Section 3.1.3	0.4	19.9	2.2	0.06	0.96	0.30	1.920	0.126	0.199
Initial 6 × 6 Covariance Matrix (Position and Velocity only)		0.4	13.0	2.1	0.04	0.63	0.30	1.827	0.122	0.121
ILS First-Order Markovs										
Localizer	Eq. (3.1-44)	0.1	3.2	9.2	0.01	0.13	0.51	0.082	0.064	0.027
Glide Slope	Eq. (3.1-45)	0.8	9.3	0.1	0.10	0.16	—	0.007	0.001	0.016
Group 15. Radar Altimeter Errors										
Bias	1 ft	0.8	7.0	—	0.03	0.11	—	0.005	—	0.010
Scale Factor	0.025	0.4	12.0	—	0.04	0.10	—	0.005	—	0.010

contributors. The rule followed in deciding which numbers to circle was to include, in any one column, the largest value, second largest value, etc., until 95% of the RSS total value was reached. The following general statements may be drawn from an examination of the System A baseline error budget:

- The projected downrange performance, in both position and velocity, is well within specs, and the filter-indicated performance is within 20% of projected actual performance. The largest contributors to downrange errors are gyro bias drifts (Group 7). Other significant error sources are accelerometer errors (Groups 2, 3 and 4), radar altimeter markov error (Group 1), glide slope errors (Groups 13, 14 and 17), IMU quantization noise (Group 1), and DME bias errors (Group 10).

- The projected vertical performance is within spec in position, but out-of-spec in velocity. The filter-indicated performance is the same as the projected actual performance in position, but almost 30% off in velocity -- erring on the optimistic side. The largest contributors to vertical velocity errors are glide slope bias error (Group 13) and the accelerometer misalignments (Group 4). Other significant contributors to vertical errors are radar altimeter errors (Group 1), glide slope markov errors (Group 14), gyro biases and mass unbalances (Groups 7 and 8), accelerometer bias and scale factor errors (Groups 2 and 3) and IMU quantization (Group 1).

- The projected crossrange performance is within spec in velocity, but out-of-spec in position. The filter-indicated performance, in both position and velocity, is optimistic -- predicting roughly two thirds of the projected actual rms errors. The largest contributors to crossrange errors are localizer errors (Groups 13 and 14). Other significant contributors to crossrange velocity errors are accelerometer scale factor errors (Group 3).

- The projected errors in estimating platform misalignments are approximately 0.2 milliradians, for misalignments about level axes, and nearly 2.0 milliradians for azimuth misalignment. The latter is significantly larger than the projected rms actual misalignment which is 0.620 milliradians --the rss value at the bottom of the System B error budget table. (Misalignments are not estimated by the System B filter).

Considering all components of position and velocity errors at touchdown, the list of major contributors includes gyro errors, accelerometer errors, and errors associated with all of the external devices except the baro-altimeter. More detailed discussion of the important error mechanisms and possible ways to reduce some of the contributions is given in Section 6.

Detailed tabulations of the error contribution time histories are given in Appendix C. For every row in Tables 5.1-1 and 5.1-2 there is a page in Appendix C, which is a reproduction of a computer print-out page summarizing important results from one error budget run.

5.1.3 Sensitivity Curves: System A

This section contains several curves illustrating the sensitivity of System A performance to variations in error source statistics. These "fixed-filter" sensitivity calculations answer the question: "What is the effect of an unknown variation in the rms value or values or an error source or group of error sources?" These calculations can be made easily, given the type of error budget information summarized in Table 5.1-1, because the appropriate error covariance equations are linear.

All of the example curves given in this section correspond to major contributors to the system performance. Similar sensitivity curves

may be constructed for any error source group for which error budget data exists in Table 5.1-1. Sensitivity curves corresponding to error sources which produce minor contributions when their nominal values are assumed are quite flat and of little interest.

To illustrate the means by which the data points for the sensitivity curves were calculated an example will be given. The sensitivity of downrange position at touchdown to gyro bias drift is shown in Fig. 5.1-3a. The baseline data point, 28.7 ft, is the total system error, which includes the effect of a 0.01 deg/hr bias drift about each platform axis. The contribution of these bias drifts is shown in Table 5.1-1 to be 17.8 ft. To compute the effect of a 0.03 deg/hr gyro drift the 0.01 deg/hr bias drift contribution is removed from the total system error and replaced with an error which is three times as large. Thus:

$$\sigma_D = \left[(28.7)^2 - (17.8)^2 + (53.4)^2\right]^{1/2}$$

$$= 57.9 \text{ ft}$$

This result is indicated in Fig. 5.1-3 as a boxed-in point. Also shown on the curve is the specification value for downrange position error (80 ft) and the corresponding gyro drift which would cause it (0.043 deg/hr) can be found from the curve. The dashed line through the origin is the asymtote approached by the total system error curve as the gyro bias drift contribution becomes large and dominates all others. The remaining points on the curve are obtained as illustrated above.

Figure 5.1-4 shows the sensitivity of vertical position and velocity errors to variations in the accelerometer misalignment angles. It is evident that the vertical velocity error won't meet the spec (0.2 ft/sec)

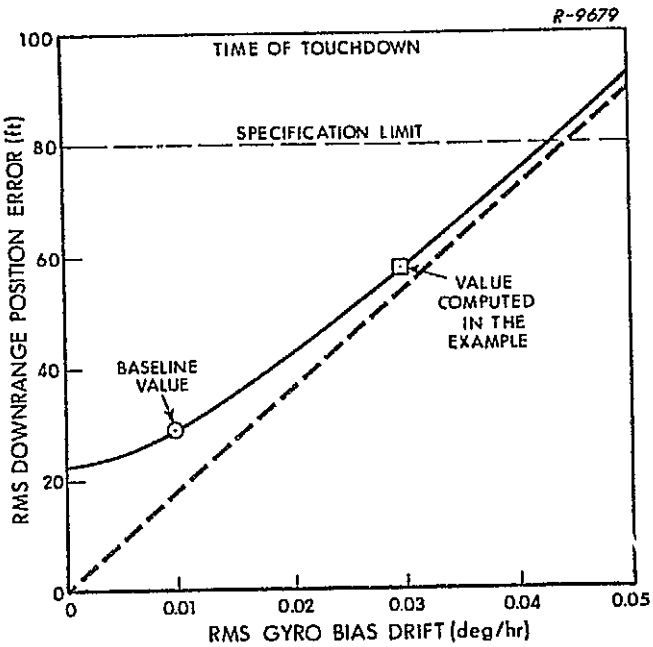

(a) Position

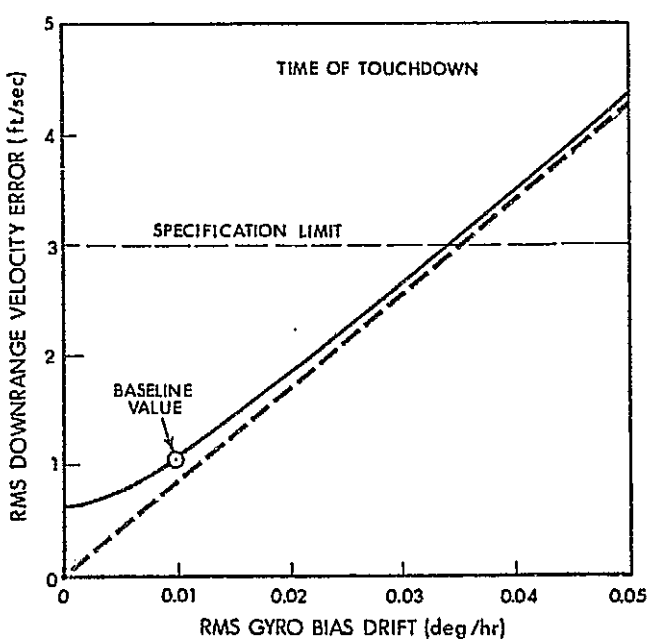

(b) Velocity

Figure 5.1-3 Sensitivity of Downrange Position and Velocity Errors at Touchdown to Gyro Bias Drift: System A

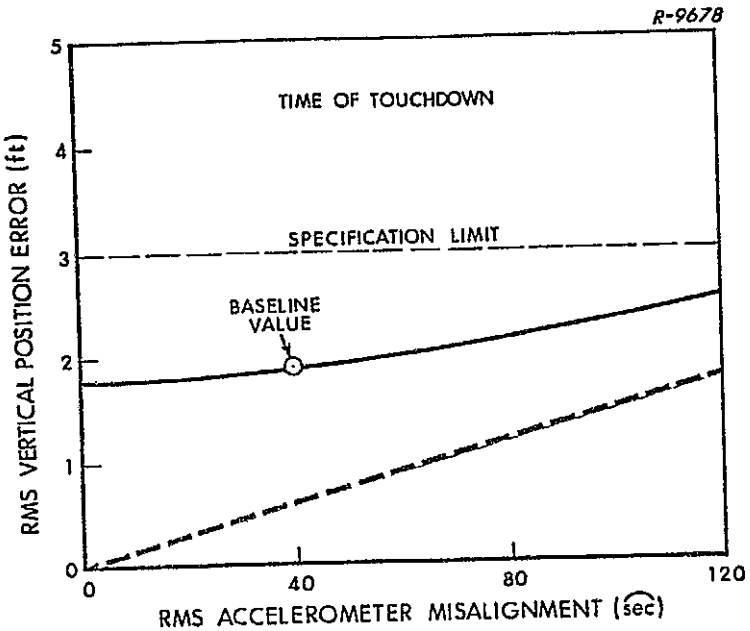

(a) Position

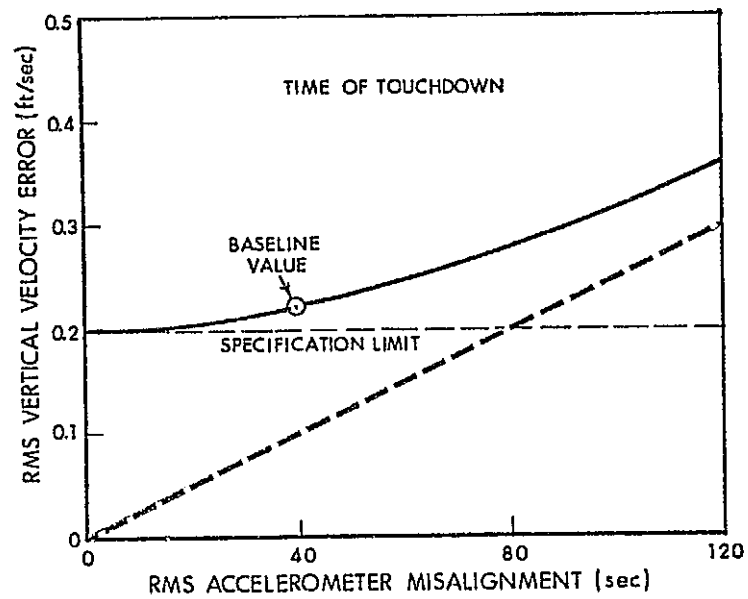

(b) Velocity

Figure 5.1-4 Sensitivity of Vertical Position and Velocity Errors at Touchdown to Accelerometer Misalignment: System A

even if the accelerometer misalignment is very small. That is, the other system error sources cause the system to just barely meet spec even with no accelerometer misalignment.

The data of Fig. 5.1-5 shows the sensitivity of vertical position error to radar altimeter markov error. The radar altimeter markov error standard deviation is a function of altitude. Thus, the ratio of the assumed function to the baseline function is used as the independent variable in this figure.

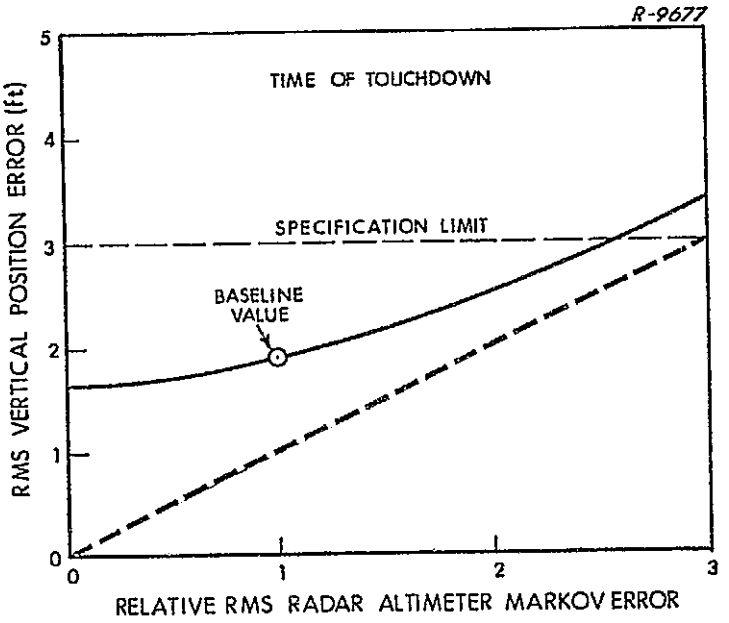

Figure 5.1-5 Sensitivity of Vertical Position Error at Touchdown to Radar Altimeter Markov Error: System A

Figures 5.1-6, 5.1-7 and 5.1-8 plot the sensitivity of crossrange errors to their three largest contributors. Figure 5.1-6 is a plot of crossrange position error as a function of localizer markov error. As in Fig. 5.1-5, the independent variable of Fig. 5.1-6 is the ratio of the assumed to the baseline function used to generate the data of Table 5.1-1.

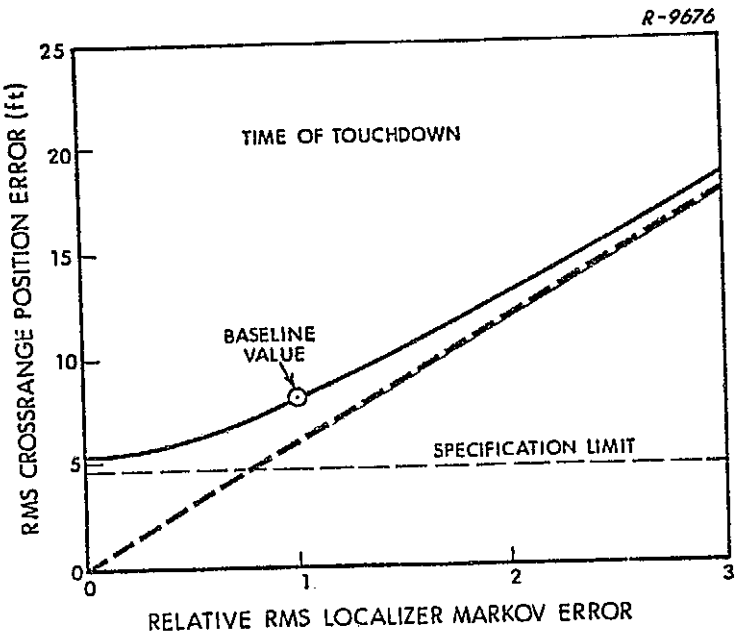

Figure 5.1-6 Sensitivity of Crossrange Position Error at Touchdown to Localizer Markov Error: System A

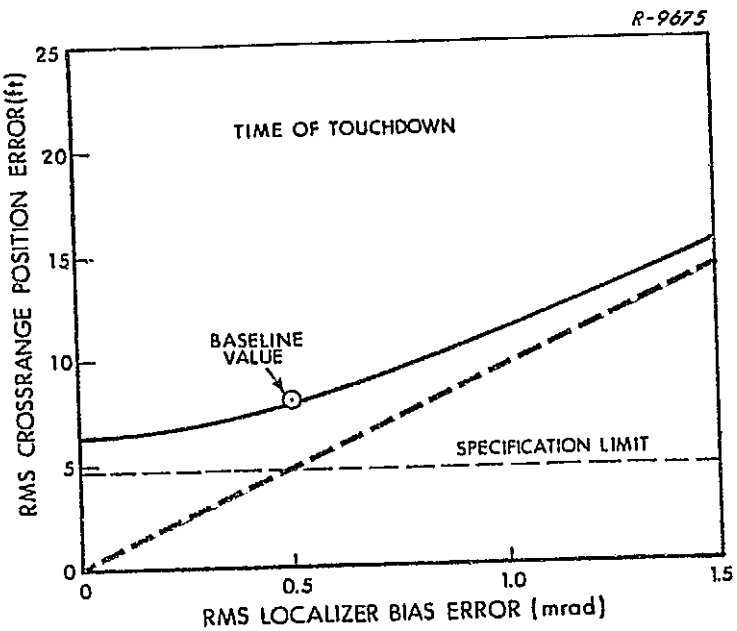

Figure 5.1-7 Sensitivity of Crossrange Position Error at Touchdown to Localizer Bias Error: System A

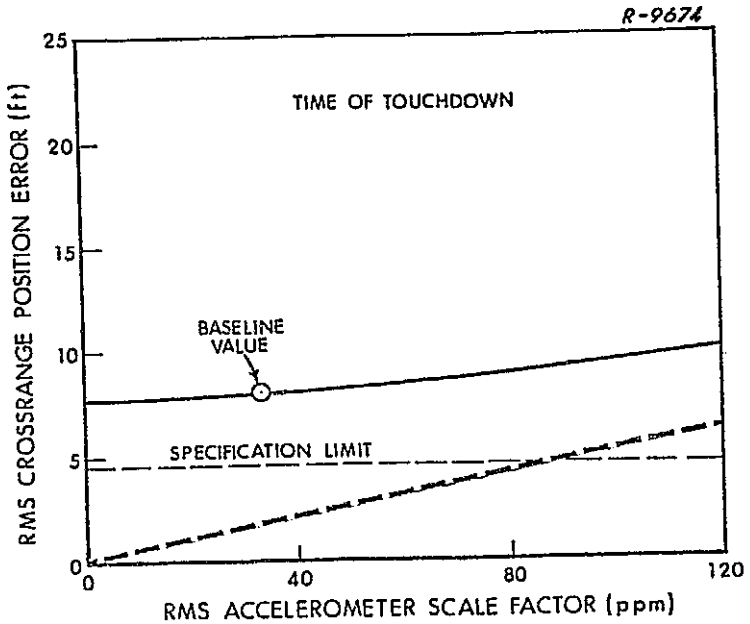

(a) Position

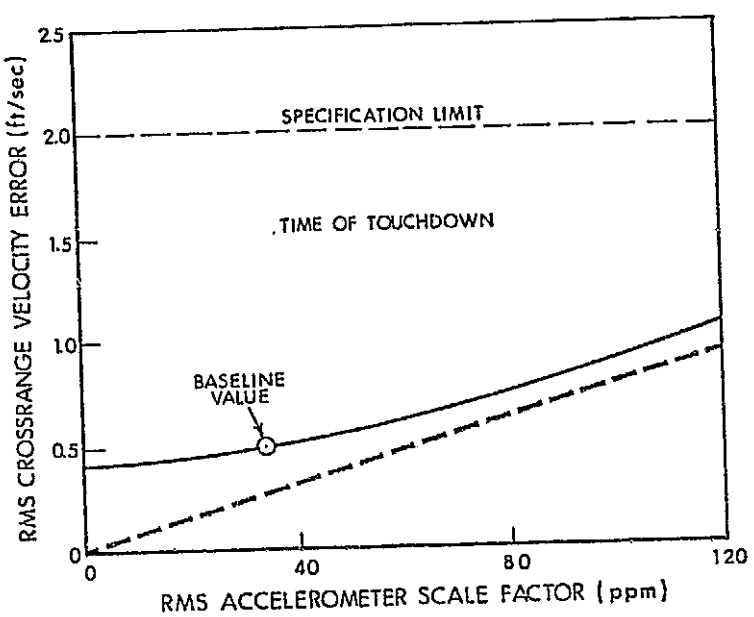

(b) Velocity

Figure 5.1-8 Sensitivity of Crossrange Position and Velocity Errors at Touchdown to Accelerometer Scale Factor Errors: System A

This is a result of the fact that the localizer markov error standard deviation is a function of the slant range to the ILS localizer antenna. Note that the spec is exceeded for all values of this error because of the other error source contributions. The crossrange position error is also exceeded for all values of localizer bias error as shown in Fig. 5.1-7. The final figure in this section, Fig. 5.1-8, shows the sensitivity of crossrange position and velocity to accelerometer scale factor error. Again, there is no value of accelerometer scale factor error for which the crossrange position error specification is met.

5.2 SYSTEM B EVALUATION

The results presented below correspond to the trajectory and measurement schedule described in Section 2 -- exactly the same as that used in the System A evaluation. A file of gain values, generated using the 6-state, square root filter covariance program described in Section 5.2, has been used repeatedly to compute detailed error contributions for this trajectory and measurement schedule.

5.2.1 Overall System Performance

Figures 5.2-1 and 5.2-2 present overall performance curves for System B, showing position error components and velocity error components, respectively. The curves plotted represent rms errors due to the combined effects of all error source groups in the baseline error budget. They were generated by root-sum-squaring individual contributions

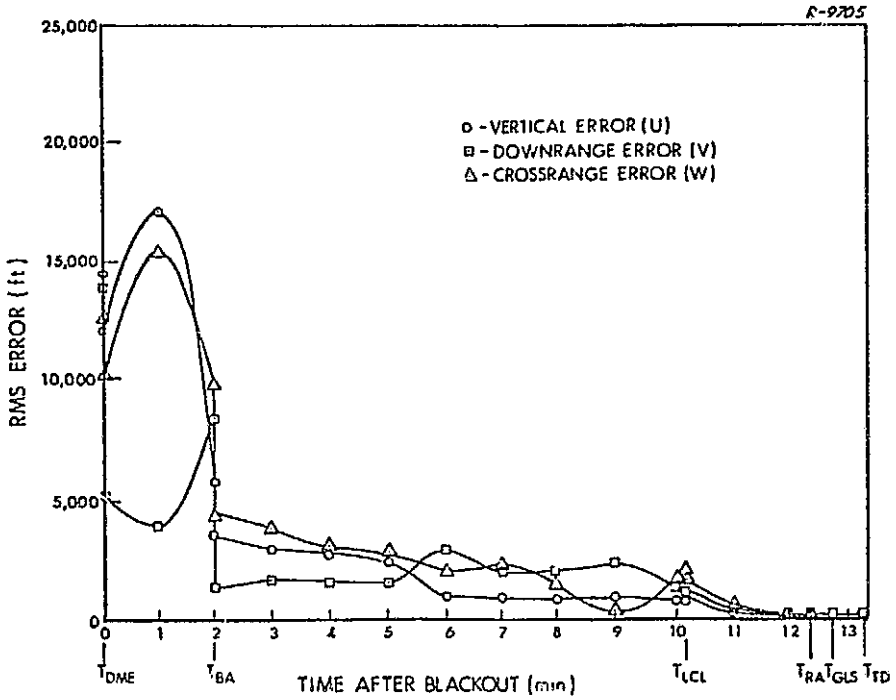

Figure 5.2-1 System B Overall Performance: Position

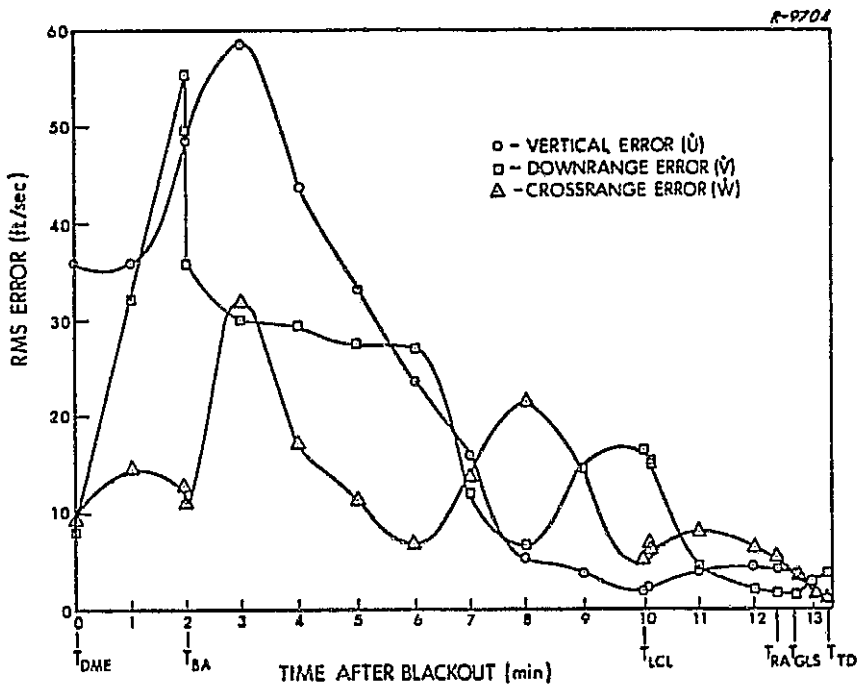

Figure 5.2-2 System B Overall Performance: Velocity

at one minute intervals. (This data is tabulated in Appendix C.) At T_{DME}, when the first DME measurements are made, and at other key times, such as T_{BA}, T_{LCL}, T_{RA} and T_{GLS}, the root-sum-square calculation was performed both before and after update. Thus, the large jumps in certain component errors, which occur at these times, are accurately shown. Otherwise, the curves are faired-in over the one-minute intervals between the calculated points.

At the time of the first DME measurements, T_{DME}, all of the position error components decrease. (Since a diagonal initial filter covariance matrix was used, no "wrong way" corrections can occur.) Following the first update the position errors generally increase over the next one or two minutes. All are reduced considerably at the time of the first baro-altimeter measurement, T_{BA}. Two of the velocity component errors increase significantly over the first three minutes. Examination of the individual contributions (as tabulated in Appendix C) shows that the major cause of these increases in position and velocity errors are the unmodeled DME bias and scale factor errors. The "humps" in the velocity component error curves near t = 8 minutes and t = 10 minutes are also largely due to the unmodeled DME errors, especially scale factor errors.

All three position error components for System B are reasonably small and well-behaved after the baro-altimeter comes into use, at T_{BA}. While the errors are generally larger than the corresponding System A errors, the problem of the large vertical errors prior to T_{RA} (exhibited by System A -- see Section 3.1-1) is avoided.

Section 6 contains further discussions of the implications of the performance curves presented in this section.

5.2.2 Detailed Error Budget

System error covariances have been calculated for each group of error sources over the entire 796 second trajectory. Table 5.2-1 is the System B Baseline Error Budget showing rms estimation errors in position, velocity and platform alignment components at touchdown. Each value is the rms contribution of the error source or sources indicated in the left hand column; it comes from a computer run in which the elements of those errors alone are set at truth-model values -- and all others are zero. The overall System B performance, or root-sum-square values, are given at the bottom of the table and compared, first with the filter's own estimate of performance based on its simplified 6-state model of system error dynamics, and second with the Shuttle landing navigation specification given in Ref. 1. Table 5.2-2 lists the System B Alternative Contributions showing how different assumptions or additional error sources would produce other contributions to position, velocity and alignment errors at touchdown.

Particular numbers have been circled in the position and velocity error columns of Table 5.2-1 to focus attention on major contributors. The rule followed in deciding which numbers to circle was to include, in any one column, the largest value, second largest value, etc., until 95% of the RSS total value was reached. The following general statements may be drawn from an examination of the System B baseline error budget:

- The projected downrange performance, in both position and velocity, is slightly out-of-spec, and the filter-indicated performance is over-optimistic by a wide margin. The largest contributors to downrange errors are DME bias errors (Group 10). Other significant error sources are gyro bias drifts (Group 7), baro-altimeter bias and scale factor errors (Group 12), radar altimeter markov error (Group 15) and glide slope bias error (Group 13).

TABLE 5.2-1

SYSTEM B BASELINE ERROR BUDGET

Error Source	Value	RMS Navigation Errors at Touchdown								
		Position (ft)			Velocity (ft/sec)			Misalignment (mrad)		
		Vertical	Downrange	Crossrange	Vertical	Downrange	Crossrange	Vertical	Downrange	Crossrange
I. UNCORRELATED NOISE										
Group 1. IMU Quantization Noise	One Pulse - cm/sec	0.2	2.7	0.4	0.05	0.14	0.08	0	0	0
Measurement Noises										
DME's	24 ft	—	0.7	—	—	0.02	—	0	0	0
Radar Altimeter	3.28 ft	(1.0)	6.9	0.1	(0.10)	0.10	0.01	0	0	0
II. IMU-RELATED STATES										
Group 2. Accelerometer Biases	60 μg	0.1	1.6	0.2	0.02	0.05	0.02	0.027	0.060	0.054
Group 3. Accelerometer Scale Factor Errors	34 ppm	—	0.7	0.1	0.01	0.03	0.01	—	—	—
Group 4. Accelerometer Misalignments	40 sec	0.2	4.1	0.5	0.04	0.16	0.06	0.088	0.192	0.173
Group 5. Accelerometer Nonlinearities	3.5 $\mu g/g^2$	—	0.1	—	—	0.01	—	0	0	0
Group 6. Gravity Anomalies and Deflections	see Table 3.1-2	0.1	1.2	0.2	0.01	0.05	0.02	0	0	0
Group 7. Gyro Bias Drifts	0.01 deg/hr	0.1	(21.4)	(2.0)	0.04	(1.11)	(0.28)	0.604	0.372	0.637
Group 8. Gyro Mass Unbalances	0.015 deg/hr/g	—	1.8	0.2	—	0.10	0.02	0.105	0.032	0.057
Group 9. Gyro Anisoelasticity	0.005 deg/hr/g^2	—	—	—	—	—	—	0.001	0.001	0.001
III. EXTERNAL-AID RELATED STATES										
Group 10. DME Bias Errors	295 ft	(0.3)	(59.2)	1.2	(0.12)	(3.13)	0.10	0	0	0
Group 11. DME Scale Factor Errors	100 ppm	(0.3)	6.0	(2.0)	(0.19)	0.48	(0.68)	0	0	0
Group 12. Baro Altimeter Errors										
Bias and Scale Factor	100 ft / 0.03	(0.3)	(36.0)	1.0	0.01	(1.04)	0.07	0	0	0
Markov and Measurement Noise	20 ft / 5 ft	—	2.7	—	—	0.07	—	0	0	0
Static Defect	1.52×10^{-4} ft/(ft/sec)^2	0.1	7.4	0.1	—	0.20	0.01	0	0	0
Group 13. ILS Bias Errors										
Localizer	0.5 mrad	—	0.8	(4.9)	—	0.01	0.18	0	0	0
Glide Slope	0.5 mrad	(0.3)	(22.4)	—	0.03	0.16	0.01	0	0	0
Group 14. ILS 2nd Order Markovs										
Localizer	Eq. (3.1-44)	0.1	1.2	(6.9)	0.01	0.02	(0.43)	0	0	0
Glide Slope	Eq. (3.1-45)	0.2	11.9	0.2	0.01	0.02	0.01	0	0	0
Group 15. Radar Altimeter Markov	Eq. (3.1-43)	(1.8)	(32.2)	0.2	(0.21)	0.28	0.01	0	0	0
Group 16. DME Survey Errors	1 ft	—	0.2	—	—	0.01	—	0	0	0
Group 17. ILS Survey Errors										
Localizer	1 ft	—	0.1	1.0	—	—	—	0	0	0
Glide Slope	1 ft	—	14.4	0.1	0.02	0.18	—	0	0	0
Total Projected Performance (root-sum-square)		2.2	85.6	9.1	0.34	3.60	0.89	0.620	0.425	0.664
Filter-Indicated Performance		1.4	21.3	4.1	0.19	0.48	0.26	Not Estimated		
Specification (Ref. 6)		3.0	80.0	4.7	0.20	3.00	2.00	Not Specified		

A "—" entry refers to a negligibly small contribution.
A "0" entry represents an identically zero contribution.

TABLE 5.2-2

SYSTEM B ALTERNATIVE CONTRIBUTIONS

Error Source	Value	RMS Navigation Errors at Touchdown								
		Position (ft)			Velocity (ft/sec)			Misalignment (mrad)		
		Vertical	Downrange	Crossrange	Vertical	Downrange	Crossrange	Vertical	Downrange	Crossrange
Group 1. Initial 9 × 9 Covariance Matrix (Position, Velocity and Alignment)	See Section 3.1.3	0.1	21.5	2.1	0.04	1.1	0.5	0.657	0.335	0.640
Initial 6 × 6 Covariance Matrix (Position and Velocity only)		—	—	—	—	—	—	0	0	0
Group 18. ILS First-Order Markovs										
Localizer	Eq. (3.1-44)	0.1	1.9	11.6	0.02	0.05	0.74	0	0	0
Glide Slope	Eq. (3.1-45)	0.3	17.9	0.3	0.03	0.27	0.02	0	0	0
Group 15. Radar Altimeter Errors										
Bias	1 ft	1.0	14.2	0.1	0.02	0.17	—	0	0	0
Scale Factor	0.025	—	58.9	0.4	0.28	0.43	—	0	0	0

- The projected vertical performance is within spec in position, but out-of-spec in velocity. The filter indicated performance is somewhat optimistic -- 35% off in position, 45% off in velocity. The largest contributors to vertical errors are the radar altimeter markov error (Group 15) and DME scale factor errors (Group 11). Other significant error sources are DME bias errors (Group 10), radar altimeter measurement noise (Group 1), baro-altimeter bias and scale factor errors (Group 17) and glide slope bias (Group 13).

- The projected crossrange performance is within spec in velocity, but out-of-spec in position. The filter-indicated performance is over-optimistic by a wide margin. The largest contributors to cross-range errors are localizer errors (Groups 13 and 14). Other significant contributions are those of DME scale factor errors (Group 11) and gyro bias drifts (Group 7).

- The projected platform misalignments (which are not estimated by the System B filter) are in the range from 0.4 to 0.7 milliradians.

Considering all components of position and velocity errors at touchdown, the list of major contributors includes gyro errors, accelerometer errors, and errors associated with all of the external devices including, in this case, the baro altimeter. More detailed discussion of the important error mechanisms and possible ways to reduce some of the contributions is given in Section 6.

Detailed tabulations of the error contribution time histories are given in Appendix C. For every row in Tables 5.2-1 and 5.2-2 there is a page in Appendix C, which is a reproduction of a computer print-out page summarizing important results from one error budget run.

5.2.3 Sensitivity Curves: System B

This section contains several curves illustrating the sensitivity of System B performance to variations in error source statistics. These curves were produced using the error budget data of Table 5.2-1. The method of generating the data for these curves is discussed in Section 5.1.2.

Similar sensitivity curves may be constructed for any error source group for which error budget data is available in Table 5.2-1. All of the error curves in this section correspond to major contributors to system performance. Sensitivity curves corresponding to error sources which produce minor contributions are quite flat.

Figure 5.2-3 shows the sensitivity of downrange position and velocity errors to DME bias errors. For System B the downrange errors do not meet the spec for either position or velocity unless the DME bias is less than the baseline value. This inability to meet spec results from the fact that the filter does not calibrate the DME 1 bias error, as the Shuttle passes over it, as is done by the System A filter. A further discussion of this problem may be found in Section 6.

The downrange position and velocity error sensitivities to gyro bias drift are shown in Fig. 5.2-4. Note that the sensitivity of System B to gyro bias drift is greater than that of System A. This is also discussed in Section 6.

The position and velocity error sensitivity to radar altimeter markov error is shown in Fig. 5.2-5. The independent variable in this curve is the ratio of the assumed standard deviation of the markov error to the baseline value. This is done since the baseline standard deviation is a function of altitude as given by Eq. (3.1-43).

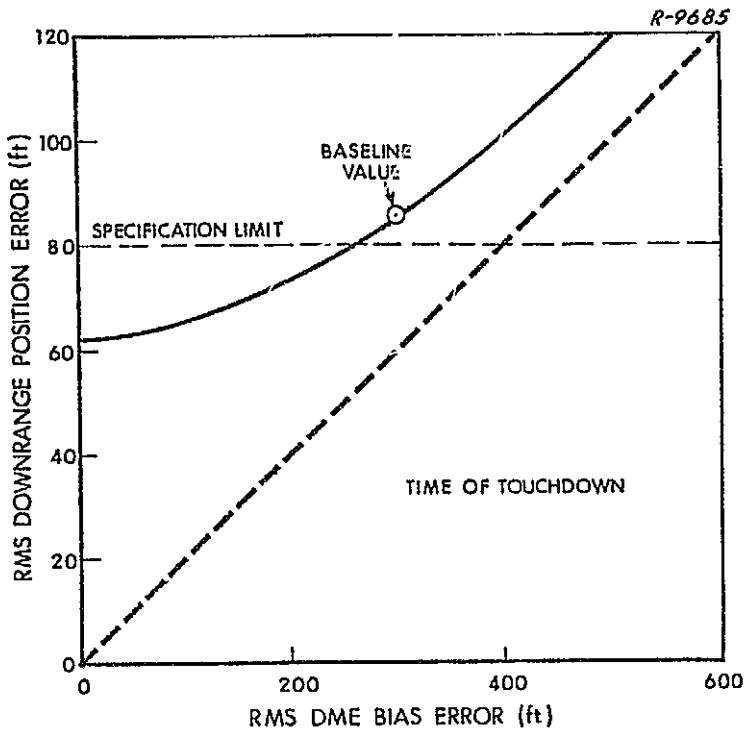

(a) Position

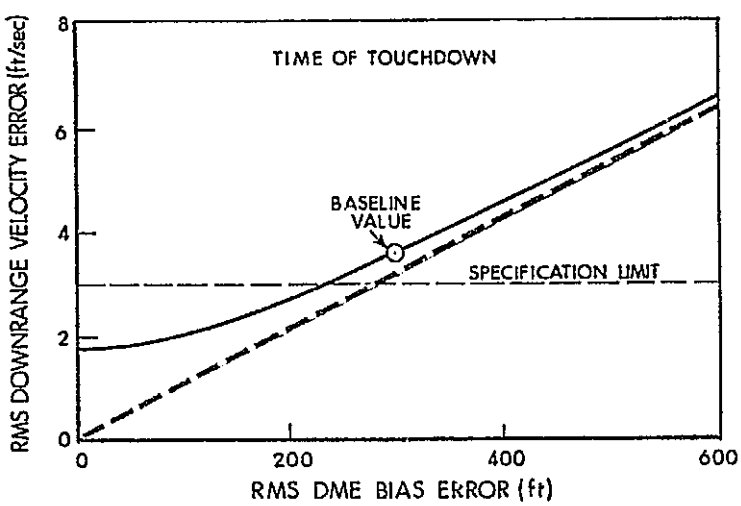

(b) Velocity

Figure 5.2-3 Sensitivity of Downrange Position and Velocity Errors at Touchdown to DME Bias Errors: System B

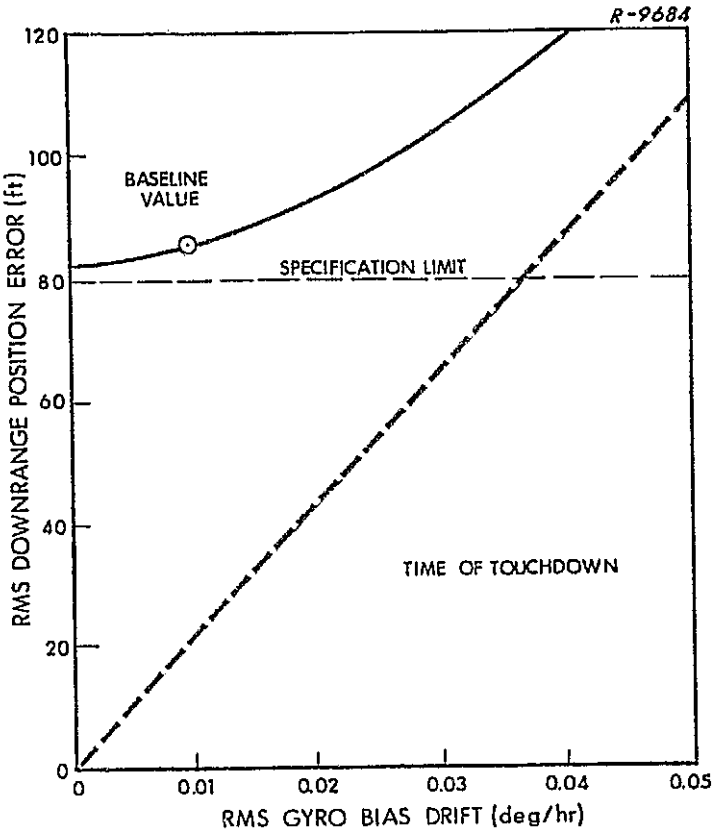

(a) Position

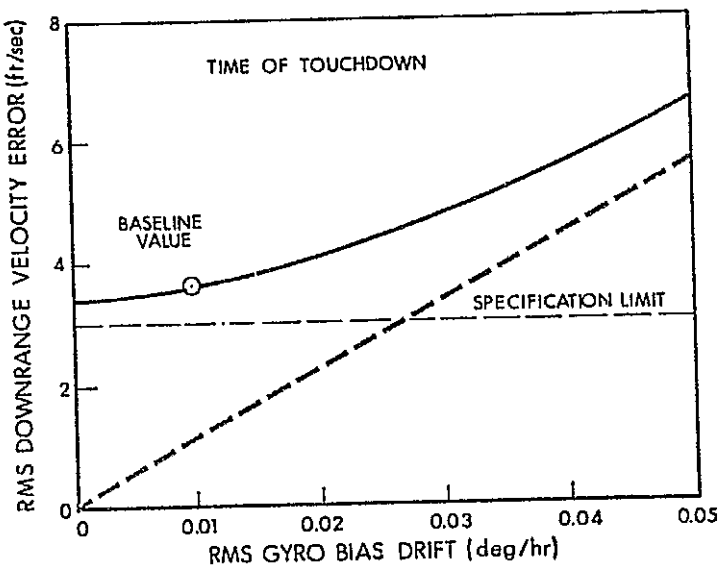

(b) Velocity

Figure 5.2-4 Sensitivity of Downrange Position and Velocity Errors at Touchdown to Gyro Bias Drift: System B

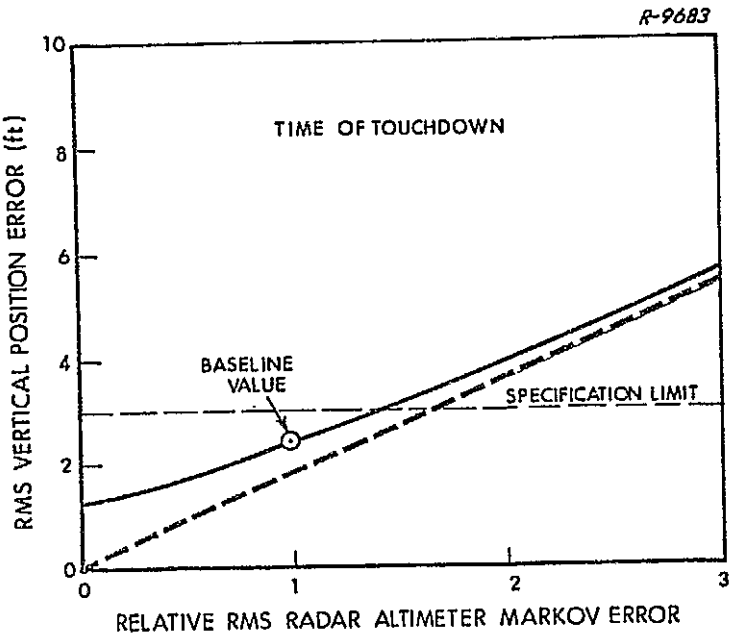

(a) Position

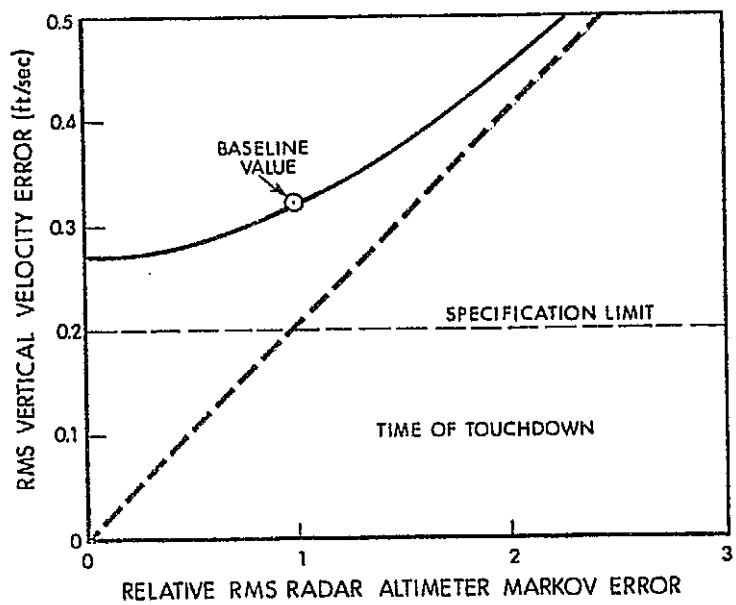

(b) Velocity

Figure 5.2-5 Sensitivity of Vertical Position and Velocity Errors at Touchdown to Radar Altimeter Markov Error: System B

Figure 5.2-6 shows the sensitivity of vertical velocity to DME scale factor error. The vertical velocity does not meet the spec for any value of DME scale factor error.

Figure 5.2-7 shows crossrange position sensitivity as a function of localizer markov error. The independent variable is again a ratio of assumed standard deviation to the baseline given by Eq. (3.1-44). It should be noted that the contributions to System A and to System B of this error source are similar. This is observed by noting the slopes of the straight lines in Figs. 5.1-6 and 5.2-7.

The final figure of this section, Fig. 5.2-8, indicates the sensitivity of crossrange position errors to gyro bias drift rate. This sensitivity of System B to gyro bias error results from the fact that the System B filter does not try to estimate platform misalignment.

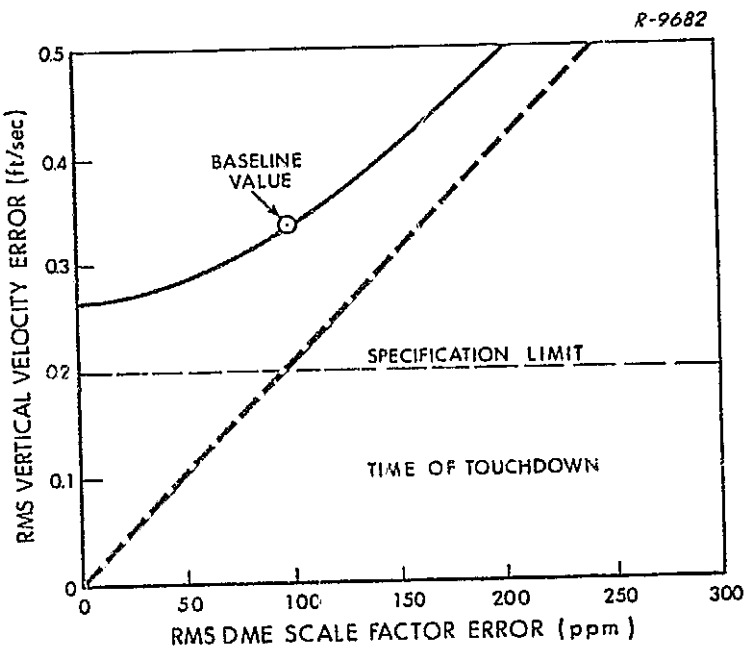

Figure 5.2-6 Sensitivity of Vertical Velocity Error at Touchdown to DME Scale Factor Error: System B

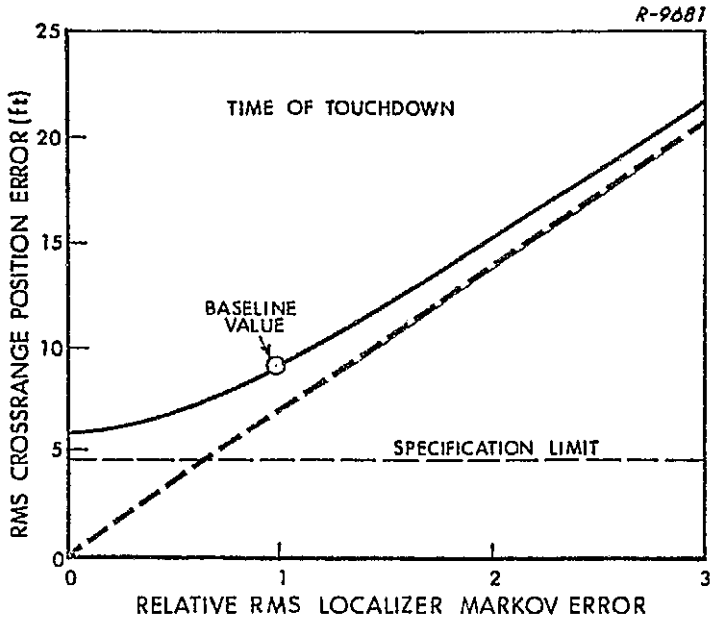

Figure 5.2-7 Sensitivity of Crossrange Position Error at Touchdown to Localizer Markov Error: System B

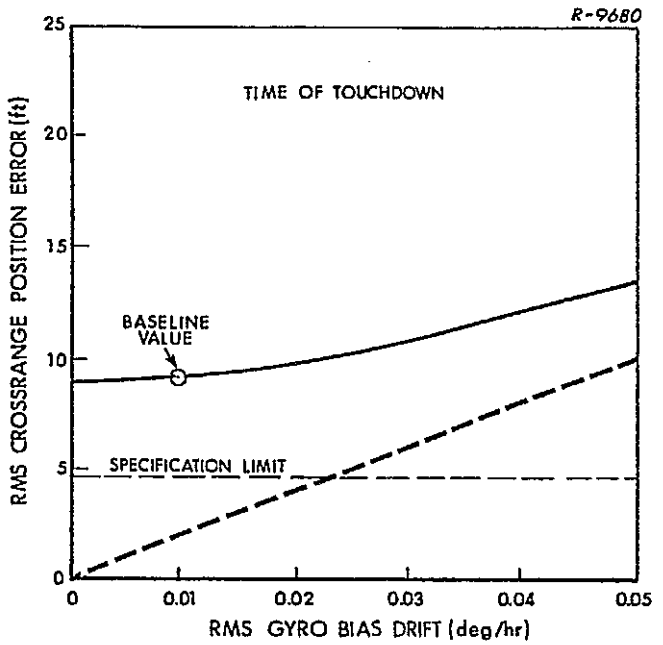

Figure 5.2-8 Sensitivity of Crossrange Position Error at Touchdown to Gyro Bias Drift: System B

5.3 SYSTEM C EVALUATION

The results presented below correspond to the trajectory and measurement schedule described in Section 2, employing a 2 second update interval for the first 720 seconds and a 0.5 second interval for the final 76 seconds. A file of gain values, generated using the 22-state filter described in Section 4.3, has been used repeatedly to compute detailed error contributions for this trajectory and measurement schedule.

5.3.1 Overall System Performance

Figures 5.3-1 and 5.3-2 present overall performance curves for System C, showing position error components and velocity error components, respectively. The curves plotted represent rms errors due to the combined effects of all error source groups in the baseline error budget. They were generated by root-sum-squaring individual contributions at one minute intervals. (These are tabulated in Appendix C.) At T_{OWD}, when the first doppler measurement is made, and at T_{BA}, when the first baro altimeter measurement is made, the root-sum-square calculation was performed both before and after update. Thus, the large jumps in certain component errors, which occur at these two times, are accurately shown. Otherwise, the curves are faired-in over the one-minute intervals between the calculated points.

At the time of the first one-way doppler measurement, T_{OWD}, some of the position and velocity component errors increase. This reflects the fact that the initial filter covariance matrix does not accurately represent the assumed real-world covariance -- just as in the System A evaluation (although the same components do not increase in both cases).

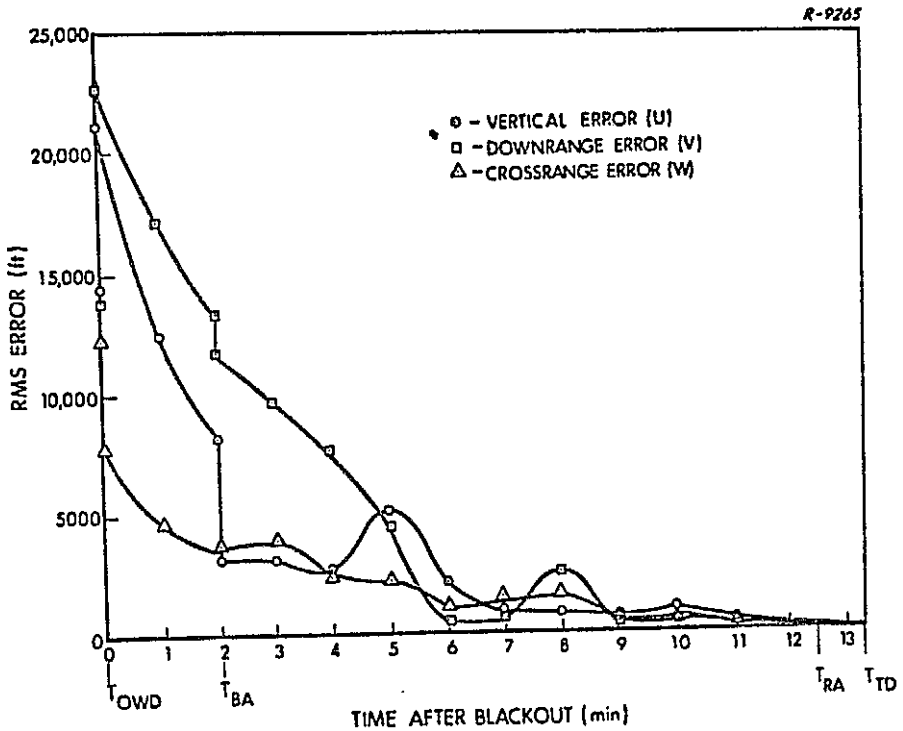

Figure 5.3-1 System C Overall Performance: Position

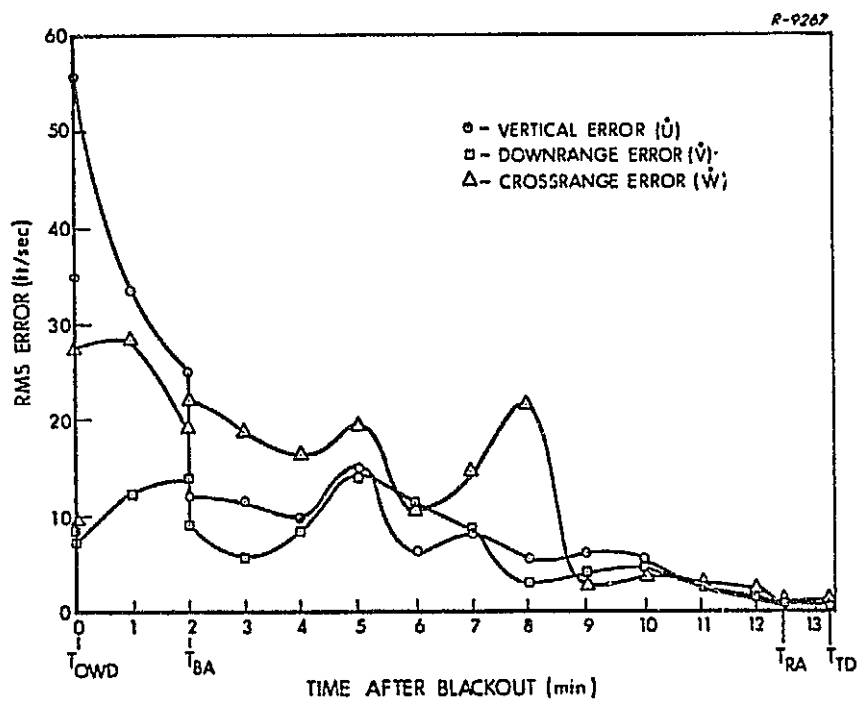

Figure 5.3-2 System C Overall Performance: Velocity

Errors then decrease rapidly over the three or four minutes following the first update. Note, especially, the large decreases in vertical position and velocity errors at T_{BA}, the time of the first baro-altimeter measurement. Figures 5.3-1 and 5.3-2 also show pronounced "humps" in certain component errors near t = 5 minutes and t = 8 minutes. The former corresponds to the interval, near Mach 1, during which baro-altimeter measurements are inhibited. The latter corresponds to a rather sharp turning maneuver. The largest single contributor during this turning maneuver is the error in antenna motion compensation. However, other contributions increase significantly at this time also.

Figure 5.3-3 re-plots the position error components over the final two minutes with an expanded scale. The most striking feature of these curves is the sharp reduction in the downrange error just after the t = 13 minutes point. This is the time at which the vehicle overflies the doppler beacon. The filter evidently is able to remove the remaining "constant of integration" error (see discussion by Lear in Ref. 10) when this overflight occurs. It is likely that the reduction would occur at an earlier time if the beacon were moved farther from the end of the runway.

Section 6 contains further discussion of the implications of the performance curves presented in this section.

5.3.2 Detailed Error Budget

The System C baseline error budget is given in Table 5.3-1, showing rms estimation errors in position, velocity and platform alignment components at touchdown. Each value is the rms contribution of the error source or sources indicated in the left hand column; it comes

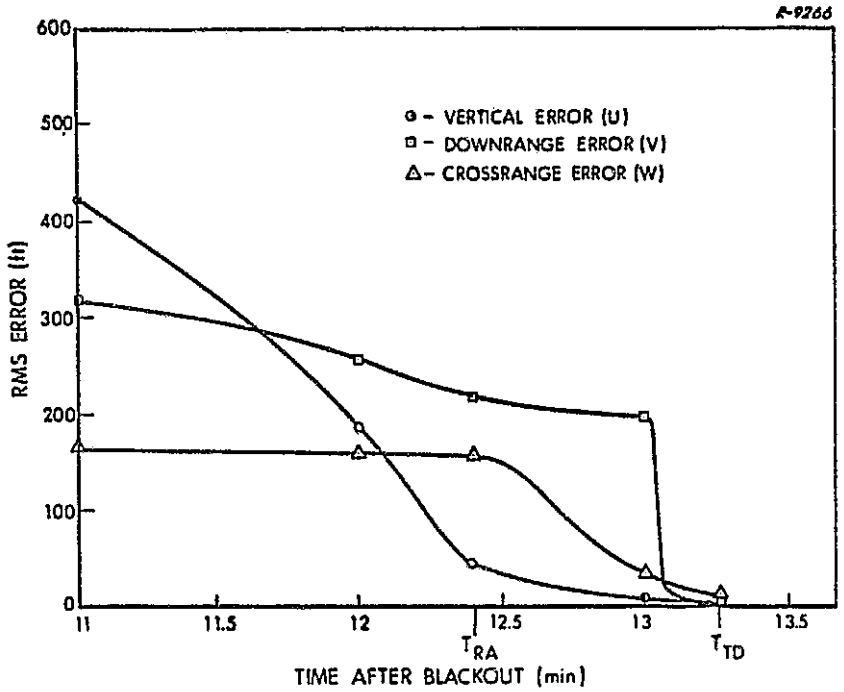

Figure 5.3-3 System C Final Approach Performance

from a computer run in which the elements of those errors alone are set at truth-model values -- and all others are zero. The overall System C performance, or root-sum-square values, are given at the bottom of the table and compared, first with the filter's own estimate of performance based on its simplified 22-state model of system error dynamics, and second, with the Shuttle landing navigation specification given in Ref. 1. Particular numbers have been circled in the position and velocity error columns of Table 5.3-1 to focus attention on major contributors. The rule followed in deciding which numbers to circle was to include, in any one column, the largest value, second largest value, etc., until 95% of the RSS total value was reached. The following general statements may be drawn from an examination of the System C baseline error budget:

TABLE 5.3-1

SYSTEM C BASELINE ERROR BUDGET

Error Source	Value	RMS Navigation Errors at Touchdown								
		Position (ft)			Velocity (ft/sec)			Misalignment (mrad)		
		Vertical	Downrange	Crossrange	Vertical	Downrange	Crossrange	Vertical	Downrange	Crossrange
I. ESTIMATED STATES AND NOISES										
Group 1. IMU Quantization Noise	One Pulse = 1 cm/sec	0.5	0.6	3.4	0.12	0.07	0.35	0.104	0.056	0.042
Measurement Noises										
One-Way Doppler	0.0357 ft	0.2	0.3	0.5	0.07	0.03	0.04	0.034	0.005	0.005
Radar Altimeter	3.28 ft	1.0	—	0.5	0.05	—	—	0.001	0.001	0.001
Radar Altimeter Markov	Eq. (3.1-43)	1.7	0.1	1.3	0.11	0.02	0.01	0.001	0.003	0.004
Doppler Rate Bias Errors										
Onboard	0.0876 ft/sec	0.4	1.8	1.5	0.09	0.15	0.08	0.029	0.009	0.036
Ground	0.0044 ft/sec	—	0.1	0.1	—	0.01	—	0.002	0.001	0.002
II. IMU-RELATED STATES										
Group 2. Accelerometer Biases	60 μg	0.6	1.8	1.3	0.12	0.01	0.16	0.560	0.059	0.060
Group 3. Accelerometer Scale Factor Errors	34 ppm	0.4	0.2	5.0	0.07	0.01	0.48	1.688	0.021	0.025
Group 4. Accelerometer Misalignments	40 sec	1.3	0.3	2.9	0.26	0.03	0.30	0.214	0.169	0.189
Group 5. Accelerometer Nonlinearities	$3.5\ \mu g/g^2$	—	—	0.1	0.01	—	—	0.002	0.002	0.001
Group 6. Gravity Anomalies and Deflections	see Table 3.1-2	0.4	0.1	0.8	0.09	0.01	0.01	0.027	0.025	0.019
Group 7. Gyro Bias Drift Rates	0.01 deg/hr	0.2	0.2	3.8	0.05	0.01	0.33	0.921	0.025	0.014
Group 8. Gyro Mass Unbalance	0.015deg/hr/g	0.1	0.1	0.9	0.02	—	0.08	0.248	0.010	0.007
Group 9. Gyro Anisoelasticity	$0.005 deg/hr/g^2$	—	—	—	—	—	—	0.005	0.001	0.001
III. EXTERNAL-AID RELATED STATES										
Group 10. Doppler Errors										
Rapid Changes in Rate Bias	0.01 ft/sec	—	0.1	0.3	0.01	0.01	0.03	0.009	0.004	0.002
Motion Compensation Errors	0.5 ft	0.6	0.8	5.6	0.10	0.11	0.65	1.171	0.076	0.054
Group 12. Baro Altimeter Errors										
Bias and Scale Factor	100 ft 0.03	—	—	—	—	—	—	—	—	—
Markov and Measurement Noise	20 ft 5 ft	—	—	—	—	—	—	—	—	—
Static Defect	1.52×10^{-4} ft/(ft/sec)^2	—	—	—	—	—	—	—	—	—
Group 15. (Not included in Baseline Error Budget)										
Group 16. One-Way Doppler Survey Survey Errors	1 ft	—	1.0	1.3	0.01	—	0.01	0.001	0.001	—
Total Projected Performance (root-sum-square)		2.6	3.0	10.0	0.39	0.21	1.01	2.346	0.207	0.216
Filter-Indicated Performance		2.1	0.6	3.5	0.21	0.06	0.33	0.264	0.065	0.055
Specification (Ref. 1)		3.0	80.0	4.7	0.20	3.0	2.0	Not Specified		

A "—" entry refers to a negligibly small contribution.

- The projected downrange performance, in both position and velocity, is far more accurate than called for in the preliminary specifications. The filter-indicated performance is even better. Significant contributors are doppler rate bias error (Group 1), accelerometer biases (Group 2), antenna motion compensation errors (Group 10), doppler survey errors (Group 16) and IMU quantization noise (Group 1).

- The projected vertical performance is within spec in position, but out-of-spec in velocity. The filter-indicated performance is within 20% of the projected actual performance in position, but almost 50% off in velocity -- erring on the optimistic side. The largest contributors to vertical velocity errors are the accelerometer misalignments (Group 4) -- contributing 0.26 ft/sec compared to a total of 0.39 ft/sec, against a spec of 0.20 ft/sec. Other significant contributors to vertical errors are radar altimeter errors (Group 1), doppler onboard rate bias error (Group 1), IMU quantization noise (Group 1), accelerometer biases (Group 2), gravity anomalies (Group 6) and antenna motion compensation errors (Group 10).

- The projected crossrange performance is within spec in velocity but out-of-spec in position. The filter-indicated performance, in both position and velocity, is optimistic -- predicting approximately one third of the projected actual rms errors. The largest contributors to crossrange errors are accelerometer scale factor errors (Group 3) and antenna motion compensation errors (Group 10). Other significant contributors are IMU quantization noise (Group 1), accelerometer misalignments (Group 4) and gyro bias drifts (Group 7).

- The projected errors in estimating platform misalignments are approximately 0.2 milliradians for misalignments about level axes, and 2.3 milliradians for azimuth misalignment. The filter-indicated performance is considerably better for all three axes. The projected rms azimuth estimation error is larger than the actual rms misalignment (0.62 mrad) -- shown as the rss vertical misalignment at the bottom of the System B error budget.

Considering all components of position and velocity errors at touchdown, the list of major contributors includes gyro errors, accelerometer errors, and errors associated with all of the external devices except the baro altimeter. The overall performance projected for System C is similar to that of System A. Significant improvement is probably possible in crossrange position and vertical velocity performance, as discussed in Section 6.

Table 5.3-2 lists the System C Alternative Contributions showing how different assumptions or additional error sources would produce other contributions to position, velocity and alignment errors at touchdown. Detailed tabulations of the error contribution time histories are given in Appendix C. For every row in Tables 5.3-1 and 5.3-2 there is a page in Appendix C, which is a reproduction of a computer printout page summarizing important results from one error budget run.

5.3.3 Sensitivity Curves: System C

This section contains several curves illustrating the sensitivity of System C performance to variations in major error source statistics. These curves were produced using the error budget data of Table 5.3-1. The method of generating the data for these curves is discussed in Section 5.1.3. Similar sensitivity curves may be constructed for any error source group for which error budget data is available in Table 5.3-1.

TABLE 5.3-2

SYSTEM C ALTERNATIVE CONTRIBUTIONS

Error Source	Value	RMS Navigation Errors at Touchdown								
		Position (ft)			Velocity (ft/sec)			Misalignment (mrad)		
		Vertical	Downrange	Crossrange	Vertical	Downrange	Crossrange	Vertical	Downrange	Crossrange
Group 1. Initial 9 × 9 Covariance Matrix (Position, Velocity and Alignment)	See Section 3.1.3	0.3	0.3	6.9	0.05	0.01	0.65	2.082	0.030	0.028
Initial 6 × 6 Covariance Matrix (Position and Velocity only)		0.2	0.3	6.2	0.03	0.01	0.58	1.939	0.018	0.024
Group 15. Radar Altimeter Errors										
Bias	Eq. (3.1-44)	1.0	—	0.7	0.01	—	0.01	0.001	0.001	—
Scale Factor	Eq. (3.1-45)	0.6	0.1	1.4	0.12	0.02	0.01	—	0.002	0.005

Figure 5.3-4 shows the sensitivity of vertical position and velocity errors to accelerometer misalignments. The vertical velocity error does not meet the spec for any value of accelerometer misalignment, even though this group is the largest single contributor. The combined effect of all other groups is represented by the intercept of the curve with the ordinate; it is 0.23 ft/sec, exceeding the spec value of 0.20. The straight line, representing the contribution of this group alone, shows that the rms misalignment would have to be less than 30 $\widehat{\text{sec}}$ for the effect of this single error source to be less than the spec value.

Figures 5.3-5 and 5.3-6 illustrate the effects of radar altimeter markov error and doppler rate bias error, respectively, on vertical position and velocity errors. The baseline radar altimeter rms error is taken to be a function of altitude, as given in Eq. (3.1-43). Thus, the ratio of the assumed function to the baseline function is used as the independent variable in Fig. 5.3-5. This is the largest contributor to vertical position error -- a ratio of 1.3 causes the total curve to exceed the spec value. The effects of radar altimeter error and doppler rate bias error on vertical velocity error are approximately the same, as indicated by the lower halfs of the two figures.

Figures 5.3-7, 5.3-8, and 5.3-9 show the sensitivity of crossrange position and velocity errors to three major contributors: antenna motion compensation error, accelerometer scale factor errors and gyro bias drifts. In all three cases the velocity error sensitivities are small relative to the spec value. The crossrange position sensitivities, however, are large and the spec cannot be met by reducing any one of the three major contributors alone.

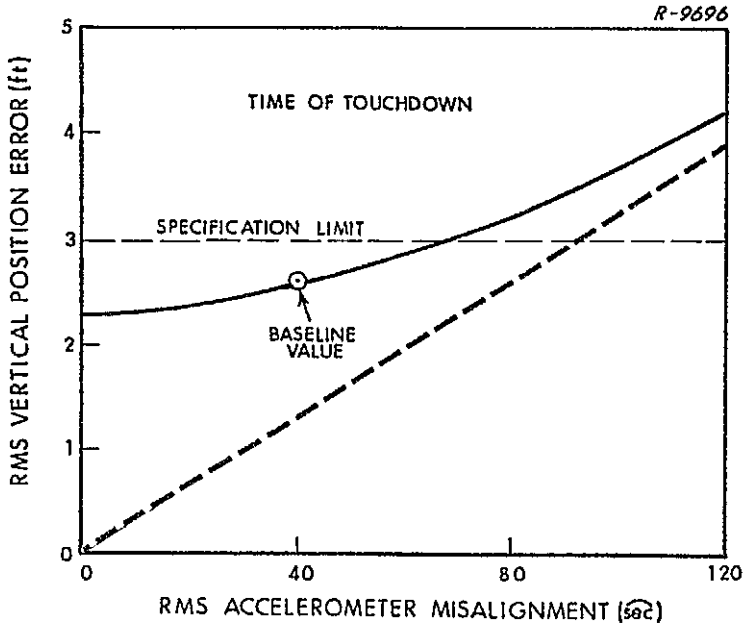

(a) Position

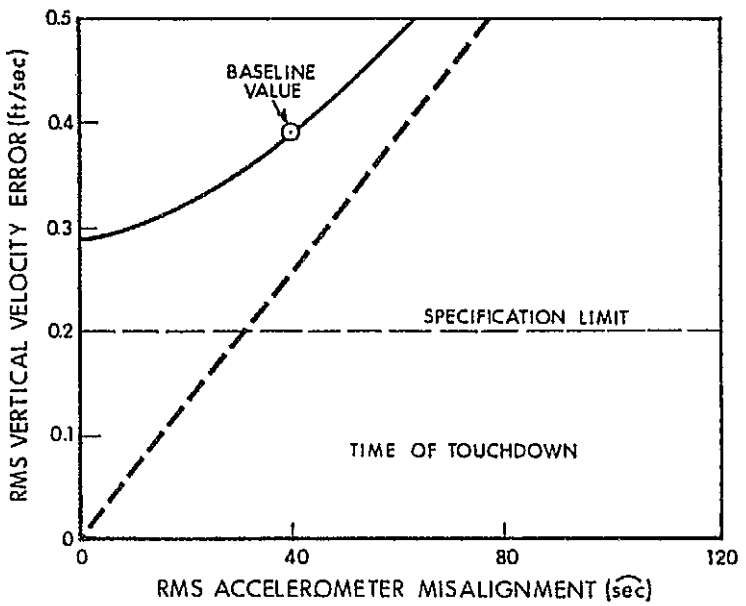

(b) Velocity

Figure 5.3-4 Sensitivity of Vertical Position and Velocity Errors at Touchdown to Accelerometer Misalignment: System C

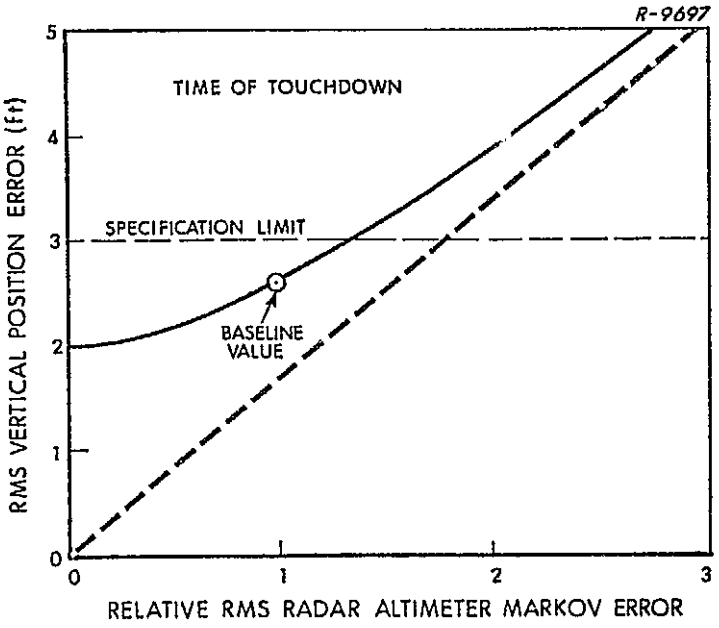

(a) Position

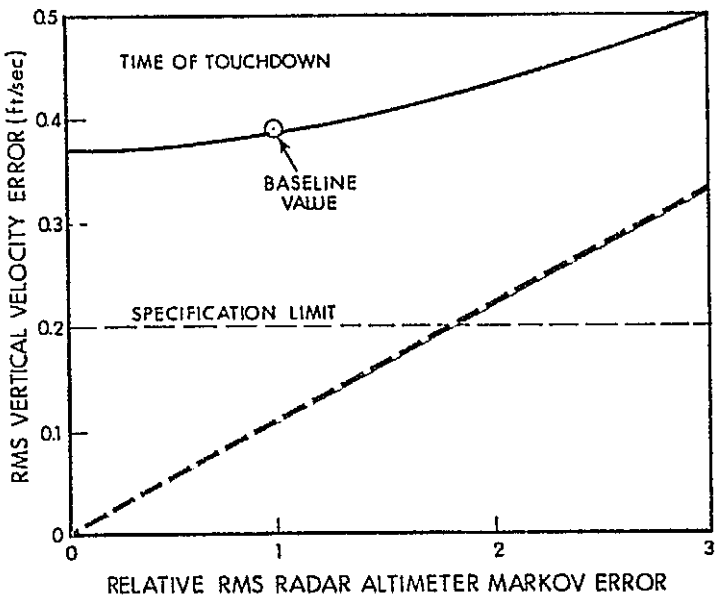

(b) Velocity

Figure 5.3-5 Sensitivity of Vertical Position and Velocity Error at Touchdown to Radar Altimeter Markov Error: System C

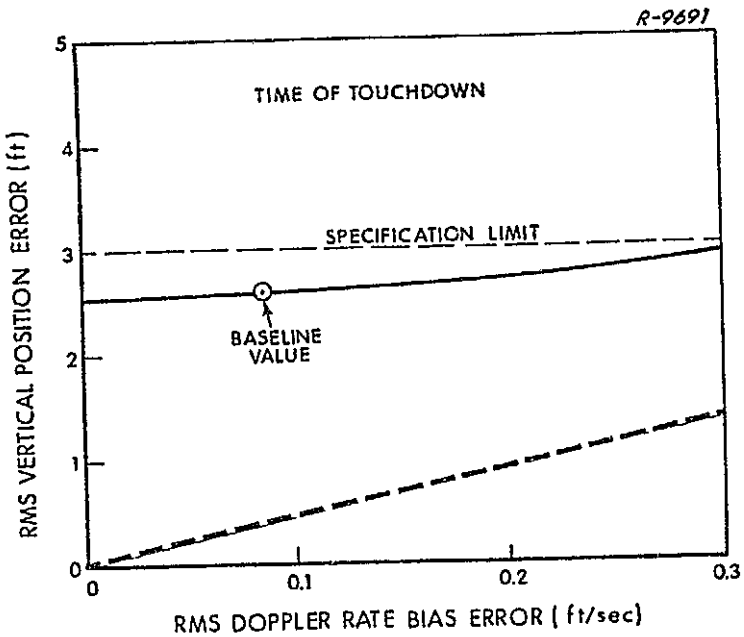

(a) Position

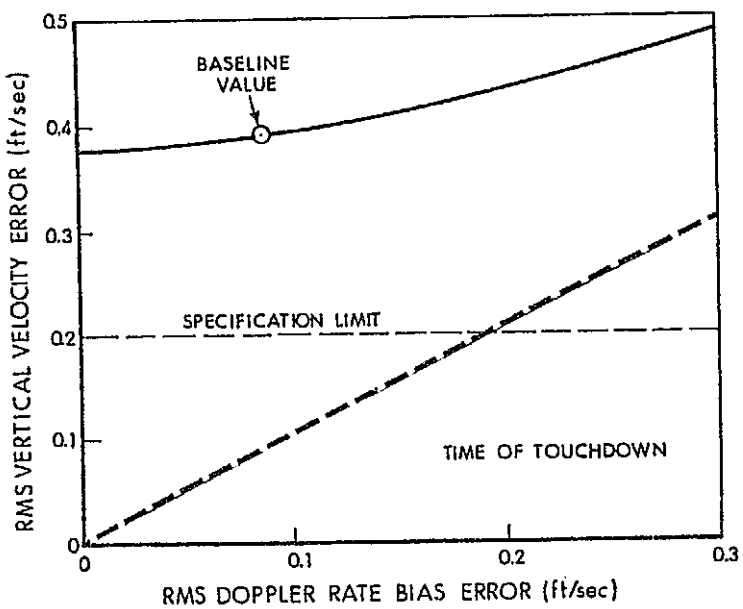

(b) Velocity

Figure 5.3-6 Sensitivity of Vertical Position and Velocity Errors at Touchdown to Onboard Doppler Rate Bias Error: System C

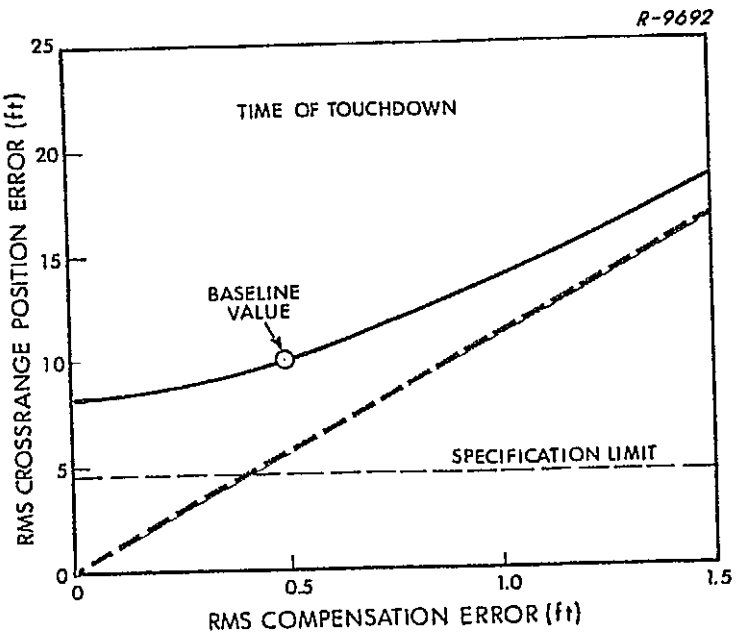

(a) Position

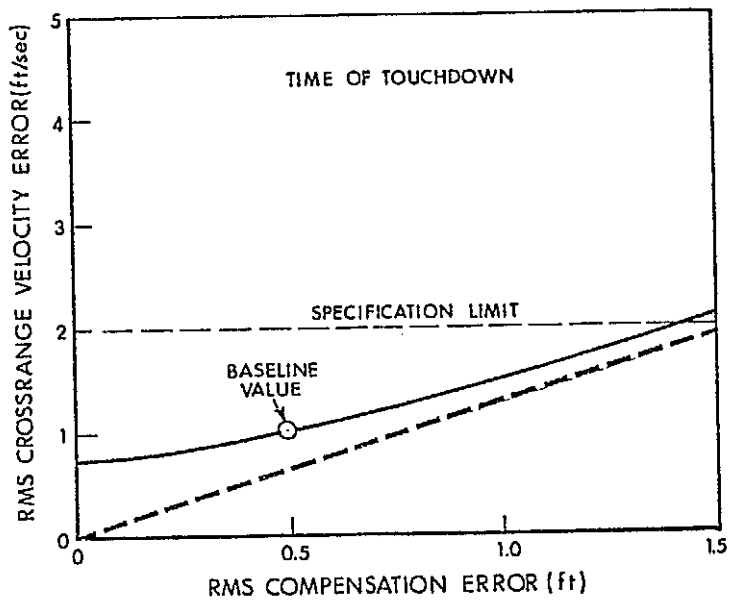

(b) Velocity

Figure 5.3-7 Sensitivity of Crossrange Position and Velocity Errors at Touchdown to Antenna Motion Compensation Error: System C

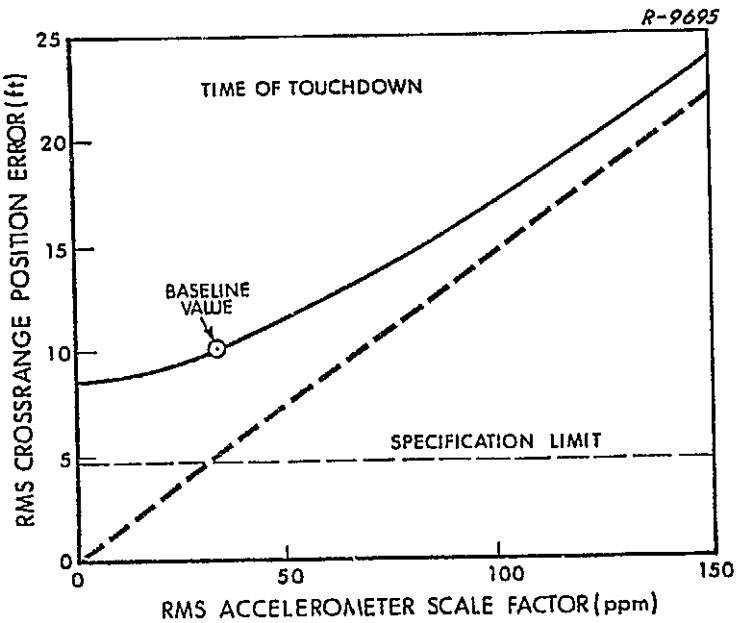

(a) Position

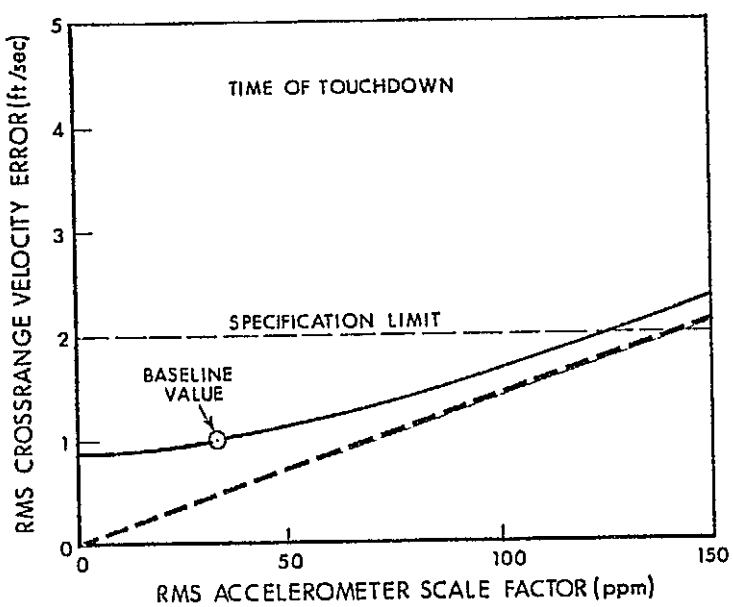

(b) Velocity

Figure 5.3-8 Sensitivity of Crossrange Position and Velocity Error at Touchdown to Accelerometer Scale Factor Errors: System C

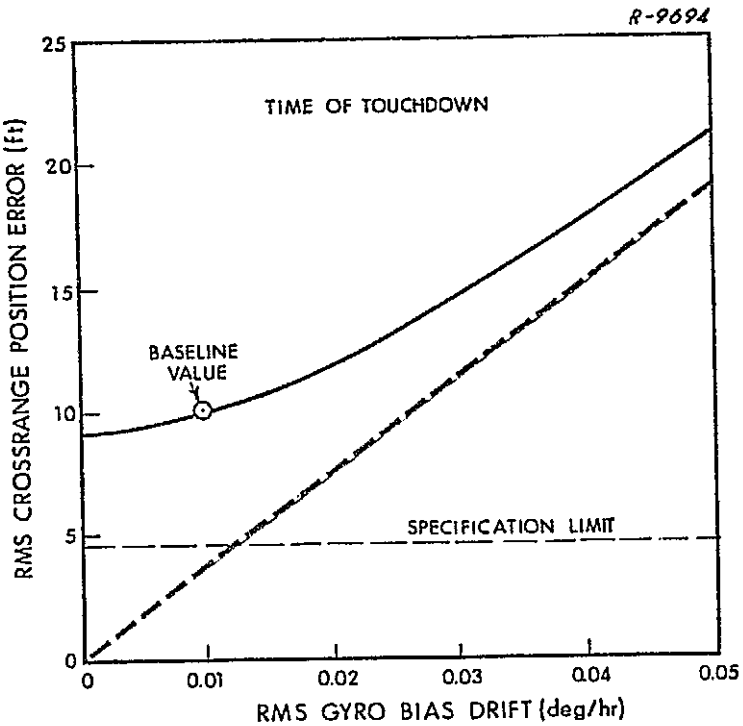

(a) Position

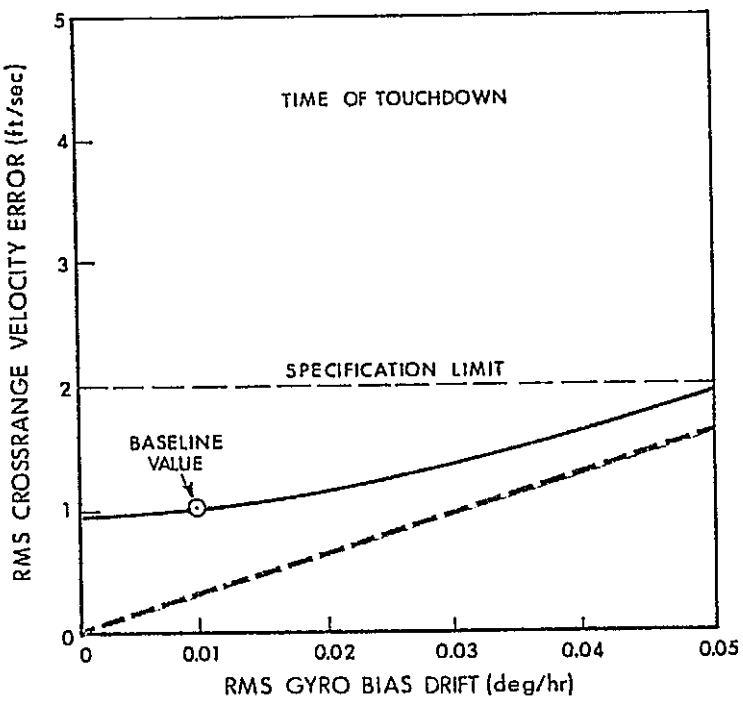

(b) Velocity

Figure 5.3-9 Sensitivity of Crossrange Position and Velocity Errors at Touchdown to Gyro Bias Drift: System C

5.4 SYSTEM D EVALUATION

The results presented below correspond to the trajectory segment, lasting 796 seconds, pictured in Fig. 2.1-1. The final five minute portion of the trajectory has the modified altitude time history described in Section 2.3 -- ending in a steeper final approach during the last minute, compared to that used in the other three system evaluations. The measurement schedule is described in Section 2.2; it employs a 2 second interval between updates for 750 seconds, followed by a 0.5 second update interval for the final 46 seconds. A file of gain values, generated using the filter covariance program outlined in Section 4.4, has been used repeatedly to compute detailed error contributions corresponding to this trajectory and measurement schedule.

5.4.1 Overall System Performance

Figures 5.4-1 and 5.4-2 present overall performance curves for System D, showing position error components and velocity error components, respectively. The curves plotted represent rms errors due to the combined effects of all error source groups in the baseline error budget. They were generated by root-sum-squaring individual contributions at one minute intervals. (These are tabulated in Appendix C.) At T_{DME}, when the first DME and VOR measurements are made, and at T_{BA}, when the first baro altimeter measurement is made, the root-sum-square calculation was performed both before and after update. Thus, the large jumps in certain component errors, which occur at these two times, are accurately shown. Otherwise, the curves are faired-in over the one-minute intervals between the calculated points.

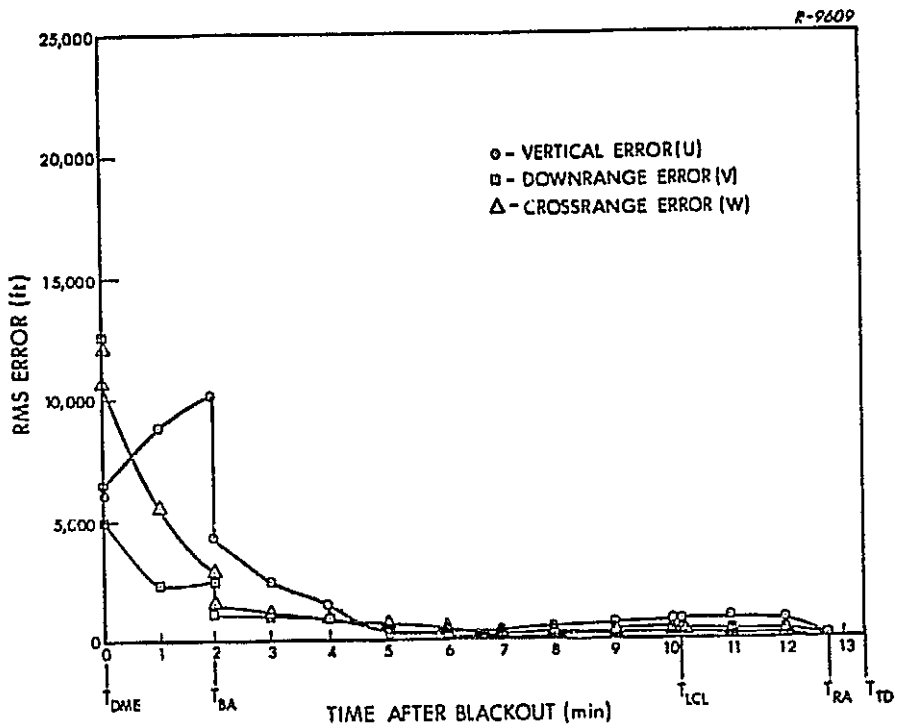

Figure 5.4-1 System D Overall Performance: Position

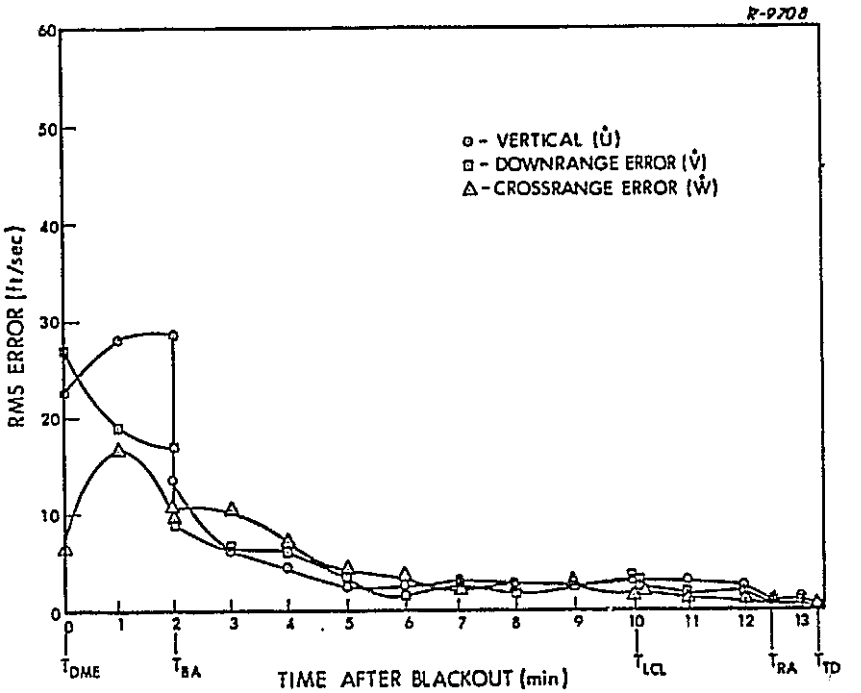

Figure 5.4-2 System D Overall Performance: Velocity

At the time of the first DME and VOR measurements there are no large increases in any of the position or velocity component errors. This result contrasts with the other three candidate system evaluations, in which drag-updating was not used prior to the end of blackout. The vertical position and velocity errors do increase significantly in the next two minutes, prior to the first baro-altimeter measurement. Examination of the individual contributions (tabulated in Appendix C) shows that the major cause of these increases is the set of initial condition errors caused by non-standard atmosphere during the drag-update interval. The increase in crossrange velocity error over the first minute is caused by the VOR markov error.

After the first baro-altimeter measurement all component errors appear to be of reasonable size and well behaved. (We are not speaking here of errors at touchdown, which cannot be judged from plots scaled as in Figs. 5.4-1 and 5.4-2. Final error performance of System D is treated in the following section.)

Section 6 contains further discussion of the implications of the performance curves presented in this section.

5.4.2 Detailed Error Budget

The System D baseline error budget is given in Table 5.4-1, showing rms estimation errors in position, velocity and platform alignment components at touchdown. Each value is the rms contribution of the error source or sources indicated in the left hand column; it comes from a computer run in which the elements of those errors alone are set at truth-model values -- and all others are zero. The overall System D

TABLE 5.4-1

SYSTEM D BASELINE ERROR BUDGET

Error Source	Value	RMS Navigation Errors at Touchdown								
		Position (ft)			Velocity (ft/sec)			Misalignment (mrad)		
		Vertical	Downrange	Crossrange	Vertical	Downrange	Crossrange	Vertical	Downrange	Crossrange
I. ESTIMATED STATES AND NOISES										
Group 1. Initial 8 x 6 Covariance Matrix(Position and Velocity)	See Section 3.4.3	0.1	(5.4)	0.5	0.05	(0.23)	0.04	0.456	0.010	0.029
Initial Position and Velocity Errors Due to Non-Standard Atmosphere during Drag Update	See Section 3.4.3	0.1	0.7	1.1	0.04	0.02	(0.13)	0.895	0.049	0.014
Initial Prelaunch Azimuth Misalignment (Optical)	60 sec	—	—	0.1	—	—	0.01	0.133	0.005	0.001
IMU Quantization Noise	One Pulse - 1 cm/sec	0.3	(4.9)	0.5	(0.12)	(0.23)	0.08	0.051	0.037	0.031
Measurement Noises										
DME	24 ft	—	(6.3)	0.2	0.01	0.07	0.06	0.008	0.011	0.009
VOR	8.5 mrad	0.1	(9.6)	0.3	0.03	(0.14)	(0.10)	0.013	0.021	0.006
Radar Altimeter	3.28 ft	(1.3)	2.5	—	(0.16)	0.05	—	0.007	0.003	0.003
First Order Markov Processes										
VOR	18.07 mrad	0.1	(11.0)	0.5	0.05	(0.32)	(0.10)	0.027	0.027	0.021
Radar Altimeter	Eq.(3.1-43)	(1.4)	(5.4)	0.1	(0.24)	(0.08)	0.03	0.012	0.007	0.005
II. IMU-RELATED STATES										
Group 2. Accelerometer Biases	60 μg	0.4	2.3	0.1	(0.21)	0.05	0.01	0.068	0.051	0.058
Group 3. Accelerometer Scale Factor Errors	34 ppm	0.2	1.2	—	0.10	0.04	—	0.034	0.017	0.009
Group 4. Accelerometer Misalignments	40 sec	(0.8)	(4.6)	0.1	(0.36)	(0.17)	0.02	0.115	0.172	0.180
Group 5. Accelerometer Nonlinearities	3.5 $\mu g/g^2$	(0.6)	1.8	0.9	(0.24)	0.08	(0.13)	0.020	0.015	0.003
Group 6. Gravity Anomalies and Deflections	see Table 3.1-7	0.3	2.4	0.2	(0.13)	(0.10)	0.02	0.042	0.023	0.010
Group 7. Gyro Bias Drift Rates	0.01 deg/hr	—	2.7	0.3	0.02	(0.12)	0.04	0.233	0.018	0.015
Group 8. Gyro Mass Unbalances	0.015 deg/hr/g	—	1.1	0.1	—	0.05	0.01	0.072	0.005	0.012
Group 9. Gyro Anisoelasticity	0.005 deg/hr/g^2	—	0.2	—	—	0.01	0.01	0.028	0.011	0.017
III. EXTERNAL-AID RELATED STATES										
Group 10. DME Bias Error	295 ft	0.2	(10.2)	0.2	0.10	0.04	(0.16)	0.084	0.022	0.007
Group 11. DME Scale Factor Error	100 ppm	—	1.8	0.1	0.01	(0.07)	—	0.009	0.001	0.010
Group 12. Baro-Altimeter Errors										
Bias and Scale Factor	100 ft 0.03 ft	—	0.1	—	0.01	—	—	0.012	0.002	—
Markov Process and Measurement Noise	20 ft 5 ft	—	—	—	—	—	—	—	—	—
Static Defect	1.52×10^{-4} ft/(ft/sec)^2	—	—	—	—	—	—	0.004	0.001	—
Group 13. ILS Localizer Bias	0.5 mrad	—	(6.3)	(5.3)	—	0.03	(0.10)	0.101	0.032	0.002
Group 14. ILS Localizer Second-Order Markov Process	Eq. (3.1-44)	—	4.3	(6.2)	0.01	0.05	(0.30)	0.107	0.051	0.009
Group 15. (Not Included in Baseline Error Budget)										
Group 16. VOR/DME Survey Errors										
DME	1 ft	—	0.8	—	—	0.01	—	0.001	—	0.001
VOR	1 ft	—	0.8	0.1	—	0.01	0.03	0.003	0.005	0.001
Group 17. ILS Localizer Survey Errors	1 ft	—	0.7	1.1	—	0.01	0.03	0.003	0.005	0.001
Group 18. (Not in System D Truth Model)										
Group 19. VOR Bias Error	5 mrad	—	0.2	0.1	—	0.01	—	0.002	—	0.001
Total Projected Performance (root-sum-square)		2.3	23.5	8.4	0.62	0.57	0.44	1.153	0.211	0.199
Filter-Indicated Performance		2.5	54.2	5.7	0.50	1.33	0.30	0.545	0.122	0.211
Specification (Ref. 1)		3.0	80.0	4.7	0.20	3.0	2.0	Not Specified		

A "—" entry refers to a negligibly small contribution.

performance, or root-sum-square values, are given at the bottom of the table and compared, first with the filter's own estimate of performance based on its simplified 23-state model of system error dynamics, and second, with the Shuttle landing navigation specification given in Ref. 1. Particular numbers have been circled in the position and velocity error columns of Table 5.4-1 to focus attention on major contributors. The rule followed in deciding which numbers to circle was to include, in any one column, the largest value, second largest value, etc., until 95% of the RSS total value was reached. The following general statements may be drawn from an examination of the System D baseline error budget:

- The projected downrange performance, in both position and velocity, is considerably more accurate than called for in the preliminary specifications; and, in fact, is more accurate than filter-indicated performance. Significant contributors are DME errors (Groups 1, 10 and 11), VOR errors (Group 1), initial condition errors (Group 1), IMU quantization noise (Group 1), radar altimeter errors (Group 1), accelerometer misalignments (Group 4), gravity anomalies (Group 6) and localizer bias (Group 13).

- The projected vertical performance is within spec in position, but out-of-spec in velocity. The filter-indicated performance is quite accurate, being slightly pessimistic in vertical position and slightly optimistic in vertical velocity. The largest contributors to vertical velocity errors are accelerometer misalignments, nonlinearities and biases (Groups 4, 5 and 2) and radar altimeter markov error and measurement noise (Group 1). Other significant contributors to vertical errors are IMU quantization (Group 1) and gravity anomalies (Group 6).

- The projected crossrange performance is within spec in velocity, but out-of-spec in position. The filter-indicated performance, in both position and velocity, is somewhat optimistic -- predicting approximately two-thirds of the projected actual rms errors. The largest contributors to crossrange errors are localizer bias and markov errors (Groups 13 and 14). Other significant contributors to crossrange velocity error are initial condition errors (Group 1),VOR errors (Group 1), accelerometer nonlinearities (Group 5) and DME bias (Group 10).

- The projected errors in estimating platform misalignments are approximately 0.2 milliradians for misalignments about level axes, and 1.2 milliradians for azimuth misalignment. The filter-indicated performance is accurate in tilt-about-crossrange and somewhat optimistic in both azimuth and tilt-about-downrange -- predicting approximately one-half the projected actual performance for these two components.

Considering all components of position and velocity errors at touchdown, the list of major contributors includes gyro errors, accelerometer errors, and errors associated with all of the external devices except the baro altimeter. Evidently, there are strong correlations between various components of error at touchdown. This accounts, for example, for VOR errors contributing significantly to downrange errors and DME bias contributing significantly to crossrange velocity error. The overall performance projected for System D is similar to that of System A, except for the larger rms vertical velocity error. The major reason for the latter is the steeper final approach trajectory used in the System D evaluation. This result and prospects for improving System D performance are discussed in Section 6.

Table 5.4-2 lists the System D Alternative Contributions showing how different assumptions or additional error sources would produce other contributions to position, velocity and alignment errors at touchdown. Detailed tabulations of the error contribution time histories are given in Appendix C. For every row in Tables 5.4-1 and 5.4-2 there is a page in Appendix C, which is a reproduction of a computer printout page summarizing important results from one error budget run.

5.4.3 Sensitivity Curves: System D

This section contains several curves illustrating the sensitivity of System D performance to variations in error source statistics. These curves were produced using the error budget data of Table 5.4-1. The method of generating the data for these curves is discussed in Section 5.1.3. Similar sensitivity curves may be constructed for any error source group for which error budget data exists in Table 5.4-1.

Figures 5.4-3 and 5.4-4 show the sensitivity of downrange position error to variations in the two largest contributors, DME bias error and VOR markov error, respectively. In both cases the overall performance stays well within spec for substantial increases in the assumed error source rms values.

Figures 5.4-5 and 5.4-6 show the sensitivity of vertical position and velocity errors to variations in accelerometer misalignment and radar altimeter markov error, respectively. The baseline performance is within spec in position, but out-of-spec in velocity. Accelerometer misalignments are the major contributor to vertical velocity error at touchdown. However, even for zero accelerometer misalignment the velocity error remains out-of-spec due to the combined effect of the other

TABLE 5.4-2

SYSTEM D ALTERNATIVE CONTRIBUTIONS

Error Source	Value	RMS Navigation Errors at Touchdown								
		Position (ft)			Velocity (ft/sec)			Misalignment (mrad)		
		Vertical	Downrange	Crossrange	Vertical	Downrange	Crossrange	Vertical	Downrange	Crossrange
Group 1 ILS First-Order Markov Localizer	Eq.(3.1-44)	—	9.1	9.7	0.02	0.10	0.44	0.159	0.073	0.015
Group 15. Radar Altimeter Errors										
Bias	1 ft	1.0	0.4	—	—	0.01	—	—	—	—
Scale Factor	0.025	0.2	5.5	—	0.21	0.01	—	0.012	0.001	0.004

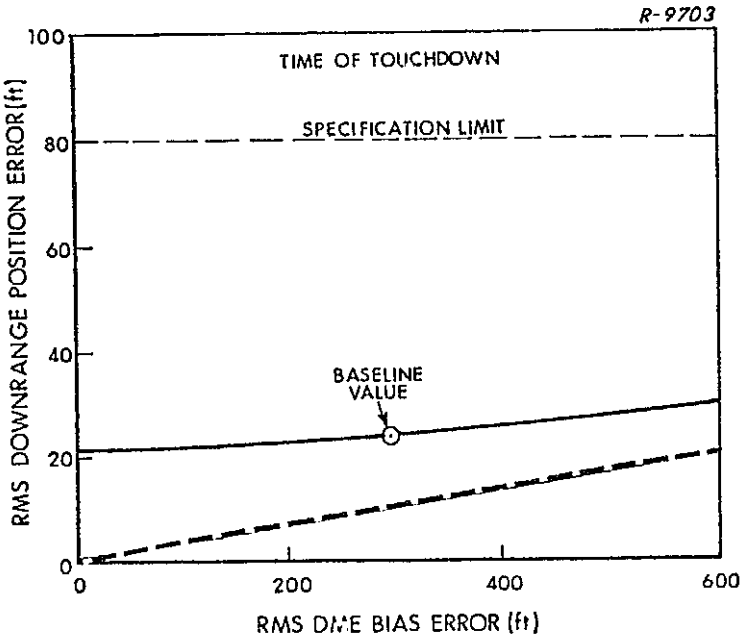

Figure 5.4-3 Sensitivity of Downrange Position Error at Touchdown to DME Bias Error: System D

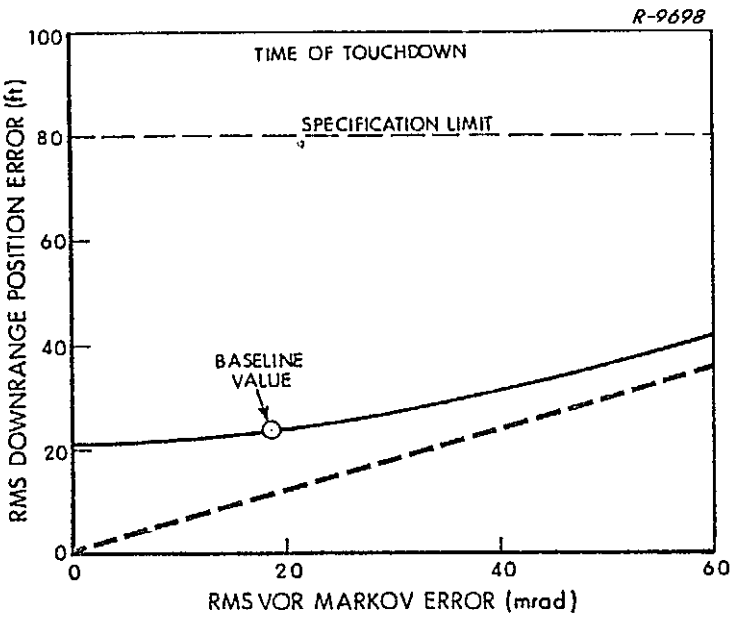

Figure 5.4-4 Sensitivity of Downrange Position Error at Touchdown to VOR Markov Error: System D

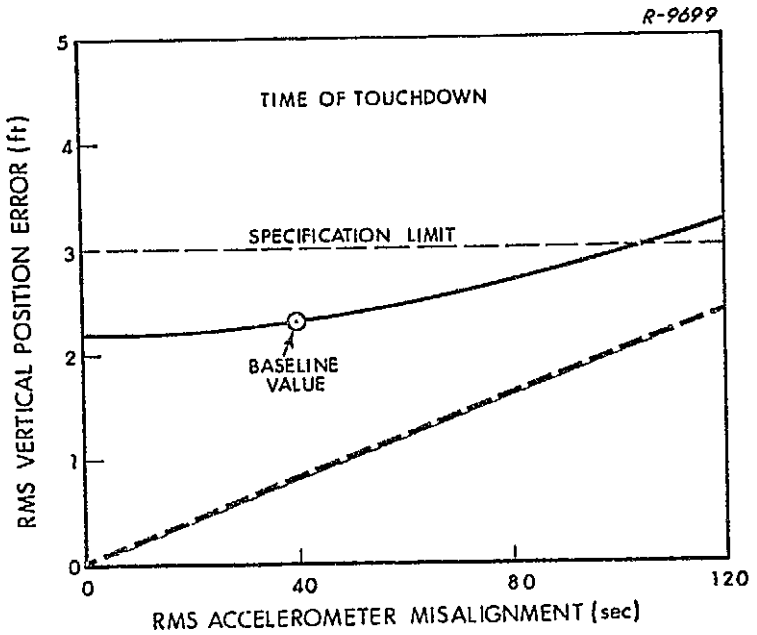

(a) Position

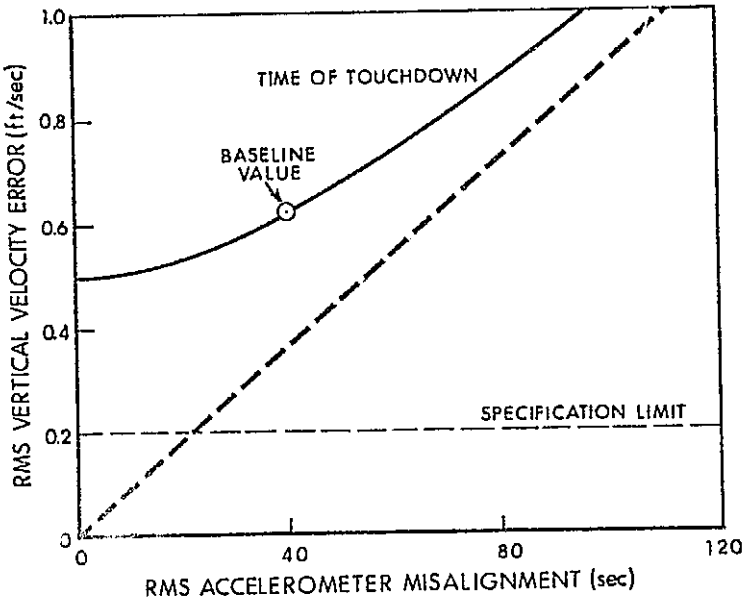

(b) Velocity

Figure 5.4-5 Sensitivity of Vertical Position and Velocity at Touchdown to Accelerometer Misalignment: System D

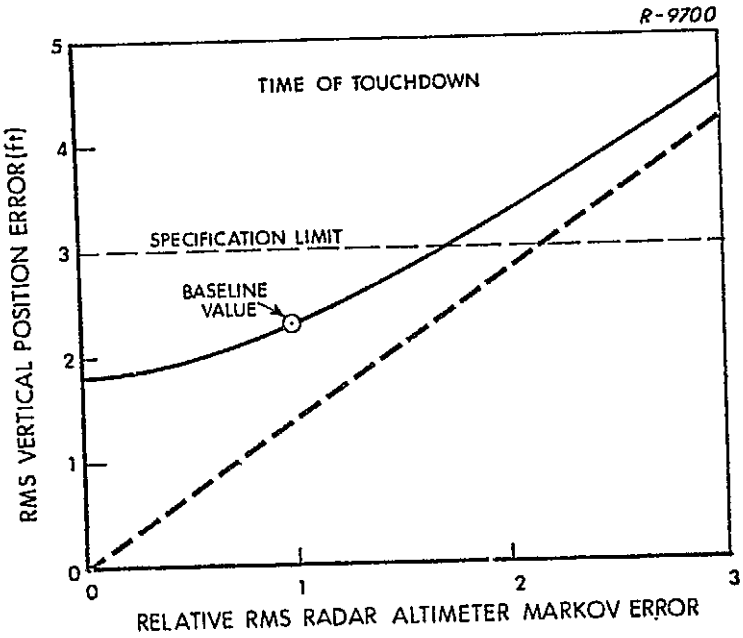

(a) Position

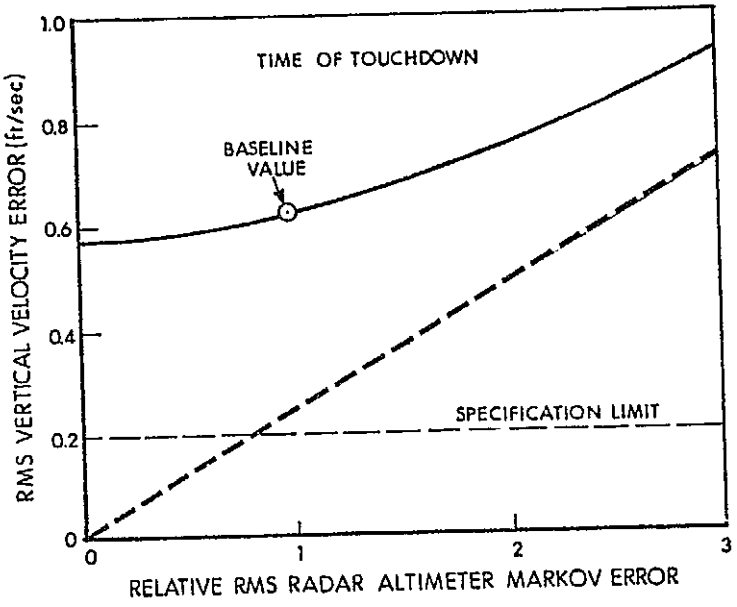

(b) Velocity

Figure 5.4-6 Sensitivity of Vertical Position and Velocity Errors at Touchdown to Radar Altimeter Markov Error: System D

error sources. An rms misalignment accuracy of 20 $\widehat{\text{sec}}$ or better is required to make this single contribution less than 0.2 ft/sec, the spec value.

Figures 5.4-7 and 5.4-8 show the sensitivity of crossrange position and velocity errors to localizer markov and bias errors, respectively. The baseline performance is well within spec in velocity, but out-of-spec in position. In order for the combined effect of these two major contributors to be within spec both would have to be reduced to approximately one-half their baseline values.

Summary — Projected overall position and velocity component errors have been plotted versus time for the four candidate systems. Detailed error budget tables and sensitivity curves related to contributions at touchdown have also been presented. All four systems are shown to be out-of-spec in crossrange position error and vertical velocity error at touchdown. System B is also slightly out-of-spec in downrange position and velocity errors at touchdown. The following section summarizes, compares and interprets these results.

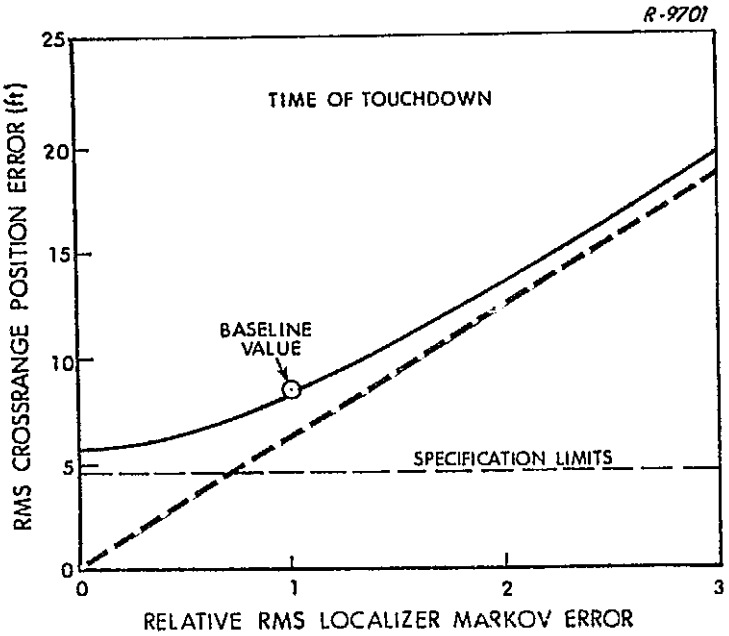

(a) Position

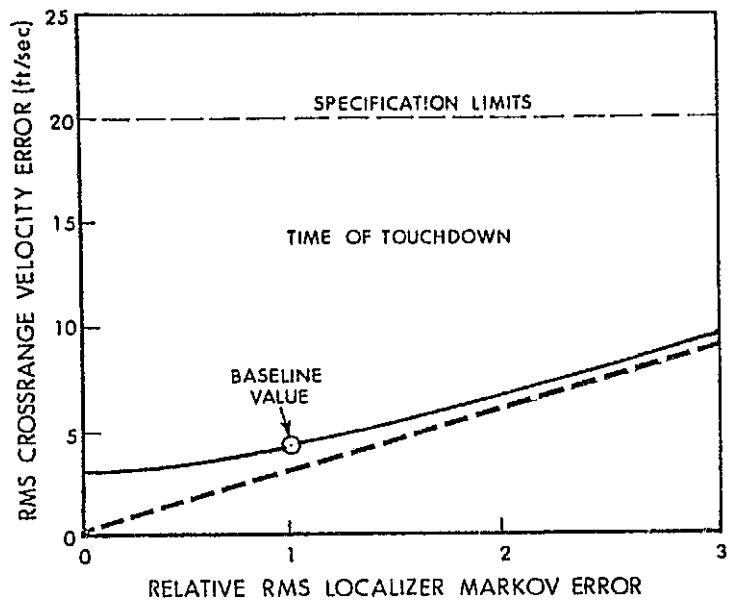

(b) Velocity

Figure 5.4-7 Sensitivity of Crossrange Position and Velocity Errors at Touchdown to Localizer Markov Error: System D

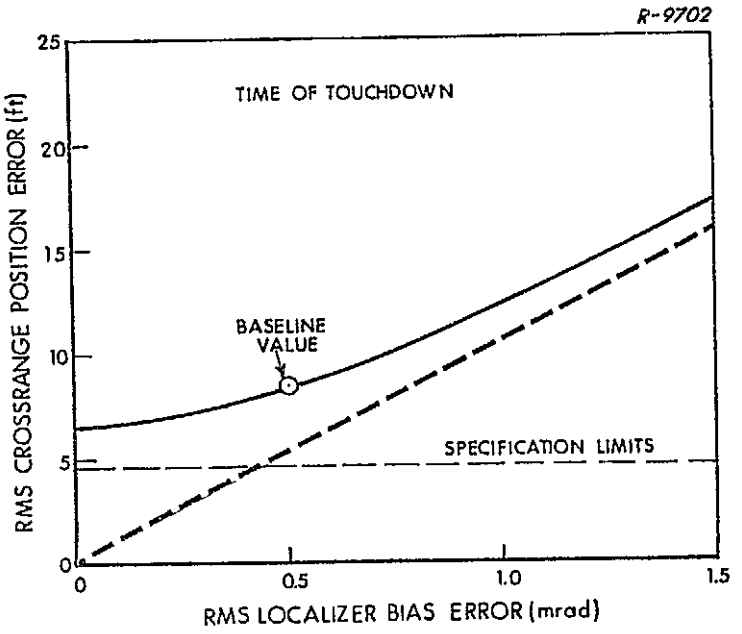

(a) Position

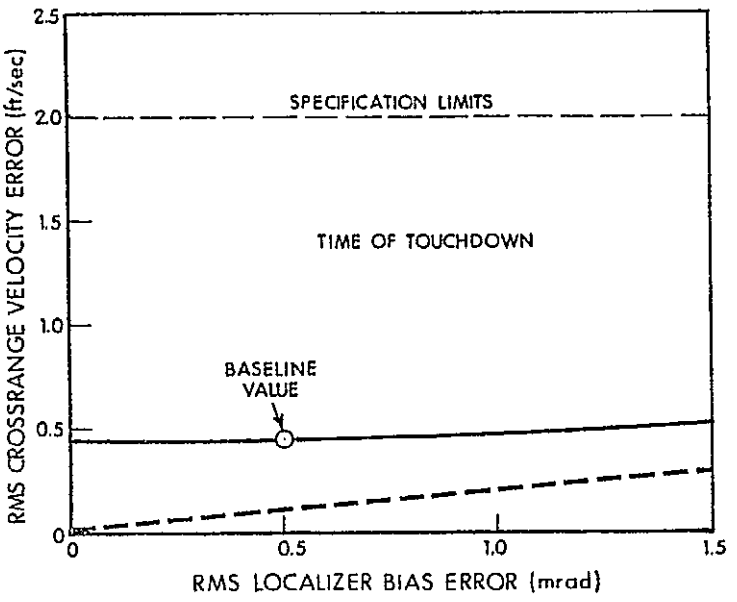

(b) Velocity

Figure 5.4-8 Sensitivity of Crossrange Position and Velocity Errors at Touchdown to Localizer Bias Error: System D

6. SUMMARY COMPARISON AND DISCUSSION

In this section the results of the four candidate system evaluations are summarized, compared, interpreted and discussed. Overall projected performance at touchdown is compared in a single table, which also lists the dominant error sources for each system. The general implications of these touchdown-point comparisons as well as comparisons of performance at earlier times of interest are reviewed. Related groups of error sources are then taken up one at a time, and their different contributions to system errors are contrasted and explained. Finally, the choices of filter states are reviewed and possibilities for improving performance through software modifications are discussed.

6 1 OVERALL PERFORMANCE COMPARISON

Table 6.1-1 presents a summary of the projected rms touchdown errors for the four systems. The table is divided vertically into four major sections corresponding to Systems A, B, C and D, respectively. The top two rows in each division are the overall system performance projections taken from the bottom of the Baseline Error Budget tables given earlier. Numbers greater than the preliminary specification values given in Table 1.2-1 represent out-of-spec performance and are boxed-in. The rows labeled "filter performance ratio" relate the filter-indicated performance, based on the filter's covariance calculation, to the projected system performance, based on the higher-dimensional

TABLE 6.1-1

COMPARISON OF PROJECTED SYSTEM ACCURACY AT TOUCHDOWN

		Vertical	Downrange	Crossrange
SYSTEM A				
RMS Errors, σ_S	Position (ft)	1.9	28.7	[8.0]
	Velocity (ft/sec)	[0.22]	1.07	0.49
Filter Performance Ratio, σ_F/σ_S	Position	1.00	1.04	0.69
	Velocity	0.73	0.84	0.69
Dominant Error Sources		Glide Slope Errors Accelerometer Misalignments Radar Altimeter Errors	Gyro Bias Drifts	Localizer Errors
SYSTEM B				
RMS Errors, σ_S	Position (ft)	2.2	[85.6]	[9.1]
	Velocity (ft/sec)	[0.34]	[3.60]	0.89
Filter Performance Ratio, σ_F/σ_S	Position	0.64	0.25	0.45
	Velocity	0.95	0.13	0.29
Dominant Error Sources		Radar Altimeter Errors DME Errors	DME Errors	Localizer Errors
SYSTEM C				
RMS Errors, σ_S	Position (ft)	2.6	3.0	[10.0]
	Velocity (ft/sec)	[0.39]	0.21	1.01
Filter Performance Ratio, σ_F/σ_S	Position	0.81	0.20	0.35
	Velocity	0.54	0.29	0.33
Dominant Error Sources		Accelerometer Misalignments Radar Altimeter Errors	Doppler Rate Bias Errors Accelerometer Biases	Accelerometer Scale Factor Errors Antenna Motion Compensation Errors
SYSTEM D				
RMS Errors, σ_S	Position (ft)	3.3	23.5	[8.4]
	Velocity (ft/sec)	[0.62]	0.57	0.44
Filter Performance Ratio, σ_F/σ_S	Position	1.09	2.30	0.68
	Velocity	0.81	2.34	0.68
Dominant Error Sources		Accelerometer Misalignments Radar Altimeter Errors Accelerometer Nonlinearities	DME Errors VOR Errors	Localizer Errors

[ ] denotes out-of-spec performance.

truth model covariance analysis. Values less than unity indicate optimism on the part of the filter. The other entries list the dominant (single largest or two or three largest) error sources -- those making major contributions to vertical, downrange or crossrange errors at touchdown.

The most striking feature of the results summarized in Table 6.1-1 is that all four systems are out-of-spec in crossrange position and vertical velocity. While System B is also shown to be out-of-spec in downrange position and velocity, this is not of great concern, as discussed below. First, we discuss the two components which have consistently emerged as troublesome.

The projected crossrange position errors for the three conventional navaid systems (A, B and D) are approximately equal and are all dominated by the same error sources -- the ILS localizer errors. This is true despite the presence of independent crossrange data, coming from the second DME station in Systems A and B, and from the VOR data in System D. These independent data sources are not nearly as accurate as the localizer data and, therefore, do not really help in reducing crossrange errors at touchdown. A related observation is that Systems A and D perform only marginally better than System B, even though the former include a state corresponding to correlated localizer errors. The state estimate is not accurate because of the lack of accurate, independent data. In summary, the crossrange performance of these conventional navaid systems is only as good as the localizer data;* sophisticated software techniques are not likely to change this result.

The projected crossrange position error for System C, the one-way doppler system, is 10 to 20 percent higher than that of the other three

*The use of some independent source of accurate data, such as precision ranging systems, would of course be effective in reducing the error.

systems. However, when the major contributors (accelerometer scale factor errors and antenna motion compensation errors) are considered, we find that there are genuine possibilities for improvement through careful software design; these are discussed later in this section and in 6.2 and 6.3. In other words, the candidate system with the largest projected crossrange error is the one most likely to be able to achieve the spec, given sufficient filter design improvement effort. We note, also, that a one-way doppler system based on two or more ground beacons, rather than the single station of System C, is likely to be capable of much improved crossrange performance. On the other hand, a potential shortcoming of the one-way doppler scheme, especially a single-station version, is that it may not work well with a "straight-in" approach. That is, the spiral approach path used in this evaluation may produce important correlations which account for the system's relatively good crossrange navigation performance.

Although the projected vertical velocity errors exceed the spec for all four candidate systems, System A comes close -- exceeding the preliminary specification value by ten percent. The System A filter generally strikes a good balance between glide slope data, IMU data and radar altimeter data, as shown by the fact that elements of all three are major (therefore somewhat equal) contributors to vertical errors. The sensitivity curve of Fig. 5.1-4(b) shows that a tighter IMU hardware specification, reducing the allowable rms accelerometer misalignment, could reduce the projected overall vertical velocity error at touchdown essentially to the spec level -- with no other changes. It may also be possible to gain improved vertical performance by filter design modifications, as suggested in Section 6.3. Since System B consists of the same hardware elements as System A, it is of course possible to reduce its errors to the level shown for System A through the addition of filter states and proper choice

of filter parameters. A careful comparison of the two error budgets indicates that only a few additional states are needed, as discussed in Section 6.3. Conversely, quite a large number could be safely omitted from the System A filter.

Before discussing the vertical performance of Systems C and D, we make the following general observation. Radar altimeter errors are a dominant source of vertical errors for all four candidate systems. Since the radar altimeter is a direct source of vertical data, it is clear that any given level of vertical navigation accuracy is possible if this data alone can be made sufficiently accurate and if the filter is designed to place sufficient weight on it.

Vertical velocity errors are also a problem for System C, the single-station one-way doppler system. Accelerometer misalignments and other IMU error sources contribute to vertical velocity errors to a somewhat greater degree than for System A. Comments already made about improving vertical velocity performance also apply to System C. That is, a tighter IMU accelerometer misalignment spec, better radar altimeter performance and filter design modifications (discussed further in Section 6.3) can all be significant.

Comparison of the projected touchdown performance of System A and System D, shown in Table 5.5-1, shows that the only important difference is in their vertical velocity accuracies. The System D rms vertical velocity error is nearly three times that of System A. There are two reasons for this difference: the lack of glide slope measurements in System D and the steeper final approach path used in the System D evaluation. The steeper path affects vertical velocity accuracy in several ways. The radar altimeter measurements begin later in the flight, there are less of

them and they are on the average less accurate (since the assumed rms error is a function of altitude, as given by Eq. (3.1-43)). Also, since the vertical velocity is changing more rapidly, the filter is less able to estimate it accurately from the sequence of vertical position measurements. An additional filter covariance calculation was made to gain insight into this problem (see Section 4.4). The results indicate that the steeper approach path is probably the major cause of increased vertical velocity error for System D. This is perhaps the most negative finding of this study -- calling into question the ability of the new Orbiter configuration to be landed safely and automatically with conventional navaids. To do so requires that the radar altimeter accuracy be considerably better than assumed in our baseline studies.

The projected downrange performance for the three systems using high-dimensional filters (A, C and D) are well within specs. System B, which includes a 6-state filter, is slightly out-of-spec in both downrange position and velocity accuracy. Since DME errors are the dominant contributors to downrange errors for System B, it seems clear that the addition of two DME bias states, as included in System A, will provide the necessary improvement. (This point is amplified in Section 6.2.) MIT/DL personnel have reported on simulations of a 6-state filter which satisfies the downrange specification. This is accomplished by proper selection of assumed measurement error variances to achieve more nearly optimal mixing of glide slope, DME and radar altimeter data. They have also simulated further improvements through the use of additional states, such as DME bias. In summary, meeting the preliminary specifications for downrange performance does not appear difficult for the hardware combinations considered in this study.

The remainder of this section is devoted to a summary of points related to earlier portions of the trajectory. The drag-updating procedure, assumed in the System D evaluation, takes places during the blackout portion of the trajectory and has a substantial effect on the "initial conditions" of the post-blackout portion. An obvious benefit to System D, as compared to Systems A and C, is evident in the error time histories of Fig. 5.4-1, as compared to those of Figs. 5.1-1 and 5.3-1. The initial errors are smaller and do not experience large increases -- due to incorrect correlation assumptions -- at the time of the first external measurements. A more subtle benefit involves the accelerometer scale factor errors (discussed in Section 6.2) which lead to incorrect azimuth alignment estimates in Systems A and C. This effect is absent in System D due to the changed initial correlation matrix. The inclusion of drag-updating, particularly in the case of System C (one-way doppler) should lead to significant improvement in crossrange error at touchdown.

A significant advantage of the VOR/DME measurements used in System D, compared to the two DME stations used in Systems A and B, involves the avoidance of filter initialization problems. These are numerical problems which can arise when large navigation corrections are made. Situations of poor measurement geometry, such as when all of the accurate measurements are associated with a given "direction" in state space, are particularly vulnerable. Nonlinear effects can also play a role in these difficulties -- for example, when an accurate range measurement is made in the presence of large uncertainties in perpendicular directions. Filter initialization problems have not occurred in generating the four baseline error budgets reported herein, using linear covariance methods. Others, however, have reported such difficulties in nonlinear simulation work. It is clear that the "angle-range" data from a single VOR/DME station always provide "good geometry" while the "range-range"

data from two DME stations provide relatively poor geometry in the early stages of the trajectory and for the station locations employed in this study. The position error time histories for System D plotted in Fig. 5.4-1 reflect this geometrical advantage in the "midcourse" portion between t = 5 minutes and t = 10 minutes. The errors are consistently low in this region as compared to those of the other three systems presented in Figs. 5.1-1, 5.2-1 and 5.3-1.

As discussed in Section 5.1.1, System A has a problem involving large vertical errors just prior to the time of the first radar altimeter measurements. The problem is associated with mis-estimates of platform tilts about level axes. System B apparently avoids the need for accurate platform data of this type by putting more faith in the baro altimeter in this region. System D minimizes the problem by actually having better tilt estimates in this region. This is apparently another advantage of the good geometry of the VOR/DME measurements.

The following sections take up individual groups of error sources, one at a time, and discusses and compares their effects on the four candidate systems.

6.2 COMPARATIVE INDIVIDUAL CONTRIBUTIONS

6.2.1 IMU Errors

Gyro bias drifts are major contributors to downrange errors for Systems A and B and significant, but relatively minor, contributors for System D. The System B contributions are somewhat larger than those of System A (21.4 ft and 1.11 ft/sec compared to 17.8 ft and 0.85 ft/sec),

even though the System A filter weights IMU data more heavily during the final approach. Examination of the detailed results and comparison with the contributions of initial errors (given in the Alternative Error Contributions, Tables 5.1-2 and 5.2-2) shows that these effects are not primarily associated with the drifting that occurs during approach and landing, but are related to the "initial" platform tilt (at 130,000 ft) caused by drifting during the major portion of the one-rev mission. The better performance for System A is due to its estimation of platform tilt. The actual rms tilt-about-crossrange is 127 $\widehat{\text{sec}}$ (System B Error Budget; 0.637 mrad), while the rms estimation error is 4 $\widehat{\text{sec}}$ (System A Error Budget; 0.018 mrad). On the other hand, System A's estimates of the drift rates themselves are poor and do not help. (They don't hurt either because the filter "knows" that these estimates are poor, as shown in Table 4.1-2.) Gyro bias drifts are also significant contributors to crossrange errors for System C (3.8 ft) and B(2.0 ft). The filters of Systems A, C and D do a reasonably good job of estimating tilt-about-downrange, which helps to hold these contributions down. For these three systems the azimuth misalignment is a greater factor in producing crossrange error at touchdown, and System C(one-way doppler) is affected the most. Other significant, but not serious, effects of gyro bias drifts involve vertical velocity errors in Systems A and C. Gyro mass unbalances (g-sensitive terms) also produce significant, but not serious, vertical errors for System A.

Accelerometer misalignments are dominant contributors to vertical velocity errors for Systems A, C and D (0.10, 0.26 and 0.36 ft/sec, respectively). The key to understanding these effects is the realization that there are six independent misalignment components, two for each instrument, resulting in a nonorthogonal triad of sensitive (input) axes. Therefore, although the orientation of the (initially) level instrument

sensitive axes may be well known, the vertical accelerometer sensitive axis direction will not be. This results in an incorrect resolution of the horizontal deceleration existing prior to touchdown, producing vertical velocity and position error growth. Between measurements these effects are about the same for System A and System B. But, the overall effect on System A is greater because it places more faith in the compensated IMU outputs. (The same is true for Systems C and D.) This faith is based on the 18 states of the filter which relate directly to the IMU. Sophisticated as this 18-state model is, it does not take nonorthogonality into account. Possible approaches to improving the filter in this regard are discussed in Section 6.3. Other significant, but not serious, effects of accelerometer misalignments involve downrange errors for Systems A and D, and crossrange errors for System C.

Accelerometer scale factor errors contribute to crossrange errors in a dominant way for System C and significantly for System A (5.0 and 1.8 ft respectively). Examination of the detailed results shows that this effect is due to a mis-estimation of azimuth misalignment. The azimuth estimation error due to this one error source group is 1.688 milliradians for System C, compared with a total actual azimuth misalignment of 0.620 milliradians due to all sources, as shown in the System B error budget. Apparently Systems A and C would perform better if they ignored their own azimuth updates. System D, on the other hand, avoids this problem because of the altered initial correlations due to drag-updating. The scale factor errors also produce significant, but not serious, contributions to vertical and downrange errors for System A.

Accelerometer nonlinearities produce negligible effects for the first three systems, but surprisingly large effects for System D. The vertical velocity error contribution (0.24 ft/sec) is among the dominant

ones for this system. This result is apparently related to the steep approach path and more abrupt flare maneuver associated with the new configuration.

Accelerometer biases are major contributors to vertical velocity error for System D (0.21 ft/sec) and significant, but not serious, contributors for Systems A and C, in both vertical and downrange directions. The size of the contributions compared with those of other significant error sources indicate that these systems generally strike a good balance between inertial errors and external measurement errors. Attempts to estimate the accelerometer biases in Systems A, C and D are not effective. (In a one-g flight condition the level biases are not distinguishable from tilts and level axes. It is only maneuvering acceleration which provides any hope of separately observing the accelerometer errors.)

IMU Quantization produces significant effects for Systems A, C and D; most notably the crossrange position error (3.4 ft) for System C. These are the systems with high-dimensional filters. They place more faith in IMU data than does System B, and are therefore more affected by the quantization. This faith is justified because of their better knowledge of platform tilts about level axes.

The interpretation of the accelerometer scale factor effects given above and further examination of the detailed error budget tables, leads to a set of implied requirements for initial azimuth alignment accuracy. In order to hold the IMU contribution to rms crossrange error at touchdown to approximately 2 feet or less, the initial rms azimuth misalignment should be approximately 2 milliradians for conventional navaid systems and approximately 1 milliradian for a single station one-way

doppler system. These requirements relate to conditions at the start of the reentry phase and apply regardless of the method used to achieve alignment prior to reentry.

6.2.2 Conventional Navaids

DME bias errors are the dominant source of downrange errors for System B (59.2 ft and 3.13 ft/sec) and significant sources for Systems A and D. This result clearly stems from the fact that DME biases are not estimated in the System B filter while the other filters estimate them quite effectively. The detailed results in Appendix C for System A, Group 10 show that the rms estimation errors for the DME filter states are 292 and 294 feet for Stations 1 and 2, respectively, compared to actual rms bias errors of 285 feet. This implies that the filter effectively calibrates the DME biases with errors of seven and nine feet. It is obviously useful to calibrate Station 1 (the station directly under the approach path) with this degree of accuracy, since this station provides the only good measure of downrange position in the final 20 or 30 seconds before touchdown. It is interesting to note that the DME noise contributions for Systems A and D are greater than for System B. This reflects the fact that, having calibrated the correlated portion of DME errors, the higher-state-size filters can (and should) put more faith in these measurements -- striking a good balance between the effects of the residual DME error and other error sources. The DME biases also contribute in a major way to vertical errors for System B, and in a significant, but not serious way to crossrange velocity error for System D. The latter effect is an illustration of the correlation previously noted between downrange and crossrange errors in the System D (VOR/DME system) evaluation.

DME scale factor errors are major contributors to vertical errors for System B (0.3 ft and 0.19 ft/sec) but relatively minor contributors for Systems A and D. This difference is a result of the lack of DME error states in the System B filter and the dynamic interaction between downrange and vertical errors in the final approach phase.

The VOR system is employed in System D only. The VOR markov error is a significant contributor to crossrange error for that system and is listed as a dominant contributor to downrange errors. The latter contributions (11.0 ft and 0.32 ft/sec) are not serious; they are listed as dominant sources only because the overall system downrange performance is very good -- there are no large contributions compared to the spec values. VOR measurement noise also produces significant, but not serious, downrange and crossrange errors for System D.

The ILS glide slope bias is a dominant contributor to vertical errors for System A and a significant but much smaller contributor for System B. The glide slope markov error also produces larger contributions for System A than for System B. This is actually a fault of the System B filter which should give more weight to glide slope measurements, striking a better balance between glide slope and radar altimeter errors. The glide slope errors also produce significant, but not serious, contributions to downrange errors for Systems A and B.

Localizer error contributions, whether modeled as second-order markov processes or bias errors, are remarkably similar for the three conventional navaid systems; even though the System A and D filters include a localizer error state and the System B filter does not. The crossrange position contributions due to the second-order markov error are 5.9, 6.9 and 6.2 ft for Systems A, B and D, respectively. This

result reflects the fact that localizer error is essentially unobservable in the postulated situation -- there is no independent source of accurate crossrange measurement, and the filter is forced to treat localizer measurements as unbiased. These contributions can only be reduced by improving the ILS system itself -- not by filter design changes.

6.2.3 One-Way Doppler Errors

The doppler beacon is included in System C only. Doppler rate bias error is listed as a dominant contributor to downrange errors (1.8 ft and 0.15 ft/sec) and a significant contributor to vertical velocity error (0.09 ft/sec). The former are not important since they are very small compared to the downrange specification values. The postulated rapidly varying rate bias error (30 second correlation time -- Group 10) is not a significant contributor. It is of interest to note that if the postulated rms value were scaled up to match that of the slowly varying component (400 second correlation time -- Group 1), the system error contributions would be approximately the same for both sources. Thus, it is not at all critical for the correlation time selected for this error state by the filter designer to be an accurate representation of the real-world error characteristic.

The antenna motion compensation error is a dominant contributor to crossrange errors (5.6 ft and 0.65 ft/sec) and a significant contributor to vertical and downrange errors. The effect on crossrange errors at touchdown is similar to that of the accelerometer scale factor errors discussed previously. During banking maneuvers, when the measurement errors are significant, the filter mis-interprets the observations and develops a platform azimuth alignment estimation error. (Note the

1.171 milliradian entry in the System C error budget.) This persists into the final approach phase and leads to significant crossrange errors through a mis-resolution of the deceleration prior to landing.

6.2.4 Altimeter Errors

The baro-altimeter errors produce negligible touchdown errors for System A, C and D and significant, but not serious, downrange and vertical errors for System B. It is worth mentioning again (see Section 6.1) that System B out-performs System A, in the region just prior to the start of the radar altimeter measurements, because it makes more use of the baro-altimeter measurements.

The radar altimeter errors are dominant contributors to vertical errors at touchdown for all four systems. This is an anticipated result since the radar altimeter is a direct source of accurate vertical data in the final approach phase. Significant contributions to downrange errors are also produced for Systems A, B and D, the conventional navaid systems. As mentioned previously the larger vertical velocity contributions for System D appear to stem from the steeper final approach path associated with the new aerodynamic configuration.

6.2.5 Survey Errors

The assumed rms value of all survey errors used in generating the baseline error budgets was 1.0 ft (for each of three components). In most cases this produced an easily predicted result such as the 1.0 to 1.1 ft crossrange errors due to localizer survey error for Systems A, B and D, or the 1.0 ft downrange error due to doppler beacon survey error

in System C. The only significant touchdown error contributions due to survey errors are the downrange position errors (7.1 and 14.4 ft) due to glide slope survey errors for Systems A and B. Examination of the detailed computations associated with these results shows that most of these contributions stem from the vertical component of survey error. The implied requirement is that the glide slope antenna should be surveyed-in carefully enough to insure that the accuracy assumed herein is met, particularly with respect to the vertical displacement from the runway level.

6.3 FILTER DESIGN

This section contains comments and suggestions pertaining to the design of the filters which form a part of each of the candidate systems. Many of these comments have been mentioned or implied in preceeding sections; some are mentioned below for the first time. First, it should be noted that this investigation has not been a filter design study per se. Such a study would involve successive calculations with specific filter states added or deleted, and would be aimed at reaching a specific recommended sub-optimal filter design for a given hardware combination. However the detailed results of this study, along with their interpretation, do provide many useful insights and inputs to such a design effort. This is especially true with respect to the comparative results for Systems A and B, which have identical conventional navaids (in the hardware sense) but very different filter designs. In fact, the System B filter was deliberately chosen to have only six states (the minimum conceivable number for this application) in order to make this comparison as useful as possible -- to indicate what additional states are most needed to achieve performance comparable to that of the 24-state filter of System A.

Based on the comparative individual error contributions discussed above some or all of the following filter states could usefully be added to System B:

- 2 DME Error States (definitely one for Station 1, probably one for Station 2 also)
- 1 Radar Altimeter Error State
- 2 Platform Level Tilt States

The Station 1 DME error state is clearly useful in bringing downrange errors within spec. It is not so obvious, from the results presented, that the Station 2 state is needed, but it may be important to have both states included in order to achieve the kind of calibration accuracy indicated in the System A results for either one. There may also be good reason to include both when consideration is given to failures and redundancy management questions. The addition of a radar altimeter error state probably will reduce the radar altimeter contribution to vertical velocity error for System B. On the other hand, if the suggestion regarding a vertical acceleration error state given later in this section is followed, this extra state may not be needed. The addition of the level tilt states will clearly reduce significant gyro drift contributions to downrange and crossrange errors. The resulting improvement in overall performance may or may not justify these additions. Perhaps the best argument for including them is that the gyro drift rate specifications, for this kind of one-rev pure-inertial-navigation (prior to approach) scenario, could be relaxed.

Based on the comparative individual contributions discussed above there are two places where major System A contributions are significantly larger than the corresponding System B contributions. These are:

- The contribution of accelerometer misalignments to vertical velocity error (0.10 ft/sec -- note the even larger contributions for System C and D).

- The contribution of accelerometer scale factor errors to crossrange position error (1.8 ft -- note the even larger contribution for System C).

A brute-force approach to the reduction of the accelerometer misalignment effect would be to add three additional filter states representing the nonorthogonality of the triad of accelerometer sensitive axes. A simpler approach would involve the use of an artificially high value of velocity state noise in the vertical direction. This would effectively result in less weight being given to the IMU vertical accelerometer outputs, and more weight given to the glide slope and radar altimeter measurements. A third approach, which might be the most fruitful of all, is given later in this section. The contribution of accelerometer scale factor errors to crossrange position error is almost entirely due to the mis-estimate of azimuth misalignment. Systems A and C would perform better if they did not attempt to estimate the azimuth component of misalignment. Alternatively, there may be value in maintaining the azimuth estimation as part of a failure detection scheme, for example, but in omitting the IMU compensation associated with it as long as it remains within some reasonable level. It should be recalled, also, that when drag-updating was included in the System D evaluation, no appreciable azimuth misalignment or crossrange error was caused by the accelerometer scale factor errors. Thus, the entire matter is largely a function of initial correlations as determined by events prior to the end of blackout.

Based on a detailed examination of the error budget calculations for the first two systems it appears that System A landing performance would not suffer if the following states were omitted from its filter:

- 3 gyro drifts
- 3 accelerometer scale factor errors
- 3 accelerometer biases
- 1 ILS localizer error
- 1 ILS glide slope error

These states do not appear to help or hurt the System A performance in any serious way -- see the discussions in Sections 6.2.1 and 6.2.2. (It is recognized that the gyro and accelerometer states may be useful in other mission phases. It is also possible that they can be useful during approach and landing as part of a failure detection scheme.) The above statements apply equally well for System D. That is, the nine IMU sensor error states and the ILS localizer error state could be omitted without appreciable effect on touchdown performance.

It is possible that the nine IMU states can also be omitted from the System C (one-way doppler) filter without loss of accuracy, but the calculations presented in this report do not provide sufficient evidence to justify such a claim. It is clear that for a single-station one-way doppler system there is no advantage in including two separate doppler rate bias error states, since they are not separately observable. (For a multiple-station doppler system, however, separate states for each station plus an added state for the onboard clock error do make sense, since all are theoretically observable.) The large contribution of antenna motion compensation error to crossrange position error for System C can be reduced by one or both of two approaches. First, the error can be reduced at the source simply by designing a highly accurate compensation scheme. Second, the contributions could probably be reduced by underweighting the doppler measurements whenever unusual angular motions occur.

A possible method for reducing vertical velocity errors of all the systems considered is to incorporate a vertical acceleration error state. This suggestion does not follow from the results presented in this report. A vertical acceleration state was used in the NASA/Ames INS/PRS aircraft landing test program (Ref. 21). It was also included in the Shuttle landing design study discussed in Ref. 14 -- also based on a set of PRS (Precision Ranging System) transponders aiding an inertial system. The purpose of this state is to compensate for the effects of vertical accelerometer errors and gravity anomaly errors. It is expected that this state would be useful, also, in compensating for the vertical accelerometer misalignment (nonorthogonality) because of the fairly steady deceleration (approximately 0.2g) during the terminal approach. With a state correlation time of about 20 seconds there should be a good opportunity to observe this combined error source while the accurate radar altimeter and glide slope measurements are being filtered. Systems A, C or D could create such a state simply by reducing the correlation time associated with the vertical accelerometer bias error state. System B would, of course, require an additional filter state.

As stated in Section 6.1 the radar altimeter accuracy will determine the ultimate vertical navigation performance achievable by the kinds of systems evaluated in this study. The sensitivity curves show, however, that none of the four systems studied can meet the preliminary vertical velocity spec (0.2 ft/sec), no matter how accurate the radar altimeter is if the filter designs are not modified. (The curves plotted are the "fixed filter" type of sensitivity curves.) Thus, if better accuracy can be obtained in radar altimeter measurements, it is necessary to use lower measurement variances, etc. in the filter in order for it to place sufficient weight on this good data. In this instance the critical factor is not so much a matter of which states are used, but the

parameter values associated with certain state or measurement statistics.

A similar comment can be made concerning the parameters associated with the baro altimeter state used in Systems A, C and D. The navigation error time histories for Systems A and B reveal an advantage for System B in the trajectory portion just prior to the start of the radar altimeter measurements. As discussed in Section 6.1, System B apparently makes better use of baro-altimeter data in this region. System A would probably benefit from using a more realistic expression and values for its correlated altimeter error state. For example, an expression combining a bias term and a scale factor term (error proportional to altitude) should result in a more proper weighting of data than that of Eq. (4.1-10) if reasonable parameters, such as those used in the truth model, are used.

In summary, it appears that software modifications alone cannot cause the systems studied to satisfy all of the preliminary specifications tabulated in Table 1.2-1. None of the candidate systems can meet the vertical velocity spec unless the radar altimeter accuracy is superior to that assumed in our truth model. Given sufficient radar altimeter accuracy, the filter design details discussed above will be very important in achieving performance within spec. Similarly, the conventional navaid systems are inherently limited in achievable crossrange position accuracy by the correlated errors of the ILS localizer, but careful attention to filter design details is necessary to keep other contributions to crossrange error small by comparison. In the case of the single-station one-way doppler system it appears that software improvements alone are potentially capable of reducing rms crossrange error at touchdown to within the specification value.

7. CONCLUSION

7.1 SUMMARY OF FINDINGS

Four candidate landing navigation systems for the Space Shuttle Orbiter have been evaluated in detail. Three of them are conventional navaid systems using combinations of DME, VOR, ILS and baro and radar altimeters aiding a gimbaled inertial system through a Kalman filter. One employs a single one-way doppler beacon and baro and radar altimeters, also aiding a gimbaled inertial system through a Kalman filter. Comprehensive truth models representing all potentially significant sources of error have been formulated and used to generate detailed error budgets and sensitivity curves. Table 6.1-1 summarizes overall performance at touchdown for the four candidate systems.

The major findings, based on interpretation of the detailed results, are as follows:

- Vertical velocity and crossrange position errors at touchdown present the only difficult challenges to the design of a system of sufficient terminal accuracy. The projected errors for all four candidate systems are out-of-spec in these two components.

- The vertical velocity problem has been made much more difficult by the steeper approach path of the new aerodynamic configuration (assumed in the fourth candidate system evaluation). The ultimate vertical performance, for the kinds of systems studied herein, depends on the radar altimeter accuracy achievable. RMS measurement errors of less than 1.0 ft are required in the terminal phase.

- For the conventional navaid systems the crossrange performance at touchdown is limited by the ILS localizer errors. RMS errors of less than 1.0 milliradian are required -- less than 0.5 milliradian if the error is a true bias or slowly varying correlated error.

- It appears that the single-station one-way doppler system could be made to satisfy the crossrange spec by software modifications alone. However, given a "straight-in" approach this system may not work well at all. On the other hand, a multi-beacon doppler system should work well with any trajectory and provide better accuracy as well.

- There are significant advantages in employing a single VOR/DME station rather than two DME stations. These advantages relate to the filter initialization phase and the "midcourse" approach phase, not primarily to touchdown accuracy.

- There are significant advantages in employing the drag-update procedure prior to the end of blackout (assumed in the fourth system evaluation). This procedure results not only in smaller initial errors, but prevents erroneous azimuth estimation errors related to initial correlations existing prior to the drag-updating.

- A better location for the one-way doppler beacon would be 6,000 to 10,000 feet from the nominal touchdown point, rather than the 3280 feet assumed in the evaluation described in this report. This would cause the sudden large reduction in downrange error to occur at an earlier time.

- The initial azimuth misalignment at the start of the entry phase should have an rms value of 2.0 milliradians or less for the conventional navaid systems and 1.0 milliradians or less for a single-station one-way doppler system -- in order to hold the IMU contribution to terminal crossrange error to 2.0 feet or less.

- A reduction in the rms accelerometer misalignment error to something less than the 40 $\widehat{sec}$ assumed herein would be helpful in reducing terminal vertical velocity errors for all the candidate systems studied.

A number of comments and suggestions regarding the choice of filter states and filter design parameters are given in Section 6.3. Comparison of the three conventional navaid systems studied indicates that a good sub-optimal filter for the approach and landing phase would include approximately 12 states. A similar number is probably appropriate for the one-way doppler system, although additional states related to accelerometer errors may be necessary. In general, software modifications alone cannot cause the systems studied to satisfy all of the preliminary specifications tabulated in Table 1.2-1. But, if sufficient sensor accuracy, especially in the radar altimeter measurements, is available, careful attention to the filter design details discussed will be vital in achieving the full potential of the overall system hardware and in avoiding various pitfalls uncovered in the course of this study.

7.2 RECOMMENDED FUTURE STUDIES

It is recommended that similar detailed error budgets be generated for additional candidate systems of interest. These can include, for example, multi-station one-way doppler systems, microwave landing systems and navigation satellite based systems. The studies should be extended backwards in time to include the blackout portion of the entry trajectory; this is necessary to obtain a proper accounting of correlations between all truth model states during drag-updating. Similar studies related to other Space Shuttle mission phases such as boost and rendezvous are also desirable.

The generation of detailed error budgets presented in this report provide a useful starting point for a filter design improvement effort. Given such an error budget based on a comprehensive truth model of about 80 states, one can define a "reduced state" approximate truth model of perhaps 30 states which account for most of the total system error. This reduced state model can then be the basis for a set of experimental calculations in which filter states, filter design parameters, ground antenna locations, trajectory, etc. are varied. Once a "good" design is approached, the designer can verify its performance using the full 80 state truth model. It is recommended that such a filter improvement effort be conducted for whatever system or systems emerge as leading candidates.

REFERENCES

1. Schiesser, E.R., "SSV Mission Navigation Requirements," FM83 (72-228), 30 August 1972.

2. Crawford, B.S., Dunn, J.C. and Sutherland, A.A., Jr., "CIRIS Design Evaluation," The Analytic Sciences Corp., TR-213-1, September 1970.

3. Crawford, B.S., "Optimal Filter Evaluation" Close Air Support System (CLASS)(U)," AFAL-TR-72-32, March 1972, CONFIDENTIAL.

4. Lear, W.M., "A Prototype, Real-Time Navigation Program for Multi-Phase Missions," TRW 17618-6003-T0-00, 1 December 1971.

5. Lear, W.M., "VOR and ILS Measurement Subroutines for the Multi-Phase Filter Program," TRW 7121-13-15, 20 December 1971, Revised 17 July 1972.

6. Kriegsman, B., "Space Shuttle GN&C Design Equation Document," (Section 9.12.2.2 Entry Navigation), April 1972.

7. Clark, C.W. and Mitchell, P.N., "Inertial Measurement Unit Performance Comparison for a Shuttle One-Rev. Mission," MSC IN 72-FM-172, 5 July 1972.

8. "Development Specification Operational Computer Program", The Singer Company, Kearfott Division, Code Ident. No. 88818, March 1971.

9. "Navigation System Characteristics," MSC IN 72-FM-190, 15 August 1972.

10. Lear, W.M., "One-Way Doppler Derivation, Discussion and Application to the Space Shuttle," MSC IN 73-FM-14, 13 February 1973.

11. Lear, W.M., "Navigation Errors Using Navigation Aids During a Space Shuttle Reentry and Landing," MSC IN 72-FM-213, 12 September 1972.

12. Levine, S.A. and Gelb, A., "Effect of Deflections of the Vertical on the Performance of a Terrestrial Navigation System," AIAA Journal of Spacecraft and Rockets, Vol. 6, No.9, September 1969.

13. "Close Air Support System (CLASS) Accuracy Control Document (U)," Litton Systems, Document No. 400824, July 1971, CONFIDENTIAL.

14. Widnall, W.S. and Morth, H.R., "Space Shuttle Landing Navigation Using Precision Distance Measuring Equipment," Intermetrics, 12 July 1971.

15. Pixley, P.T., "Times of Output, Output Coordinate Systems, and Station Location Errors for TASC," FM82 (72-240), 6 September 1972.

16. Lear, W.M., "Calculation of Shuttle Altitude During Reentry from Drag Measurements," TRW 20029-6011-T0-00, 28 July 1972.

17. Lear, W.M.,"Modification #1 to the Multi-Phase Filter Program," TRW 7121-4-09, 10 December 1971.

18. Robertson, W.M., "Numerical Integration of the W-Matrix by the Average-G ("Heun") Method," MIT/DL, 23A STS Memo No. 47-72, 16 August 1972.

19. McAllister, D.F. and Wilcox, J.C., "Digital Computer Program for Generalized Inertial Guidance System Error Analysis, Version II (GEAP II)," TRW 08768-6009-7000, 11 May 1967.

20. "Shuttle Tracking Systems Data Packages," Lockheed Electronics Company, MSC/TCSD Document No. 1902, November 1971.

21. Schmidt, S.F., "Precision Navigation for Approach and Landing Operations," AIAA preprint 14-3, August 1972.